MARINE AND NON-LOCAL SOURCES OF SULFUR SPECIES AND ORGANIC MATERIAL IN THE EQUATORIAL PACIFIC MARINE BOUNDARY LAYER

A DISSERTATION SUBMITTED TO THE GRADUATE DIVISION OF
THE UNIVERSITY OF HAWAI'I AT MĀNOA
IN PARTIAL FULFILLMENT OF THE REQUIREMENTS FOR THE
DEGREE OF

DOCTOR OF PHILOSOPHY

IN

OCEANOGRAPHY

December 2015

By

Rebecca M. C. Simpson

Dissertation Committee:

Barry Huebert, Chairperson
Steven Howell
Antony Clarke
Christopher Measures
Jennifer Griswold

Acknowledgments

I would like to thank my committee for volunteering so much of their time to guide me through the dissertation process. Drs. Barry Huebert, Steven Howell, Antony Clarke, Chris Measures, and Jennifer Griswold. It is an honor to graduate under their supervision and to have gained their esteem. I look up to each one in many ways and am amazed at their achievements and insights.

I am deeply grateful for the mentoring and instruction received from Barry and Steve throughout my entire graduate career. I hold them both in the highest regard as scientists and am glad to now call them friends. For as long as I've known, my projects have mostly been a group effort as a trio. They have contributed a great deal of time and effort to my development and the development of my papers. Barry has cultivated my critical eye, challenging measurements and assumptions, daring me to defend every claim. Ever the analytical physical chemist, Barry has shown me the ways of careful science, leaving no paper unread and no error unpropagated. Steve has instilled in me the importance of always considering every detail and angle, especially the one where you might be wrong. Steve's curiosity and genuine love for science are undeniably uplifting as they constantly remind me why I spent 8 years (give or take) of my life studying invisible things. They have trained me in immeasurable ways, and I have been deeply humbled during this experience.

Although I was not his advisee, Tony Clarke invited me to work with him on his PASE paper, which turned out to be an exciting experience and one that revealed to me a different approach to aerosol measurements and their interpretation. His determination and almost magical foresight make tedious data mining a treasure hunt. I am grateful for his comments, advice, and good spirit. I am glad that I met Jennifer Griswold during my time at UH. She has provided me a big dose of lively encouragement and advice for future endeavors. She has been very generous

and kind, much needed during a stressful time.

My funding for PASE and for a portion of the data analysis came from the National Science Foundation (NSF). The NSF funded my Masters work under a generous grant (ATM-0627942). Many people were necessary to execute such a large field campaign, and I would like to acknowledge the RAF flight crew and all those that contributed both data and intellectual support. A big thank you goes to Zhuang, who analyzed all the aerosol chemical composition samples at UH while we were in the field. Ian Faloona, Steve Conley, John Merrill, Brian Heikes, Byron Blomquist, and the late Alan Bandy shared important interpretations and insights that inspired various pieces of my work. Though I take certain PASE authors to task for some of their statements, I may not have had nearly as much to write about!

The majority of my funding for my Ph.D. came from the Department of Oceanography through a teaching assistantship. I would like to thank Chris Measures and Eric DeCarlo for their immense support and trust during my time as Head Teaching Assistant. They allowed me a great deal of responsibility that, though stressful at times, aided my maturation and gave me a sense of accomplishment when my own research became frustrating. Because of my years teaching students and overseeing other TAs, I believe that I will be walking away from the department with many valuable skills beyond scientific research. In that sense, I am grateful to all the graduate students that taught with me as well as the other professors who lectured in OCN 201. The undergraduate student body is one of the most diverse in the country, and I had the pleasure of teaching a wide variety of these students. They made me feel young at times and, more recently, old at times, but they always reminded me that curiosity and love of learning are infectious.

The hard-working women of the Oceanography Department office have been incredibly helpful through the years. Catalpa is a unique and loving soul who is constantly running our errands, getting food for our parties, and quietly cleaning

up our messes. She is always there to listen to grievances and has been especially helpful during my time as Head TA. Catalpa is always eager to pitch in for the students even when she's not asked. Pamela has been very quick to help me get logistics settled, particularly for OCN 201. There is no expressing how integral Kristin Uyemura Momohara is in ensuring that we students don't slip through the cracks. Like clockwork, Kristin already has all the paperwork and forms printed out and ready for signing even before you realize you need them to make it through the next hurdle.

I would like to thank all my friends for always being present and ready to help when called upon. Pat Drupp was my first good friend in grad school when we were 20-something twerps and has remained important to me through all the tumultuous growing up we had to do. As fortune would have it, we both defended our dissertations during the same week. Anela Choy tolerated me when I was learning to surf and then spent many hours with me in that marvelous Hawai'ian water during invaluable surf sessions, some unforgettable, some challenging. She has been my closest friend, and I will always cherish our island adventures. Anela opened my eyes to a completely different side of local culture that I would have otherwise not experienced. Kristen Fogaren has become a treasured confidant for issues ranging from personal dilemmas to fantasy football lineups. I wish her luck and look forward to new excitement on the mainland. I will always think fondly upon my first days as a grad student with the 2007 cohort including Sherril, Saulo, Max, Pavica, Tina, Victoria, and Eun Jung, my first office mate. Other grad students over the years have shared good times (Tracy), mostly commiserating lately (Donn and Shimi). I still miss the Mānoa house and my roommates Matt, Justin, John, Mattie B, and Steph. That was by far the best group and most fun I've ever had living with peers. Matt continues to be a great friend; he is thoughtful and always young at heart. Tobi and Fiona, or the Germans, have been great friends since nearly the beginning. We started out as climbing buddies, but

the days at Mokulēʻia have long since passed for us, especially since surfing became an addiction. I hope to see all these people again.

This dissertation would not have been possible without the unwaivering support and unconditional love from my family. I am incredibly fortunate to have my mother (Suzette), father (Larry), sister and her new husband (Emily and Dan), Nana, step-mother (Cindy), and step-siblings (Stephanie and Rob). As this chapter of my life draws to a close, I realize that even though they have been physically distant, their belief in me is the foundation of my confidence and the security I need to pursue my goals. Even when I am feeling small and invisible, these loved ones always make me feel seen and appreciated.

Abstract

Marine aerosol and gases in the remote marine boundary layer (MBL) form a critical link between the ocean and atmosphere by regulating aerosol optical properties, cloud formation and properties, photochemistry, and biogeochemical cycles. The sources of marine aerosol were once thought to be relatively simple: large, primary sea salt aerosol (SSA) from wave-breaking and small, secondary non-sea-salt-SO_4^{2-} (NSS) from condensed oxidation products of the organo-sulfur gas dimethylsulfide (DMS) in the atmosphere. With the advent of faster, more sensitive measurements, contributors to the marine organic and sulfurous aerosol population are coming into sharper focus. Of course, new complications inevitably appear.

This dissertation explores components of this increasingly complex chemical story using a rich dataset collected during an airborne experiment in the remote equatorial Pacific. Rapid sulfur gas measurements coupled with size-resolved aerosol chemistry enabled the construction of balanced DMS, SO_2, and NSS budgets that include entrainment and divergence. These two dynamic terms turn out to be critical mechanisms for adding oxidized sulfur to (entrainment) and removing it from (divergence) the remote MBL. Even in cleaner conditions, entrainment of continental material from 10 000 km away can match DMS as a source of NSS to the MBL. During episodes of enhanced long-range transport, distant sources such as biomass burning can eclipse the low-background marine atmosphere.

In addition to some entrainment of submicrometer organic species, we were able to detect submicrometer organic aerosol concentrations that varied according to satellite chlorophyll *a* multiplied by wind speed. This connection strongly suggests emission from the marine biology. The natural marine signal near equatorial upwelling was up to 4x stronger than other organic aerosol signals.

Methanesulfonic acid (MSA), a natural organo-sulfur gas, is often measured but

poorly understood. Through our exploration of a unique vertical gradient in high-resolution MSA measurements in the MBL, we highlight large unknowns in DMS oxidation chemistry as well as the emerging importance of gas-particle partitioning. We find strong evidence for MSA vapor degassing from small particles in the mixed layer near the warmer, drier ocean surface. There remains much debate and study and concerning the sources of natural aerosol and cloud condensation nuclei.

Contents

Acknowledgments v
Abstract vii
List of Figures xiii
List of Tables xiv
Notation xvi

1 Introduction 1
1.1 The Marine Atmosphere 1
1.2 PASE 5
1.2.1 Original Vision 5
1.2.2 Sampling Strategy 6
1.2.3 Findings and Successes 7
1.2.4 PASE in Context 11
References 16

2 Dimethyl sulfide (DMS) may be less important than long-range transport as a source of sulfate to the remote tropical Pacific marine boundary layer 21
2.1 Introduction 22
2.2 Methods 28
2.2.1 Experimental 28
2.2.2 Chemical Budget Analysis 31

2.3 Results . . . 36
2.3.1 DMS Processes and Budget . . . 39
2.3.2 SO_2 Processes and Budget . . . 41
2.3.3 NSS Aerosol Processes and Budget . . . 46
2.3.4 What Fraction of DMS Becomes NSS? . . . 50
2.3.5 DMS Versus Long-Range Transport of Sulfur in MBL NSS . 50
2.3.6 Context of PASE Results . . . 52
2.4 Conclusions . . . 56
References . . . 81

3 Submicrometer organic aerosol in the equatorial Pacific marine boundary layer: Links to chlorophyll *a* and entrainment from the free troposphere . . . 95
3.1 Introduction . . . 96
3.2 Experimental . . . 98
3.2.1 Aerosol and Gas Measurements . . . 99
3.2.2 Use of CO to Differentiate between Clean Marine Air and Continentally Influenced Air . . . 100
3.2.3 Estimating Flight-Averaged Chlorophyll *a* . . . 101
3.3 Results and Discussion . . . 102
3.3.1 OA Profiles and Properties . . . 102
3.3.2 Wind-Driven Species Concentrations . . . 105
3.3.3 OA Correlation with Chlorophyll *a* . . . 106
3.3.4 A Note on SOA in PASE . . . 111
3.3.5 Continental OA in the Remote Marine Atmosphere . . . 111
3.4 Conclusions . . . 112
References . . . 123

4 Revising concepts of methanesulfonic acid (MSA) formation in the remote tropical Pacific marine boundary layer using high-resolution measurements and a thermodynamic model of aerosol chemistry . . . 135
4.1 Introduction . . . 137
4.2 Measurements and Calculations . . . 142
4.2.1 PASE . . . 142
4.2.2 Aerosol and Gas Measurements . . . 143
4.2.3 Aerosol Property Model: *E-AIM* . . . 145
4.3 Results . . . 146
4.3.1 MSA Vapor Observations . . . 146
4.3.2 Particulate MS^- Observations . . . 147
4.3.3 MS^- Size Distributions . . . 147
4.4 Discussion . . . 148
4.4.1 LML Sources of MSA . . . 148
4.4.2 MBL Particulate MS^- Measurements Support Hypothesized MSA Processes . . . 163
4.4.3 Gas-phase MSA production . . . 169
4.4.4 FT Sources of MSA . . . 170
4.5 Conclusions . . . 173
References . . . 192
Appendix . . . 207

List of Figures

1.1 PASE research flight tracks and example flight pattern from Research Flight 03. 14

2.1 Model of subsidence, entrainment, and divergence in the central Pacific MBL and FT system. 62

2.2 Schematic of remote marine boundary layer processes and notation used in our sulfur budget. 63

2.3 Altitude-segregated NSS during PASE flights. 64

2.4 Project-average ML size distributions for NSS, MS^-, NO_3^-, and Na^+. 65

2.5 **(a)** [DMS] and **(b)** [SO_2] profiles. 66

2.6 Flight-average vertical profiles of CO, DMS, and SO_2 during RF03 (Low-CO) and RF11 (High-CO). 67

2.7 Project-average profiles of NSS from MOI, DMA mass, and AMS SO_4^{2-} in 100-m bins. 68

2.8 Diurnal concentrations from the 1994 experiment. 69

2.9 Project-mean PASE concentrations and processes. 70

2.10 DMS-OH and SO_2-OH reaction rates versus TOD. 71

2.11 DMS, SO_2, and LWC during BuL cloud penetrations in RF03. . . . 72

2.12 Downwelling UV irradiance versus time during upper-ML leg, just under clouds. 73

2.13 PASE process rates in $\mu mol\, m^{-2} d^{-1}$, "units," for Low-CO air. . . . 74

2.14 Comparison of NSS measured from aircraft campaigns in the lower FT of the remote Pacific. 75

3.1 Equatorial Pacific monthly average MODIS Chl *a* for August, 2007, when PASE was in the field. 115

3.2 24 h HYSPLIT back trajectories (gray lines) for Research Flight 06 (ML flight track shown in black) plotted with MODIS Chl *a*. 116

3.3 PASE altitude profiles of AMS submicrometer non-refractory OA, corrected using a factor of 5.5 derived from NSS comparisons between the AMS and impactor samples. 117

3.4 OA profiles in 300 m altitude bins for PASE and VOCALS C-130 (SE Pacific). 118

3.5 AMS OA averaged by 5 ppbv CO bins in the mixed layer (<550 m) and buffer layer (550 m - 1250 m). 119

3.6 FT CNhot (refractory aerosol >10 nm after heating) versus OA (a) colored by CO ppbv and (b) fit to a linear function for only HCO air. 120

3.7 PASE OA (a), Na^+ (b), and DMS (c) averaged per 1 m s^{-1} wind speed bins. 121

3.8 Flight-averaged AMS OA as a function of 24 h upwind MODIS Chl *a* concentrations and wind speed (WS). 122

4.1 Simple DMS oxidation scheme in the remote tropical marine boundary layer. 175

4.2 a) PASE MSA gas profile (CIMS 10 s data) with 200 m-bin mean and median traces. 176

4.3 PASE MS^- aerosol profile showing total, coarse-mode (>1um), and fine-mode (<1 µm) concentrations (a) measured by the MOI. 177

4.4 a) PASE MS^- mean mass distribution in the LML, TML, and BuL and b) ML $Na^+/10$, NSS, and $MS^-\times 10$ mass distributions. RF05 is excluded as it was an outlier. 178
4.5 MSA versus simultaneous wind speed measured from the plane in the PASE LML. 179
4.6 MSA and H_2SO_4 profiles and 200 m-bin means. 180
4.7 $\log_{10}$(MSA) and $\log_{10}(H_2SO_4)$ versus OH molecules/cm^3 (a and b, respectively) and versus %RH (c and d, respectively) in the PASE ML. 181
4.8 AMS submicrometer NH_4^+ neq/m^3 versus SO_4^{2-} neq/m^3 averaged for 30 min level legs in the ML, color-coded by flight number. 182
4.9 Calculated flux of MSA vapor to/from PASE particles in the LML and TML. 183
4.10 Comparison of size-resolved MOI MS^- aerosol molar concentration with calculated total daily fluxes (dotted lines) of MSA vapor to/from each MOI stage. 184
4.11 $\log_{10}$(MSA) versus submicrometer $[SO_4^{2-}]$ molality (mol kg^{-1}) in ambient particle volume in the LML and TML. 185
4.12 Correlations between a) MSA and b)MS^- and coarse-mode SSA. . . 186
4.13 Potential temperature (θ) profiles colored by a) MSA molecules/cm^3 and b) DMS pptv. 187
4.14 $\log_{10}$(MSA molecules/cm^3) versus DMS /pptv in the upper BuL (upper 300 m) colored by %RH, with the lower 200 m of the FT (black triangles) plotted on top. 188

List of Tables

1.1 Organic Sulfur Compounds of the Marine Atmosphere with Chemical Formulas. 15

2.1 Mixed Layer and Buffer Layer Sulfur Species in ppt. 76
2.2 DMS Budget Summary of Calculated Terms from Equation 2.10. . . 77
2.3 Example Calculation of Oxidation of SO_2 in Cloud Passes. 78
2.4 SO_2 Budget Summary of Calculated Terms from Equation 2.11. . . 79
2.5 NSS Budget Summary of Calculated Terms from Equation 2.14. . . 80

4.1 *E-AIM* Inputs and Outputs. 189
4.2 PASE MSA and MS^- Concentrations in Layers of the Central Pacific Marine Atmosphere. 190
4.3 Comparison of Total Calculated MSA Gas-to-Particle Fluxes Assuming Different K_H Values for MSA. 191

Notation

Symbol	Description
NSS	Non-sea-salt [SO_4^{2-}].
OA	Organic aerosol.
mOA	Marine organic aerosol.
POA	Primary organic aerosol.
SSA	Sea salt aerosol.
S	Sulfur species.
$\langle S \rangle$	Column-average sulfur concentration.
CCN	Cloud condensation nuclei.
ppt/ppb	parts-per-trillion/billion; molar mixing ratio.
γ	yield of SO_2 from DMS oxidation; 0.75 in this study.
PASE	Pacific Atmospheric Sulfur Experiment.
VOCALS	VAMOS Ocean-Cloud-Atmosphere-Land Study.
MBL	Marine Boundary Layer (ML + BuL).
ML	Mixed Layer.
LML	Lower Mixed Layer.

TML	Top of Mixed Layer.
BuL	Buffer Layer.
FT	Free Troposphere.
TWI	Trade wind inversion.
z_0	Ocean surface; 0 m.
z_1	Mixed layer height; 550 m.
z_2	Trade wind inversion height; 1250 m.
LRT	Long-range transport.
ω_e	Entrainment velocity ($\mathrm{mm\,s^{-1}}$).
$J_{0\,\mathrm{S}}$	Sulfur species surface flux.
$J_{z_2\,\mathrm{S}}$, $\omega_e[S]_\mathrm{F}$	Entrainment flux of S.
D_S	Divergence loss.
div	Horizontal divergence.
$R_{\mathrm{M\,S\,O_3}}$	Reaction of $[\mathrm{SO_2}] + [\mathrm{O_3}]$ in ML SSA.
C	Flux of $\mathrm{SO_2}$ into cloud.
ξ	in-cloud conversion efficiency.
V_d	dry deposition velocity.
1 flux "unit"	$\mathrm{\mu mol\,m^{-2}\,d^{-1}}$ of S.
TOD	Time of day.
ITCZ	Inter Tropical Convergence Zone.
LCO	Low CO; CO $<$ 63 ppbv.
HCO	High CO; CO $>$ 63 ppbv.
Chl *a*	Chlorophyll *a*.
VOC	Volatile Organic Compound.
E-AIM	Extended AIM Aerosol Thermodynamics Model.

Chapter 1

Introduction

1.1 The Marine Atmosphere

The tropical marine atmosphere is an important region for Earth's radiation budget owing to its very high solar irradiance and low albedo. Marine aerosol and gases in the remote marine boundary layer (MBL) form a critical link between the ocean and atmosphere by regulating aerosol optical properties, cloud formation and properties, photochemistry, and biogeochemical cycles.

Formed through either primary (wave-breaking and bubble-bursting) or secondary processes (gas-to-particle conversion), marine aerosol is differentiated by size and chemical composition, with sea-salt aerosol (SSA) dominating the supermicron (>1 µm) mode and non-sea-salt sulfate (NSS) dominating the submicron (<1 µm) mode. Other organic and inorganic species present in seawater are emitted with SSA. Organic matter emitted with sea spray is termed primary marine organic aerosol (mOA) and has been shown to be enriched on small primary SSA under some circumstances (*Facchini et al.*, 2008; *Keene et al.*, 2007), though the mostly unknown sources of these compounds make them virtually indistinguishable from secondary mOA, which forms by condensation of oxidized volatile organic

compounds (VOCs) on pre-existing particles.

Diverse interactions between marine particles, gases, and clouds modulate feedbacks between marine ecosystems and climate, but we have too little understanding of the details to predict the magnitudes of these feedbacks. As a consequence of its size and remoteness, the ocean-aerosol-cloud-climate system is one of the largest sources of uncertainty in global climate projections.

The CLAW hypothesis (*Charlson et al.*, 1987), a seminal idea in modern marine atmospheric chemistry, proposed that a complete negative feedback loop exists between phytoplankton and climate. Through the water-side biochemical production of a compound that is released to the atmosphere as dimethyl sulfide (DMS), marine microbes provide the precursor material for subsequent photochemically induced oxidations to produce climate-relevant SO_4^{2-} particles, either through nucleation or cloud-mediated growth. In theory, an increase in the DMS flux leads to an increase in the number of SO_4^{2-} particles and thus more cloud condensation nuclei (CCN), which enhances cloud persistence and albedo to the extent that photosynthetically active radiation reaching the ocean surface is reduced, in turn reducing phytoplankton biomass.

From the beginning, CLAW was tenuous. There was no evidence for some of the steps (like reduced sunlight reducing DMS), and even those with theoretical support (e.g., more DMS leads to more CCN) were not proven. Since 1987, much work (e.g., *Clarke et al.*, 1999, 2006; *Quinn and Bates*, 2011) has shown that the CLAW mechanism cannot operate as originally described. Nevertheless, the component connections are real, and the amount of productive research inspired by the hypothesis justifies its intellectual legacy.

In agreement with earlier findings, I argue against the primary CLAW DMS-to-SO_4^{2-} route in Chapter 2, because DMS does not control SO_4^{2-} particle concentrations in some very remote parts of the ocean. The CLAW hypothesis has proven to be an important paradigm for understanding and studying the relationships be-

tween marine biota, air-sea exchange, atmospheric chemistry, aerosols and CCN, cloud physics. and radiative transfer. None of these operates in isolation from the others, and must be studied in concert, even though we show that the precise thermostatic feedback loop described by Charlson, Lovelock, Andreae, and Warren does not operate as proposed.

Recent insights into the ocean-atmosphere system point to increasingly significant roles for non-DMS sources of CCN, including emissions of mOA particles from the ocean surface and material of continental origin entrained into the MBL from the free troposphere (FT). In Chapter 3, we quantify the marine and distant sources of organic aerosol, and find a very close coherence between mOA and (Chl a) as inferred from satellites. The background marine CCN population seems to only be weakly sensitive to DMS flux variability (*IPCC-AR5*, 2013), though there is a high likelihood that such an inference does not hold for all marine ecosystems in all conditions. Despite the effort made thus far to test the CLAW hypothesis, we have yet to see the collection of a well-posed, comprehensive set of atmospheric and seawater measurements in a single oceanic region. Thus, natural aerosol feedbacks are still not well constrained on regional or seasonal scales, and substantial uncertainty persists surrounding aerosol-cloud interactions (*Carslaw et al.*, 2010; *Mahowald et al.*, 2011; *IPCC-AR5*, 2013).

Long-range transport (LRT) of aerosol particles in the stable FT is an effective means of delivering continental aerosols to the remote ocean. In isolated areas of the ocean such as the central Pacific, sparse continental influence means that local CCN concentrations are highly susceptible to small changes in particulate physicochemical properties (*Lohmann and Feichter*, 2005). Beyond affecting MBL atmospheric chemistry, the deposition of continental material such as mineral dust and volcanic ash in low-nutrient regions (meso- or oligotrophic, for example) represents a longer-term indirect biogeochemical effect that aerosols have on global processes that lead to complicated non-linear feedbacks (*Mahowald et al.*, 2011).

Characterizing marine aerosol composition needs added attention so that models can not only predict background aerosol forcings but also reduce the uncertainty in the reference scenarios from which models determine the magnitude of anthropogenic aerosol radiative forcings. To accurately parameterize marine aerosol properties, we need to understand the sources and sinks of gas and particle-phase substances. This requires distinguishing between natural and distant anthropogenic sources that arrive by LRT. DMS oxidation products lofted into the FT by deep convection in the Inter Tropical Convergence Zone (ITCZ) can advect and subside into other MBL environments. Furthermore, natural SO_2 and NSS from volcanic degassing can contribute to the NSS burden downwind.

In current climate models, the most disagreement with observations and with other models stems from the simulated sensitivity of MBL clouds to changing conditions (*Bony and Dufresne*, 2005; *IPCC-AR5*, 2013). There are many approaches that can be taken to increase knowledge about the radiative response of MBL clouds, but to understand the atmospheric processes controlling CCN concentrations, an airborne field experiment in a pristine, archetypal MBL is the best means of acquiring real chemical and physical data to construct constrained budgets to improve models (*Hamilton et al.*, 2014).

This chapter introduces an airborne sampling approach undertaken in 2007 to characterize the major chemical and dynamic processes of the remote MBL. All field measurements analyzed in Chapters 2, 3, and 4 of my dissertation derive from the Pacific Atmospheric Sulfur Experiment (PASE). In the remainder of this chapter, I will describe: 1) the strategy taken in PASE to increase our understanding of the natural sulfur cycle in the marine atmosphere, 2) the main findings and the strategy's success, 3) the contextual significance of my dissertation and its contributions to contemporary marine atmospheric chemistry.

1.2 PASE

1.2.1 Original Vision

A remote site in the tropical Pacific was chosen in order to study as many facets of CLAW-inspired DMS chemistry as possible in the MBL without the added complexities of unstable meteorology and anthropogenic sulfur emissions. Christmas Island (2° N, 157° W) is at least 10 000 km from any continent and meteorologically located in the southern hemisphere due to the position of the ITCZ (5° to 10° N) at the time of the experiment in August and September of 2007. With mean east-southeasterly winds of $8\,\mathrm{m\,s^{-1}}$ and sparse trade wind cumulus clouds limited to the buffer layer (BuL) over the mixed layer (ML; ML + BuL = MBL), the tropical Pacific trade wind regime during PASE provided the dynamic consistency desired to permit quantitative budgeting of major sulfur species. Because cloud chemistry involves quantifying aqueous processes that are notoriously difficult to observe, the initial intent was to restrict the experiment to the ML.

The upwind distance from Christmas Island to South America was virtually rain-free ($<1\,\mathrm{mm\,d^{-1}}$ for August and September), simplifying the gas-phase chemistry and reducing the need to estimate aerosol wet-depositional fluxes in the ML. Though this region typically experiences low cloud cover, the month-long dryness can partly be attributed to the La Niña, or cold phase of the El Niño-Southern Oscillation (ENSO), which has significant influence over equatorial Pacific climate. This region experiences strong large-scale subsidence, which entrains dry FT air into the humid ($\sim$80 %) MBL below on a timescale of 1 d to 2 d.

Set in the biologically active equatorial upwelling zone, PASE was well positioned to observe any natural marine biological signal over the low background of the remote southern hemisphere. Though this oceanographic ecosystem is mesotrophic, its sustained primary production year-round is substantial due to the

region's large geographical expanse. With a slight peak in September, this moderate upwelling supports the largest total yearly amount of primary production in the ocean. The prevailing La Niña further strengthened the divergence-induced upwelling along the equator, increasing the chances of observing emissions of marine biological material.

Because PASE is representative of a large portion of the tropical trade wind regime, many of its insights are relevant to the tropical ocean. The logistical constraints of an airborne experiment based on an atoll in the central Pacific were many and in some cases prevented full closure of chemical cycles. Regardless, PASE was the most comprehensive and widely applicable remote sulfur experiment to date, and as my dissertation's chapters demonstrate, there is no substitute for a well-designed field experiment.

1.2.2 Sampling Strategy

The program consisted of 14 research flights (Figure 1.1) that sampled the MBL, which is divided into the mixed layer (ML; ∼0 m to 550 m) and overlying buffer (cloud) layer (BuL; ∼550 m to 1250 m). The FT (>1250 m) resides above the trade wind inversion (TWI). For the most part, the C-130 aircraft flew chevron patterns at level altitudes for 30 min, with 15 min per leg. Semi-Lagrangian, or more accurately Eulerian as noted in Chapter 2, budget analyses were made possible by flying so that the apex of the chevron patterns advanced slightly upwind with each successive stack (Fig. 1.1b).

As mentioned, we primarily sampled in the ML to keep the gaseous budget analyses simple, even though it somewhat detracted from the aerosol budget analyses and ultimately was unfavorable for both owing to the integral role played by clouds chemically and dynamically. Sampling in the BuL was hence limited and mostly restricted to cloud-free regions, biasing our cloud statistics low. Rapid pro-

files into the FT were flown roughly three times a flight with little sampling time and no level altitude legs with which to collect size-resolved aerosol chemistry.

The simultaneous atmospheric measurements – photochemical species (CO, O_3, OH, H_2O_2, CH_3O_2H, HO_2, RO_2), gaseous sulfur (DMS, SO_2, H_2SO_4, MSA), and size-resolved (e.g., NSS, MS^-, NO_3^-, Na^+) and high time resolution (submicron OA, SO_4^{2-}, NH_4^+) aerosol species – collected versus altitude during PASE were successful and unmatched for a remote experiment. These were enriched by aerosol physical and optical properties and CCN concentrations at a range of supersaturations (*Clarke et al.*, 2013; *Hudson et al.*, 2011). Concomitant meteorological measurements (wind, RH, etc.) provided context for the chemical observations to assess the extent to which dynamics or air mass origin controls chemical profiles and diurnal variations.

1.2.3 Findings and Successes

The on-board atmospheric pressure ionization mass spectrometers (APIMS) made available high-resolution ($\sim$25 Hz) DMS and SO_2 observations with very high precision due to the isotopically labeled internal standard method that they use to obtain internally calibrated ambient samples (*Bandy et al.*, 2002). These uniquely reliable DMS and SO_2 measurements enabled rigorous computations of eddy-covariance (EC) fluxes and flux divergences, thereby allowing us to quantify ambient reaction rates of DMS and SO_2, the core gases of the CLAW hypothesis sulfur cycle. The chemical ionization mass spectrometer (CIMS) supplied fast measurements of OH radical, the primary DMS oxidant in the MBL.

With these well-constrained ML EC fluxes of DMS and SO_2 and concentrations of OH, PASE investigators were able to construct sulfur budgets and agree that OH was the primary DMS (and SO_2) oxidant, with a small possibility for low [BrO]. Yet different approaches, including that of Chapter 2, shaped the very different

conclusions concerning the yield (γ) of SO_2 from DMS oxidation by OH (*Conley et al.*, 2009; *Faloona et al.*, 2010; *Gray et al.*, 2010). The seemingly incongruous findings are a result of semantics; the definition of γ differed in *Faloona et al.* (2010). Because of our agreement with *Gray et al.* (2010) on the meaning of γ, our evaluation of γ in Chapter 2 was based on their model-derived value. However, we arrive at different conclusions concerning the fate of SO_2.

On the SO_2 front, we differ more drastically from *Faloona et al.* (2010); they attribute the largest portion ($\sim$57 %) of their SO_2 sink to heterogeneous loss to aerosol without support of empirical evidence. Because their budget was confined to the ML on a day-long timescale, *Faloona et al.* (2010) lacked a large sink in clouds – which we deemed the single most important for SO_2 loss – and therefore had a large residual of SO_2 that they called heterogeneous uptake since the other known removal fluxes had been computed. In our month-long sulfur budget, I constrain the loss of SO_2 to large particles by demonstrating nearly undetectable amounts of NSS mass on the largest stages of the impactor. Whereas measuring large-particle chemistry from a plane is typically fraught with losses due to tubing and shatter, the low-turbulence inlet (LTI, *Huebert et al.* (2004)) used upstream of the impactor greatly reduces these losses and is extremely well characterized. We can therefore confidently dismiss the hypothesized uptake of SO_2 onto coarse sea salt (*Sievering et al.*, 1991) as insignificant in the tropical MBL.

In their 1-D chemical transport model, *Gray et al.* (2010) also report that heterogeneous loss to aerosol is a large loss term at 19 % of SO_2, but at least they included loss to the BuL where a dominant portion is scavenged in cloud. Dry deposition of SO_2 to the ocean surface was their largest SO_2 sink (48 %), whereas it was a smaller sink (20 %) in our budget and smaller than divergence (35 %). Besides inclusion of the cloudy BuL, the largest contrast between our sulfur budget and those of the other PASE authors is the treatment of entrainment and divergence. As two of the mechanisms responsible for significant oxidized sulfur sources and

losses, respectively, entrainment and divergence cannot be excluded in subsidence regions. Further interpretations of our sulfur budget and its implications are in Chapter 2.

The main shortcoming of our measurements is the missing window of evening hours (∼5 p.m. – 2 a.m.), which prevents closure of the diurnal cycle. Because we operated in such a remote location, making measurements outside of the ML daytime plan was not possible due to safety concerns. Additionally, having only two "night" flights that took off at 2 a.m. was inadequate, as we probably missed nighttime and even sunrise MBL dynamics and chemistry by not having a large enough sample size.

Considerable effort was made to measure dimethyl sulfoxide (DMSO) and dimethyl sulfone $DMSO_2$ (Table 1.1), but these APIMS instruments failed early in the project and could not be revived. The absence of the DMSO measurement rendered us incapable of quantitatively evaluating (and thus confirming) the hypothesized multiphase pathway for coarse MS^- formation from DMSO uptake onto large sea salt particles in Chapter 4. DMSO is a critical intermediate whose fate (homogeneous destruction by OH, deposition on particles, or scavenging by cloud) determines the product distribution of the DMS-OH addition channel.

Due to the scarcity of relevant measurements, the large role likely played by multiphase chemistry, and the difficulty of simulating the reactions in a lab under low-NO_x ambient conditions, DMS-OH addition chemistry in the remote MBL has been poorly understood. Beyond DMSO, this uncertainty has obscured MSA vapor's origins and its connection to MS^- aerosol, which is more concentrated by $\sim$ 2 orders of magnitude. Fast MSA measurements from the CIMS enabled the observations of a MSA gradient that led to the uncovering of a previously undescribed pathway to MSA vapor. In Chapter 4, I explain this hypothesized pathway that has not yet been seriously considered in the literature. In doing so, I warn against the temptations of applying overly simple models to ambient

DMS chemistry. When fitting a model to data one must ensure that any necessary sources or sinks are physically realistic.

Though we sought out simplicity during PASE, we discovered that thorough treatments of the chemical budgets truly require the complexity of multiphase reactions, especially clouds, even in a subsidence region with relatively low cloud cover (∼16 %). Additionally, the sampling strategy designed to simplify the gaseous budgets created more uncertainty in the aerosol budgets due to the lack of statistics in the BuL and FT. While the rapid gaseous measurements made fine-scale interpretations and budgeting possible, the size-resolved aerosol chemistry could only be measured once for every 30 min level leg, leaving many fewer samples. The arid conditions were convenient for the gases but murky for the longer-lived aerosols (and CCN), which were never sufficiently removed by wet deposition to discern whether a diurnal cycle existed.

Another phenomenon that contributed to obscuring the aerosol variation was the entrainment of polluted non-local air, which was observed in nearly half the research flights and added SO_2 and NSS mass to the remote MBL. The low background CO (a combustion indicator) in the southern hemisphere tropics made the CO and particulate (CNhot) pollution signal discernible. The La Niña increased not only the likelihood of high-altitude transport of air from South America but also the dry conditions experienced during the unusually intense Amazon fire season. Thus observations of LRT of biomass-burning type continental outflow in PASE were more favorable than in non-La Niña years. In Chapter 2, I evaluate the contribution of local DMS oxidation to the NSS mass and compare it to the NSS derived from LRT of continental material to the MBL.

Not all aerosol measurements were successful. The total aerosol sampler (TAS) exhibited a build-up of ions that became increasingly large and inconsistent with the impactor throughout the project, leading us to suspect accumulated residue from shattered cloud droplets on the C-130 that were never washed off the plane

or TAS inlet. Due to this contamination, TAS data was not used. The MS^- on the filters could not be resolved when extracted by ion chromatography (IC), and so we turned to earlier MS^- size distributions from a project at Christmas Island in 1994 (*Huebert et al.*, 1996) to constrain their concentrations, which we believe do not exceed 10 % of the total MS^- mass. Nevertheless, the aerosol measurements proved invaluable for quantifying the chemical budgets without particles, the MBL story is fragmented at best.

Once thought unsuccessful, the submicron organic aerosol (OA) measured by the aerosol mass spectrometer (AMS) proved to be usable, albeit on longer time scales (1 d) than originally intended (10 s), and a surprising addition to the PASE story. By making use of a comparison of NSS concentrations between the impactor and AMS, a correction was applied to the OA. Project-average profiles suggested a surface source. In Chapter 3, I investigate whether our OA measurements can be linked to satellite-derived chlorophyll-a to indicate a mOA source. I also attempt to differentiate the marine and continental OA sources.

1.2.4 PASE in Context

PASE is arguably one of the few pristine MBL regimes globally that seldom experiences continental influence (*Hamilton et al.*, 2014). Hence, we were able to characterize the sulfur budget in a representative trade wind region and found that DMS chemistry is not likely as significant for sulfate aerosol (and CCN, *Clarke et al.* (2013)) production in the remote MBL as proposed by the CLAW hypothesis. The movement toward a weaker DMS-sulfate-cloud cycle is reflected in the work of others (e.g., *Quinn and Bates*, 2011), though reductions in future anthropogenic sulfur emissions in response to climate legislation invite future reassessments.

Remote trade wind regions are indeed very sensitive to inputs from distant sources. We observed a strong indication of this as LRT of CO, SO_2, and NSS

eclipsed the natural DMS-generated NSS at times. It may be that we sampled rare LRT events (and perhaps volcanic influence) that only occur during favorable climate states. A brief survey of the estimated yearly intensities of Amazon biomass burning seasons reveals that 2007 had an exceptionally large area of forest burned (NASA satellite products). However, global biomass burning emissions are increasing, much of it advecting and depositing over oceans.

The equatorial Pacific has a marine biological surface OA source that is stronger than the background and OA entraining from the FT. HYSPLIT back trajectories in the stable trade wind regime can be used to define a 1 d fetch. Our linear relationship between submicron OA and MODIS Chl a $\times$ wind speed provides a practical parameterization for the low-Chl a tropical regions that are more productive than oligotrophic ecosystems but much less productive than coastal upwelling or bloom regions. Refinement of OA measurements is leading to greater emphasis on the potential for marine OA to contribute substantially to the MBL CCN population.

Though the CLAW hypothesis has been diminished, there yet remains a great deal unknown about ambient DMS chemistry. DMSO, MSIA, and $DMSO_2$ measurements in the gas and aqueous phases are needed to begin to address these gaps in knowledge (see Table 1.1 for formulas and structures). Our hypothesized pathway to MSA vapor production through uptake and aqueous oxidation of DMSO in cloud droplets and particles needs further study as do the other possible reactions of DMSO and its products and their subsequent interactions with the condensed phase.

Results of this dissertation can be used by modelers to 1) reduce uncertainty in tropical yield of NSS from DMS (in pristine versus continentally influenced conditions), 2) include the marine sulfur cycle perturbation from addition of CO-linked LRT (biomass burning/anthropogenic) input, 3) parameterize submicron OA flux to the ML in low-productivity waters using MODIS Chl a and wind speed,

4) increase the importance of multi-phase chemistry in aerosol-gas interactions and processes, 5) diminish the use of large sea salt particles as absorbers of SO_2.

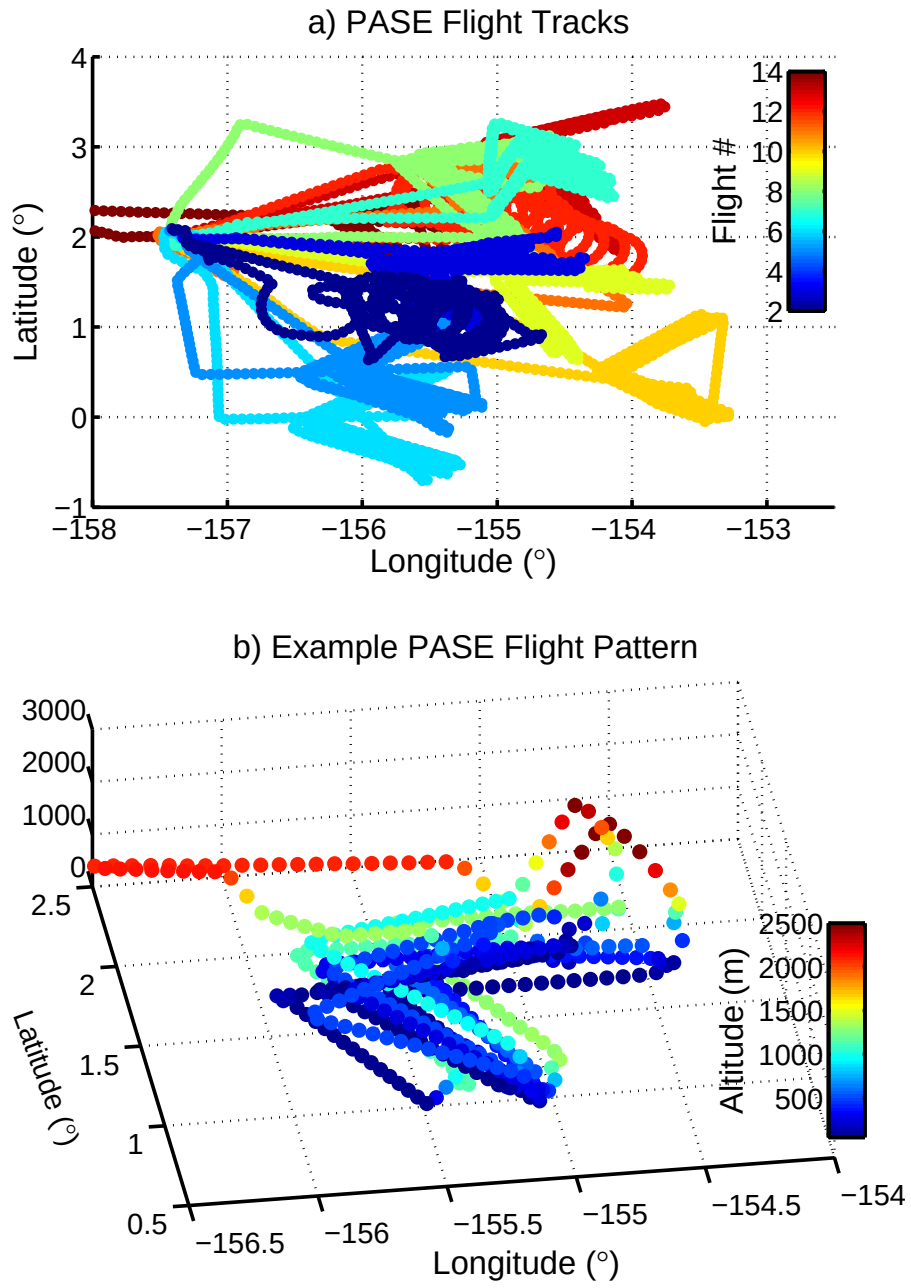

Figure 1.1: PASE research flight tracks and example flight pattern from Research Flight 03.

dimethylsulfide	DMS	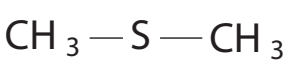
dimethyl sulfoxide	DMSO	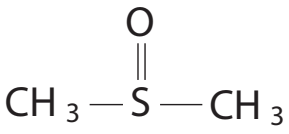
dimethyl sulfone	DMSO2	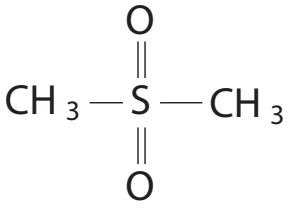
methanesulfinic acid	MSIA	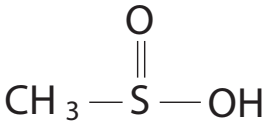
methanesulfonic acid	MSA	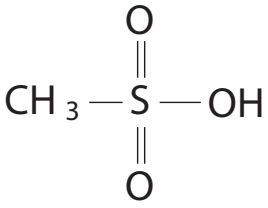
sulfuric acid	H_2SO_4	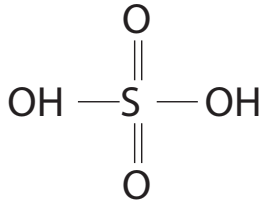
sulfur dioxide	SO_2	

Table 1.1: Organic Sulfur Compounds of the Marine Atmosphere with Chemical Formulas.

References

Bandy, A. R., D. C. Thornton, F. H. Tu, B. W. Blomquist, W. Nadler, G. M. Mitchell, and D. H. Lenschow (2002), Determination of the vertical flux of dimethyl sulfide by eddy correlation and atmospheric pressure ionization mass spectrometry (APIMS), *J. Geophys. Res.*, *107*, doi:10.1029/2002JD002472.

Bony, S., and J.-L. Dufresne (2005), Marine boundary layer clouds at the heart of tropical cloud feedback uncertainties in climate models, *Geophys. Res. Lett.*, *32*(20).

Carslaw, K., O. Boucher, D. Spracklen, G. Mann, J. Rae, S. Woodward, and M. Kulmala (2010), A review of natural aerosol interactions and feedbacks within the Earth system, *Atmos. Chem. Phys.*, *10*(4), 1701–1737.

Charlson, R. J., J. E. Lovelock, M. O. Andreae, and S. G. Warren (1987), Oceanic phytoplankton, atmospheric sulphur, cloud albedo and climate, *Nature*, *326*(6114), 655–661.

Clarke, A., F. Eisele, V. Kapustin, K. Moore, D. Tanner, L. Mauldin, M. Litchy, B. Lienert, M. Carroll, and G. Albercook (1999), Nucleation in the equatorial free troposphere: Favorable environments during PEM-Tropics, *J. Geophys. Res.*, *104*(D5), 5735–5744.

Clarke, A., S. Freitag, R. Simpson, J. Hudson, S. Howell, V. Brekhovskikh, T. Cam-

pos, V. Kapustin, and J. Zhou (2013), Free troposphere as a major source of CCN for the equatorial Pacific boundary layer: Long-range transport and teleconnections, *Atmos. Chem. Phys.*, *13*(15), 7511–7529.

Clarke, A. D., S. R. Owens, and J. Zhou (2006), An ultrafine sea-salt flux from breaking waves: Implications for cloud condensation nuclei in the remote marine atmosphere, *J. Geophys. Res.*, *111*(D6).

Conley, S. A., I. Faloona, G. H. Miller, B. Blomquist, D. Lenschow, and A. Bandy (2009), Closing the dimethyl sulfide budget in the tropical marine boundary layer during the Pacific Atmospheric Sulfur Experiment, *Atmos. Chem. Phys.*, *9*(22), 8745–8756.

Facchini, M. C., M. Rinaldi, S. Decesari, C. Carbone, E. Finessi, M. Mircea, S. Fuzzi, D. Ceburnis, R. Flanagan, E. D. Nilsson, et al. (2008), Primary submicron marine aerosol dominated by insoluble organic colloids and aggregates, *Geophys. Res. Lett.*, *35*(17).

Faloona, I., S. Conley, B. Blomquist, A. Clarke, V. Kapustin, S. Howell, D. Lenschow, and A. Bandy (2010), Sulfur dioxide in the tropical marine boundary layer: dry deposition and heterogeneous oxidation observed during the Pacific Atmospheric Sulfur Experiment, *J. Atmos. Chem.*, *63*(1), 13–32, doi: 10.1007/s10874-010-9155-0.

Gray, B., Y. Wang, D. Gu, A. Bandy, L. Mauldin, A. Clarke, B. Alexander, and D. Davis (2010), Sources, transport, and sinks of SO_2 over the equatorial Pacific during the Pacific Atmospheric Sulfur Experiment, *J. Atmos. Chem.*, pp. 1–27, doi:10.1007/s10874-010-9177-7.

Hamilton, D. S., L. A. Lee, K. J. Pringle, C. L. Reddington, D. V. Spracklen, and

K. S. Carslaw (2014), Occurrence of pristine aerosol environments on a polluted planet, *P Natl Acad Sci*, *111*(52), 18,466–18,471.

Hudson, J. G., S. Noble, and V. Jha (2011), On the relative role of sea salt cloud condensation nuclei (CCN), *J. Atmos. Chem.*, *68*(1), 71–88.

Huebert, B., D. Wylie, L. Zhuang, and J. Heath (1996), Production and loss of methanesulfonate and non-sea salt sulfate in the equatorial Pacific marine boundary layer, *Geophys. Res. Lett.*, *23*(7), 737–740.

Huebert, B. J., B. W. Blomquist, J. Hare, C. Fairall, J. E. Johnson, and T. S. Bates (2004), Measurement of the sea-air DMS flux and transfer velocity using eddy correlation, *Geophys. Res. Lett.*, *31*(23), L23,113.

IPCC-AR5 (2013), *Climate Change 2013: The Physical Science Basis. Contribution of Working Group I to the Fifth Assessment Report of the Intergovernmental Panel on Climate Change*, 1535 pp., Cambridge University Press, Cambridge, United Kingdom and New York, NY, USA, doi:10.1017/CBO9781107415324.

Keene, W. C., H. Maring, J. R. Maben, D. J. Kieber, A. A. Pszenny, E. E. Dahl, M. A. Izaguirre, A. J. Davis, M. S. Long, X. Zhou, et al. (2007), Chemical and physical characteristics of nascent aerosols produced by bursting bubbles at a model air-sea interface, *J. Geophys. Res.*, *112*(D21), D21,202.

Lohmann, U., and J. Feichter (2005), Global indirect aerosol effects: a review, *Atmos. Chem. Phys.*, *5*(3), 715–737.

Mahowald, N., D. S. Ward, S. Kloster, M. G. Flanner, C. L. Heald, N. G. Heavens, P. G. Hess, J.-F. Lamarque, and P. Y. Chuang (2011), Aerosol impacts on climate and biogeochemistry, *Ann. Rev. Environ. Resources*, *36*, 45–74.

Quinn, P., and T. Bates (2011), The case against climate regulation via oceanic phytoplankton sulphur emissions, *Nature*, *480*(7375), 51–56.

Sievering, H., J. Boatman, J. Galloway, W. Keene, Y. Kim, M. Luria, and J. Ray (1991), Heterogeneous sulfur conversion in sea-salt aerosol particles: the role of aerosol water content and size distribution, *Atmos. Environ. A*, *25*(8), 1479–1487.

Chapter 2

Dimethyl sulfide (DMS) may be less important than long-range transport as a source of sulfate to the remote tropical Pacific marine boundary layer

This chapter is published in the journal Journal of Geophysical Research: Atmospheres with the following complete citation: Simpson, R., Howell, S. G., Blomquist, B. W., Clarke, A. D., and Huebert, B. J. (2014). Dimethyl sulfide: Less important than long-range transport as a source of sulfate to the remote tropical Pacific marine boundary layer. *Journal of Geophysical Research: Atmospheres* 119.14 (2014): 9142-9167.

Abstract

During the Pacific Atmospheric Sulfur Experiment (PASE), dimethyl sulfide (DMS) was not the principal source of non-sea salt sulfate (NSS) mass in the remote marine boundary layer (MBL), according to an Eulerian sulfur budget based on observations of chemical concentrations from the NCAR C-130 in relatively dry, subsiding regions of the tropical Pacific. Our three (DMS, SO_2, and NSS) monthly average budgets are mutually consistent. The PASE-average DMS emission was 3.0 ± 0.5 µmol m^{-2}d^{-1} (our budget "units"). SO_2 sources include DMS + OH (1.4 ± 0.4 units, assuming 75% of reacted DMS forms SO_2) and entrainment from the free troposphere (FT) (0.8 ± 0.2 units). Clouds were the most important chemical reactors for SO_2 (-1.0 ± 0.5 units). SO_2 loss terms also include divergence (-0.9 ± 0.3 units), dry deposition (-0.5 ± 0.2 units), and OH + SO_2 (-0.22 ± 0.05 units). The total SO_2 loss balanced the SO_2 source. We assume that no SO_2 was lost to ozone oxidation on sea salt particles; we found negligible NSS on particles from 2.6 µm (the sea salt mass peak) to 10 µm diameter. Fine-particle NSS sources include in-cloud oxidation of SO_2 by H_2O_2 (1.0 ± 0.5 units), OH + SO_2 (0.19 ± 0.05 units), and entrainment (1.1 ± 0.3 units in clean conditions; twice that when continental pollution is present). NSS sources balance NSS loss to divergence. Only about 1/4 of emitted DMS becomes NSS. FT entrainment supplied 2/3 and DMS oxidation produced 1/3 of MBL NSS, rather similar source terms.

2.1 Introduction

Sulfate is a major component of marine particulate matter (*Junge*, 1963; *Clarke et al.*, 1987; *Huebert et al.*, 1998). The amount of marine sulfate virtually always exceeds that which could be derived from seawater alone, implying a source of non-sea salt sulfate (NSS) (*Bates et al.*, 1992; *Huebert et al.*, 1996; *Clegg and Toumi*,

1998). Most NSS is in particles smaller than 1 µm in diameter, in contrast to the sea-salt aerosol (SSA) mass, which is generally in a > 1 µm mode. The distinction is important because the direct (*Kiehl and Briegleb*, 1993; *Charlson et al.*, 2002) and indirect (*Charlson et al.*, 1992; *Boucher and Lohmann*, 1995) aerosol radiative forcings of climate depend on particle size.

Shaw (1983) postulated a link between marine biota and climate via the ocean-derived gas dimethyl sulfide (DMS). The "CLAW" hypothesis (*Charlson et al.*, 1987) refined his idea by including the potential impact of DMS on cloud radiative properties: the emission of DMS to the atmosphere might modify the number of cloud-condensation nuclei (CCN), thus changing the albedo of clouds and the radiation budget of the Earth. Essential to the functioning of this potentially negative feedback mechanism is the control of CCN number by DMS oxidation. The chemical and physical linkages between DMS, SO_2, and NSS are therefore critical for evaluating the DMS-emission-to-NSS-mass portion of the CLAW hypothesis.

The hypothesis that DMS controls CCN and cloud droplet number concentrations has largely been refuted by *Quinn and Bates* (2011). Nonetheless, the provenance of NSS mass in the remote marine boundary layer remains an interesting question, which we address here. How much NSS derives from DMS and how much from continental emissions?

The oxidation of DMS to SO_2 can occur by a variety of pathways, but OH attack is the most common (*Davis et al.*, 1999; *Yang et al.*, 2009). OH either adds to the S atom or abstracts an H atom. Gamma (γ), the moles of SO_2 formed per mole of DMS oxidized, directly controls the supply of SO_2 from DMS yet cannot be reliably modeled (*Gray et al.*, 2010). Most of the studies cited in *Faloona* (2009) are large-scale (often global) models where the reported γ is that value which yields the best agreement between a model and some set of concentration measurements. *Gray et al.* (2010) put forward an argument that γ is likely to be around 0.73, (0.75 in the tropics) based on laboratory kinetic data. The abstraction:addition ratio for

OH reacting with DMS under tropical MBL conditions implies a γ of about 0.75. We will use 0.75 for γ. In fact, the choice of γ has little impact on our conclusions.

It is worth noting that *Faloona et al.* (2010) define γ differently, as the *total* SO_2 source divided by the DMS loss rate. A non-DMS source of SO_2 (such as entrainment) could therefore elevate their γ above 1.0.

A molecule of SO_2 has four possible fates. The three reactions and one deposition are:

$$SO_2 + OH \xrightarrow{+O_2+H_2O} H_2SO_{4(v)} + HO_2 \tag{2.1}$$

$$SO_2 + H_2O_2 \xrightarrow{\text{cloud}} H_2SO_4 \tag{2.2}$$

$$SO_2 + O_3 \xrightarrow[\text{SSA}]{+H_2O} H_2SO_4 + O_2 \tag{2.3}$$

$$J_{0\,\mathrm{S}} = V_{d\mathrm{SO}_2}[SO_2] \tag{2.4}$$

Where $J_{0\,\mathrm{S}}$ is the dry flux of SO_2 to the surface (z_0), and $V_{d\mathrm{SO}_2}$ is the dry deposition velocity. Of these loss mechanisms, only Eqn 2.1 can increase total particle number or CCN number (*Clarke et al.*, 1998; *Weber et al.*, 1999). Aqueous-phase pathways (Eqns 2.2 & 2.3) reduce the gas-phase SO_2 concentration and therefore the potential for new particle formation. However, freshly nucleated particles must still grow and coalesce to become effective as CCN. It is possible that materials such as continental soot or primary marine organics from sea-spray (*Clarke and Kapustin*, 2002; *Quinn and Bates*, 2011) control the initial nuclei number, rather than the condensation of H_2SO_4 vapor from OH oxidation. DMS could still play a role in growing those nuclei to the CCN size range.

Aqueous-phase oxidation of SO_2 to SO_4^{2-} by H_2O_2 (Eqn 2.2) in cloud droplets has been postulated to be the most important pathway for conversion of SO_2 to NSS (*Hegg*, 1985; *Pandis and Seinfeld*, 1989; *Chin et al.*, 2000), though this is debated by some who argue that SSA dominates the production (Eqn 2.3) and

removal of NSS (*Sievering et al.*, 1991; *Chameides and Stelson*, 1992; *Faloona et al.*, 2010).

In cloudwater typical of marine conditions with a pH $\leq$ 5 (*Lenschow et al.*, 1988; *Heath and Huebert*, 1999; *Yang et al.*, 2011), H_2O_2 is the dominant oxidant (Equation 2.2), since its reaction with SO_2 is pH-independent (*Penkett et al.*, 1979). Oxidation of SO_2 by O_3 (Equation 2.3) is only important at pH $>$ 6, making alkaline SSA particles an ideal reaction medium. Although alkalinity is supplied by seawater (pH $\approx$ 8), production of sulfuric acid and condensation of acidic vapors (H_2SO_4, HCl, and HNO_3) may consume the alkalinity, dropping the pH and terminating the oxidation of SO_2 by O_3 (Eqn 2.3).

Many decades of effort have been expended trying to quantify sulfur sources, oxidation pathways, reaction rates, branching ratios, and transport and mixing dynamics (e.g. *Penkett et al.*, 1979; *Schwartz*, 1988; *Huebert et al.*, 1996; *Davis et al.*, 1999; *Gurciullo et al.*, 1999; *von Glasow et al.*, 2002; *Zhu et al.*, 2006) that together determine NSS and CCN production rates. Laboratory studies have been used to estimate ambient DMS and SO_2 oxidation rates and product distributions (*Niki et al.*, 1983; *Hatakeyama et al.*, 1985; *Yin et al.*, 1990; *Barone et al.*, 1996; *Turnipseed et al.*, 1996; *Ravishankara*, 1997).

It is hard, though, to constrain some ambient process rates from just lab studies and modeling: too many critical factors are highly variable in the real world. For example, the two heterogeneous SO_2 oxidation rates (Eqns 2.2 and 2.3) depend on particle size, diffusion rates to and within the condensed phase, the supply of oxidants, pH and relative humidity (RH) and their variation with altitude, and a host of other factors. Computing these process rates from the best imaginable lab studies still cannot be expected to represent ambient reaction rates with much fidelity.

Chemical process rates are intimately tied to the physical and dynamic context in which they occur. When describing the chemical environment in an air

volume, one must consider both inputs and outputs of air and chemicals from outside the volume. We define a study volume based on the three-layer conceptual model defined by *Betts* (1973) and refined by *Albrecht et al.* (1979) and *Bretherton and Park* (2008) where marine boundary layer (MBL) dynamics are simplified in regions of subsidence. This is sketched in Figure 2.1. They equate the net downward transport of FT air to the loss of MBL air through the sides of the volume by horizontal divergence. Subsidence inexorably moves air into the MBL. As shown in Figure 2.2, we divide the MBL into two layers: the Mixed Layer (ML, also denoted by subscript $_{\mathrm{M}}$) and the Buffer Layer (BuL, or cloud layer, also denoted by subscript $_{\mathrm{B}}$).

Since the height of the capping inversion (z_2) is roughly constant over a month-long period ($\sim$1250 m during the project described below), the entrainment and divergence volumes will be nearly equal (albeit $\mathrm{P}z_2 < \mathrm{P}z_0$, where P is the ambient pressure), even though this parity may not obtain from hour to hour.

The Pacific Atmospheric Sulfur Experiment (PASE) airborne field campaign sampled the remote equatorial Pacific troposphere near Christmas Island during August and September of 2007. The National Center for Atmospheric Research (NCAR) C-130 flew multiple 30-min legs at altitudes from $\sim$40 m ASL throughout the MBL and BuL with periodic profiles into the FT (*Conley et al.*, 2009). Rapid measurements of DMS and SO_2 enable us to compute SO_2 oxidation in clouds and dry deposition of SO_2 to the ocean surface. Concomitant measurements of OH, H_2SO_4, MSA, H_2O_2, O_3, H_2O vapor, CO, and dynamic and thermodynamic parameters proved valuable as well.

Our PASE data enable us to address two principal questions about remote marine sulfur chemistry:

1. What are the relative contributions of DMS and long-range transport (LRT) to NSS in the equatorial mid-Pacific MBL?

2. What fraction of DMS becomes NSS?

The first of these is the natural-vs-anthropogenic issue. In a relatively calm volcanic year, anthropogenic sources are thought to be responsible for 2/3 or more of global atmospheric sulfur (*Chin and Jacob*, 1996; *Faloona et al.*, 2010). How much of this reaches remote parts of the globe, including "clean" marine boundary layers? If particle and CCN number are controlled by biomass burning, mineral dust, or other local primary sources of aerosol number, that eliminates control by DMS (as argued by *Quinn and Bates* (2011)).

If the long-range transport (LRT) of S from continental sources were significant relative to natural DMS, that would also reduce the leverage of DMS as a principal controller of remote NSS mass. It would also suggest that the remote MBL might be amenable to some degree of management, by control of continental S sources. Since wet and dry removal limit S lifetimes in the MBL, the FT is the main conduit for LRT.

The second question addresses one of the major outstanding questions about the CLAW hypothesis: how much of the emitted DMS actually becomes NSS? Several products can be formed and deposited, depending on branching that is controlled by environmental conditions. In order to answer this question, we compute the rates of homogeneous and heterogeneous processes in the remote MBL to quantify the DMS to sulfate oxidation paths. We also estimate transport from FT to MBL.

Our goal is to produce three mutually consistent month-long budgets for DMS, SO_2, and NSS, using only measured concentrations, fluxes, chemical kinetics, and a minimum of dynamical assumptions to estimate process rates for each substance. We do this also for the most- and least-polluted FT conditions to assess the impact of LRT on MBL NSS. Our multi-week time scale is very different from the diel scale frequently used in micrometeorological studies of MBL dynamics.

It is perhaps to be expected that different authors will reach different conclusions from the same data. *Faloona et al.* (2010) and *Gray et al.* (2010) have published PASE sulfur budgets in which they reach conclusions unlike ours, having made quite different assumptions and using different approaches. *Faloona et al.* (2010) confined their SO_2 budget to the ML while *Gray et al.* (2010) created a 1-D model fit to concentration profiles. Neither study systematically evaluated all pertinent process rates as we do. We wish to stimulate discussions of which process rates are accurately known and which important ones need more theoretical work, laboratory studies, or targeted observations.

Obviously our budgets will not represent all parts of the globe. However, we will show that PASE reasonably represents much of the remote tropical Pacific.

2.2 Methods

2.2.1 Experimental

Rarely has an airborne program been equipped to quantify supermicrometer aerosol chemistry with a definable uncertainty, due the difficulty of passing large particles through inlets and tubing. During PASE, however, we measured aerosol composition versus size at a variety of altitudes with a well-characterized low-turbulence inlet (LTI), transport tubing, and measurement system. The result is a dataset well-posed to address the formation and loss of NSS on coarse sea salt aerosol.

The NSF/NCAR C-130 flew to the east of Christmas Island (Kiritimati), in the equatorial Pacific upwelling regime. Thirteen research flights were flown within 152–157°W, 0–2.5°N. One other flight was focused on a convective region to the northwest and excluded from our analysis. On a typical research flight, the aircraft flew three stacks of V-shaped legs that consisted of a low-ML leg (∼40 m above the ocean), a mid-ML leg (∼300 m), a top-ML leg (∼500 m), and a BuL leg, which

varied between 800 m and 1200 m, depending on the height of the MBL. BuL legs were usually just at or above cloud tops; cloud penetrations were common. A profile penetrating into the FT was flown between each stack. Flights were originally intended to drift with the wind in Lagrangian fashion, but obvious contamination from aircraft exhaust prompted us to move slowly upwind, resulting in nearly stationary patterns (*Conley et al.*, 2009). Flights were directed to relatively cloud-free areas, yet averaged 15% cloud cover (*Simpson*, 2010). Ambient conditions were very close to an atmospheric chemist's standard ambient temperature and pressure, SATP: 1 Atm and 298 K.

All but 2 flights were daytime flights, which generally took off at 0900 local and landed at approximately 1700. The 2 early morning flights (RF6 and RF13) that spanned sunrise took off at 0200 and landed at 1000 local time. Highly convective regions were avoided, causing a low bias in our cloud statistics. PASE observations reported in this study draw from flights 2, 3, and 5–14. We excluded portions of RF09 and RF10 due to aircraft data system failures.

An upgraded MSP Model 131 high-flow multi-orifice impactor (MOI, *Kline et al.*, 2004) allowed us to collect size-resolved ambient aerosol with a $100\,\mathrm{L\,min^{-1}}$ flow rate. The MOI had nominal 50% cut sizes of 10, 5, 1.4, 0.8, 0.44, and 0.25 µm diameter; a backup Teflon filter collected everything smaller than the stage 6 cutoff. MOI samples were analyzed at the University of Hawai'i in Mānoa by ion chromatography (IC) for: MS^- (methane sulfonate), SO_4^{2-}, Na^+, Cl^-, NO_3^-, Br^-, Ca^{2+}, $C_2O_4^{2-}$, K^+, and Mg^{2+}. Analytical procedures are described in *Simpson* (2010) and *Huebert et al.* (1998). NSS-SO_4^{2-} was calculated using the bulk seawater Na^+/ SO_4^{2-} mass ratio of 0.251. To achieve suitable sensitivity each impactor stack sampled for one 30 min constant-altitude leg. Data for each stage were plotted and analyzed at geometric means between 50% cut sizes.

A TSI Model 3321 aerodynamic particle sizer (APS) measured detailed super-micrometer physical size distributions every minute. The APS 0.8 µm to 20 µm

number distributions were converted to volume and mass distributions by assuming humidity-dependent diameters and densities for sea-salt. LTI flow modeling (*Huebert et al.*, 2004a; *Wilson et al.*, 2004) quantified the inertial enhancement of supermicrometer particle concentrations in the LTI, so that apparent concentrations of particles up to 10 µm dry were corrected to ambient concentrations. Corrected APS number distributions were then used with the LTI efficiency computations to derive correction factors (*Simpson*, 2010) for each MOI stage during every sample.

Often, a long differential mobility analyzer (LDMA) was used in tandem with the APS to produce comprehensive size distribution information at all altitudes. The LDMA provides submicrometer aerosol size distributions spanning mobility diameters of 0.01 µm to roughly 0.5 µm on a time scale of approximately 85 seconds. This combination of data was used to discern changes in ML, BuL, and FT mass distributions. To compare with MOI mass distributions, we converted APS aerodynamic and LDMA mobility diameters to geometric using a density of $2.2\,\mathrm{g\,cm^{-3}}$ for sea salt and $1.7\,\mathrm{g\,cm^{-3}}$ for NSS.

A time-of-flight aerosol mass spectrometer (AMS; *DeCarlo et al.*, 2006) was used to quantify submicrometer NSS mass in the FT. It used an inlet chamber controlled at 600 hPa, modeled after one described in *Bahreini et al.* (2003), and used a vaporizer temperature of 700°C to vaporize SO_4 as quickly as possible (at the expense of sensitivity to organic material). Nominally, the AMS submicrometer size range is ∼0.05 µm to 1 µm vacuum aerodynamic diameter (*Liu et al.*, 2007), but in practice, the range is closer to 0.03 µm to 0.6 µm, where this upper limit is not a sharp cutoff. Comparisons between the MOI and AMS in the MBL allowed us to normalize the AMS NSS measurements.

DMS and SO_2 concentrations were measured at 10 Hz using two Atmospheric Pressure Ionization Mass Spectrometers (APIMS; *Bandy et al.*, 2002). In addition to enabling eddy covariance flux measurements, the rapid APIMS response allowed

us to make detailed DMS and SO_2 altitude profiles to complement our level-leg-only MOI aerosol data. Their rapid response also enabled observations of DMS and SO_2 concentrations even during very brief cloud penetrations. For our month-long computations, the fast gas data was averaged over specific aerosol-sampling periods.

OH and H_2SO_4 vapor concentrations were measured using the method of selected ion chemical ionization mass spectrometry (SICIMS) (*Mauldin et al.*, 1998). This instrument has been adapted for aircraft platforms and is capable of making 30-second measurements.

CO was measured using a vacuum UV resonance fluorescence instrument similar to that of *Gerbig et al.* (1999). Precision is reported as ± 3 ppbv and accuracy as better than 10% for a mixing ratio of 100 ppb (*Pfister et al.*, 2010).

2.2.2 Chemical Budget Analysis

Meteorological dynamics illustrated in Figure 2.2 present a natural laboratory for in-situ studies of chemistry in the marine boundary layer. Within the hypothetical study region or grid-cell "box" below the capping trade wind inversion (TWI), a generalized chemical budget for species S may be specified as follows:

$$\frac{d\langle \mathrm{S} \rangle}{dt} = J_{0\,\mathrm{S}} + C_{\mathrm{S}} + \omega_e[\mathrm{S}]_{\mathrm{F}} - D_{\mathrm{S}} - u\frac{d\langle \mathrm{S} \rangle}{dx} \tag{2.5}$$

The left hand side of Eqn 2.5 represents the time rate of change in the column concentration from the surface to the TWI, and [S] is the density concentration ($\mu\mathrm{mol\,m^{-3}}$, standard). For convenience, the units for all budget terms employed in this study are $\mu\mathrm{mol\,m^{-2}d^{-1}}$, hereafter referred to as simply "units".

Terms on the right hand side of Eqn 2.5 are: $J_{0\,\mathrm{S}}$, the surface flux of S (deposition or emission); C_{S}, the column-integrated in-situ chemical production or loss; $\omega_e[\mathrm{S}]_{\mathrm{F}}$, the flux at the capping inversion from subsidence of free tropospheric

air; D_S, the loss of S from the sides of the "box" due to wind divergence; and $u\frac{d\langle S\rangle}{dx}$, variable advection of S into the box. We adopt the sign convention that any process adding mass of S to the MBL study volume is positive.

We evaluate the terms in Eqn 2.5 on a long-term (∼monthly: Fig 2.3) mean basis, using the entire dataset of measurements from the PASE campaign. Where possible, we independently evaluate the terms in Eqn 2.5 to establish a budget for each substance.

The exact form of the surface flux and chemical production/loss terms in (Eqn 2.5) will vary depending on the species. Specific details for these terms will be addressed in the budget discussion for each species. But, a few further general clarifications on the other terms will be presented here in the methods section.

In a 1994 Christmas Island experiment, the nighttime decrease in MBL NSS concentrations was attributed to dilution by FT air, with an entrainment velocity of 5.0 ± 2.0 mm s^{-1} (*Huebert et al.*, 1996). *Wood and Bretherton* (2004) report a similar entrainment velocity in the equatorial Pacific of 4.8 ± 1.0 mm s^{-1}. *Conley et al.* (2011) calculated a project-average entrainment rate for PASE of 6.6 ± 3.8 mm s^{-1} using the O_3 flux and (a small) concentration gradient between the BuL and ML. We will use $\omega_e = 5 \pm 2$ mm s^{-1} in our calculations as a consensus value rather than the *Conley et al.* (2011) value, which includes 5 mm s^{-1} and yet has a large uncertainty.

Entrainment of FT species into the MBL occurs by the mechanism diagrammed in Figure 2.1. With $z = 1.25$ km and $\omega_e = 5$ mm s^{-1}, over a third (35%) of the MBL is replaced by FT air each day. The rate at which a chemical is entrained is

$$J_{z_2\,S} = \omega_e[S]_F \tag{2.6}$$

We chose to use the mean of [S] from the z_2 of each flight, up to 1000 m above z_2

for computing entrainment. This is in part because of the difficulty of identifying z_2 amidst the undulating nature of convective cloud tops (which could be thought of as occasional contamination of the lowest FT with BuL air); and partly because the FT air to be entrained between this flight and the next was in the km just above z_2.

Entrainment from above is always a positive flux into the MBL, even when FT concentrations are smaller than in the MBL. (Of course, entrainment is accompanied by divergence, so the net effect is typically negative.) In this budget analysis we separate airmass subsidence or entrainment ($\omega_e[\mathrm{S}]_\mathrm{F}$) from wind divergence within the MBL, D_S. This contrasts with the usual budgetary treatment of subsidence and divergence as a net entrainment term, $\omega_e([\mathrm{S}]_\mathrm{F}$ - $[\mathrm{S}]_\mathrm{M})$. There are two reasons for this: source attribution and the vertical structure of divergence.

Note that in atmospheric literature, there are two uses for the term divergence. One use is strictly meteorological, defining divergence as the horizontal derivative of the wind field. The other use refers to losses of air volumes and is the divergence that we employ. Acknowledging that these two terms are confusing, we lay out our approach below.

Divergence losses are calculated by integrating horizontal divergence *div* through the depth of the column:

$$D_\mathrm{S} = \int_0^{z2} div(z)[\mathrm{S}](z)dz \tag{2.7}$$

As will be shown later, chemical concentrations are nearly constant in the mixed layer from the surface to z_1 and then decrease approximately linearly to the FT value at z_2. A review of divergence data from the ECMWF reanalysis in the PASE area averaged over August and September 2007 shows a similar pattern, with *div* near zero at the TWI, gradually increasing to a roughly constant value in the ML. Given this pattern and defining $\mathrm{S_F}$ and $\mathrm{S_M}$ as the FT and ML concentrations of S

and D_{M} as ML horizontal divergence, Eqn 2.7 can be integrated to produce

$$D_{\mathrm{S}} = D_{\mathrm{M}}\mathrm{S}_{\mathrm{M}}z_1 + \frac{1}{6}D_{\mathrm{M}}(\mathrm{S}_{\mathrm{F}} + 2\mathrm{S}_{\mathrm{M}})(z_2 - z_1) \tag{2.8}$$

D_{M} can be determined by observing that ω_e is just the integral of *div* over the column, yielding $D_{\mathrm{M}} = 2\omega_e/(z_1 + z_2)$ for the divergence profile we are using. Substituting D_{M} into Eqn 2.8 and simplifying, we get

$$D_{\mathrm{S}} = \frac{2\omega_e\mathrm{S}_{\mathrm{M}}}{z_2 + z_1}\left[z_1 + \left(\frac{1}{3} + \frac{1}{6}\frac{\mathrm{S}_{\mathrm{F}}}{\mathrm{S}_{\mathrm{M}}}\right)(z_2 - z_1)\right] \tag{2.9}$$

The full derivation of Eqn 2.9 appears in the appendix.

The additional benefit of separating the entrainment and divergence terms in (Eqn 2.5) is that source attribution becomes more straightforward. Marine versus continental source attribution depends on comparing the S derived from DMS with S that actually entrained across the TWI from FT to MBL. Note that divergence removes material from our study volume, but it is not a "sink" in the sense of ultimate removal of that S from the atmosphere. Ours is an Eulerian model.

Over a month-long average the advection term in Equation 2.5 is negligible. There were day-to-day changes in all species, but the overall trend was small. From a nearly Lagrangian perspective, *Conley et al.* (2009) concluded that "on average, advection contributes nothing to the DMS budget." Advection will be neglected henceforth.

The form of our model has a few somewhat nonintuitive consequences in addition to the always positive contribution from the FT mentioned above. Due to subsidence and consequent horizontal divergence, the amount of air leaving our box horizontally exceeds that entering. This is expressed as either increased wind speed, a broadening of the trade wind region downwind, or higher z_2 at the exit of the box, or some combination. Similarly, if the terms in Eqn 2.5 balance, yielding

$d\langle S\rangle/dt = 0$, the concentration of S advecting from the box equals that entering, but the flux of S is higher–there is a net addition to the MBL, but it matches the divergence, so concentrations are constant. Another way to think about this is that divergence removes S from the box, but not from the atmosphere, so flux must go up even if concentrations remain constant.

What use is there for a month-long MBL sulfur process framework? It is not well posed for evaluating aerosol lifetimes, for example, since divergence will at times remove aerosols from our study volume faster than deposition can. To be frank, no set of observations has done very well at constraining aerosol lifetimes. But it is useful for evaluating the import of dynamics and chemistry in controlling concentrations. It is also very similar to the formulation one would use for computing concentration changes in and export from a grid cell in a chemical transport model.

Finally, the reader will note that while measured concentrations are in molar mixing ratio units (pptv), the budget is specified in density units ($\mu\text{mol}\,\text{m}^{-3}$), integrated through the depth of the air column to become $\mu\text{mol}\,\text{m}^{-2}\text{d}^{-1}$. P and T variability through the MBL will cause airmass volume to vary, but to a degree (10% or less) that will cause little impact on our conclusions. We convert $\mu\text{mol}\,\text{m}^{-2}\text{d}^{-1}$ to pptv d^{-1} by dividing by z_2 and using $1\,\text{mole gas} = 0.0245\,\text{m}^3$ at the mean ($z_2/2$) T and P.

Process uncertainties have been derived by propagating uncertainties in concentrations and rate constants. We derived concentration uncertainties from the analytical uncertainty for each substance and the Standard Error of the Mean (SEM) of its concentration (both in Table 2.1). We use the SEM because we are concerned with the correctness of mean concentrations. These concentration uncertainties are combined as roots of sums of squares, then propagated similarly with entrainment velocities, divergence rates, chemical reaction rate constants, or other variables to produce the uncertainties shown after each process rate.

2.3 Results

The MOI collected a detailed chemical size distribution for aerosols on every level flight leg. Project-average size distributions for NSS, MS^-, NO_3^-, and Na^+ are illustrated in Figure 2.4. Multi-stage size-dependent major ion chemistry has rarely if ever been measured at altitude in the MBL. Both short sampling times and aerosol inlets make coarse-particle sampling more troublesome from aircraft than from ships (*Huebert et al.*, 1990; *Baumgardner and Huebert*, 1993; *Howell and Huebert*, 1998; *Blomquist et al.*, 2001; *Huebert et al.*, 2004a; *Wilson et al.*, 2004). We corrected the material on each MOI stage for inlet efficiency (*Simpson*, 2010). Of course, intensive variables (such as ion ratios on each stage; $[SO_4^{2-}]$ / $[Na^+]$) are unaffected by inlet enhancement.

Three of these four ions have their mass peaks in the coarse mode, between 2 µm and 3 µm (Figure 2.4). NSS is the exception, decreasing from its peak on the backup filter to nothing on the largest two stages. NSS resides almost entirely in the accumulation mode (Table 2.1). Photochemically produced nitric acid is taken up by sea salt particles, putting nearly all nitrate on the coarse mode. MS^- is typically bi-modal in the marine atmosphere. MSA has a low vapor pressure and is a reasonably strong acid but not as strong as H_2SO_4, meaning MSA can be driven to the less acidic environment of the coarse SSA mode.

It is important to note that we excluded RF06 from the average in Fig 2.4. This flight alone showed evidence of dust entraining from the FT and had elevated coarse SO_4^{2-} and Ca^+ typical of dust. Since this SO_4^{2-} was clearly not locally derived NSS, we decided that including it in Fig 2.4 would misrepresent the discussion of DMS-SO_2-NSS photochemistry.

The shaded area in Figure 2.4 is the project-average single-particle volume distribution, measured by the APS and LDMA. Not surprisingly, chemical peaks of Na^+, NO_3^-, and MS^- all coincide with the physical volume (sea salt) peak. Although

there are too few submicrometer stages to define the NSS peak diameter, it is well below 0.4 µm.

The concentration of NSS (sum of all MOI stages) did not change dramatically (>50% from the mean) throughout the program (Figure 2.3). While the lowest concentrations were BuL samples (due to the entrainment of lower-concentration FT air), there were (polluted) flights late in the program in which the smallest NSS concentration was in the ML.

The DMS and SO_2 instruments could measure concentrations during soundings into the FT between flight stacks (Figure 2.5). Since one of our objectives is to quantify the impact of distant sources on remote MBL sulfur chemistry, we stratified all our DMS and SO_2 data by simultaneous CO concentration. The CO frequency distribution (shown in *Clarke et al.* (2013)) exhibits two modes, with an antimode around 63 ppbv. Accordingly, we have colored DMS and SO_2 values red (CO > 63 ppbv) and blue (cleaner, CO < 63 ppbv) (Fig 2.5). When each is averaged into 200 m altitude blocks, the mean of DMS is higher in the more polluted samples. This relationship between CO and DMS is surprising, as DMS is not a combustion product. In contrast, SO_2 is apparently affected little by [CO], even though it is typically associated with pollution. We shall explore this in a later paper.

Fig 2.5a demonstrates that the Mixed Layer (ML, lower 550 m) is vertically mixed far better than the BuL. The bottom of the BuL resembles ML air, while at the top it resembles the FT. Flight average profiles from flights RF03 and RF11 (Figure 2.6) demonstrate the difference between layers in cleaner and more polluted flights. In both flights the ML is relatively well mixed (less so for sulfur gases in RF03). Keep in mind that during a sounding, the aircraft is moving 30 or more times as fast horizontally as vertically, as if climbing a ramp. Some of the apparent noise in profiles is no doubt due to mesoscale horizontal concentration inhomogeneities encountered during the sounding maneuvers. Those inhomogeneities are

largely averaged out in the project-average binned profiles of Figure 2.5.

CO, which is mostly produced in combustion, is relatively low (< 63 ppbv) in RF03, but considerably higher (64–85 ppbv) in RF11. The 1700 m [CO] peak in RF11 suggests that a continental pollution plume in the FT was impacting the MBL. Substantially elevated values of SO_2 support the idea that long-range pollution transport influenced the sulfur budget during this flight.

CO does have a local sea surface source in the tropical MBL (*Blomquist et al.*, 2012). *Bates et al.* (1993) data for springtime at 10° S – 15° N suggest a typical CO surface emission flux of 4 µmol $m^{-2}d^{-1}$. This is dwarfed by the entrainment of FT CO: Assuming ω_e = 5 mm s^{-1} at 900 mb (90 000 Pa), T = 281 K, and $[CO]_F$ = 80 ppbv, the downward flux of CO through the inversion is 1300 µmol $m^{-2}d^{-1}$, 300× the CO surface emission flux. Variability in the entrainment flux is much more likely to drive variability in CO than is variability in surface flux.

The MOI-derived NSS altitude profile (Figure 2.7) shows the similarity between ML (<550 m) and BuL (∼550 m to 1250 m) concentrations of NSS. We had a paucity of data in the FT, so to increase the amount of FT information, we have added data from the AMS, normalized to MBL MOI concentrations. Figure 2.7 also contains NSS inferred from the PASE project-average particle volume in the FT. (Only 2 level FT flight legs were flown in PASE, and one had MOI contamination.) $[NSS]_F$ is about a third of $[NSS]_{MBL}$.

Even though PASE sampled only during the day, we assumed the diel cycles had the same shape as the 24-hour observations from a previous experiment. Figure 2.8 illustrates the mean diel cycles measured during our tower-based around-the-clock sampling at Christmas Island (Kiribati) in 1994 (*Huebert et al.*, 1996; *Bandy et al.*, 1996). The daytime project-average concentrations of DMS, SO_2, and NSS are shown in Figure 2.9. Each of these concentrations results from averaging to the exposure time of an MOI sample, classifying by CO concentration, averaging over layer altitudes, normalizing to a daytime average using Figure 2.8, and averaging

over the project.

Each budget term was computed using the concentrations as depicted in Figure 2.9. In a 1.25 km MBL, 1 µmol $m^{-2}d^{-1}$ of S = 1 unit $\approx$ 19 pptv d^{-1}.

2.3.1 DMS Processes and Budget

The DMS budget in the MBL is relatively simple (Eqn 2.10). It includes five terms, the sum of which would equal zero if [DMS] were at steady-state over a month's time.

$$\begin{aligned} z_2 \frac{d[\mathrm{DMS}]_{\mathrm{MBL}}}{dt} = & \\ & J_{0\,\mathrm{D}} \text{ (a)} \\ -z_1 k_{\mathrm{D}} [\mathrm{OH}]_{\mathrm{M}} [\mathrm{DMS}]_{\mathrm{M}} - (z_2 - z_1) k_{\mathrm{D}} [\mathrm{OH}]_{\mathrm{B}} [\mathrm{DMS}]_{\mathrm{B}} & \text{ (b)} \\ & +\omega_e [\mathrm{DMS}]_{\mathrm{F}} - D_{\mathrm{D}} \text{ (c)} \end{aligned} \tag{2.10}$$

Just two terms are positive (sources), and one of those (entrainment: $\omega_e[\mathrm{DMS}]_{\mathrm{F}}$ or $J_{z_2\,\mathrm{D}}$ as in Eqn 3.1) is insignificant. There is virtually no DMS in the lower FT to entrain (*Lenschow et al.*, 1988; *Faloona et al.*, 2005; *Conley et al.*, 2009). That leaves surface emission of DMS, $J_{0\,\mathrm{D}}$, as the sole source of DMS to the MBL. There are two types of negative terms (losses): oxidation by OH and divergence (second term of 2.10c; see Eqn 2.9) out the sides of the box.

We averaged the eddy-covariance (EC) DMS emission flux for all flights reported in Table 2 of *Conley et al.* (2009) for the $J_{0\,\mathrm{D}}$ term, which is 3.0 ± 0.5 units (Table 2.2). This is slightly below their reported 3.1 ± 1.5, which included a correction for diel changes that were noted though poorly defined due to the lack of night flights. Because the average and standard deviation reported by *Conley et al.* (2009) over-represent two flights with only a few pre-dawn hours of data, we

instead report an evenly weighted project average and standard error of the mean, which is the more appropriate statistic. At the standard error of the mean, the uncertainty of the $J_{0\,\mathrm{D}}$ term is about 20%.

Loss to OH (2.10b) can be calculated with a relatively high degree of confidence. We computed DMS oxidation (2.10b) from all PASE simultaneous 10-second DMS and OH concentrations and the well-known reaction rate constant (k_{D}) at 298 K (6.7×10^{-12} cm^{3}molecule^{-1}s^{-1}; *Sander et al.* (2006)). These rates have been plotted against time of day (TOD) in Figure 2.10. Numerous lab, field, and theoretical studies of OH attack on DMS have ensured that this reaction rate constant is very well known. The considerable uncertainty in the DMS-OH product distribution contributes no uncertainty to our DMS loss rates. DMS loss to OH was -1.5 ± 0.5 units in the ML and -0.4 ± 0.1 units in the BuL. *Conley et al.* (2009) found good agreement between flux divergence-inferred photochemical losses and calculated loss to OH, so concluded that no other oxidants needed to be considered.

To adjust our 8 hr measurements to a 24 hr cycle, we correct our data using the tower-derived DMS diurnal cycle from the 1994 Christmas Island experiment (Figure 2.8) as a guide to compute the ratio of 24 hr average [DMS] / $[\mathrm{DMS}]_{\mathrm{avg}}$ for the times of day we flew. Details of these calculations can be found in *Simpson* (2010). Average nighttime DMS concentrations inferred from the shape of the 1994 data allowed us to calculate the nocturnal portion of the DMS divergence term.

Propagating the uncertainty using the SEM of DMS (7%) and OH (12%) and assuming a maximum uncertainty of 15% in the DMS-OH rate constant, the total uncertainty for loss to OH is $\pm$ 20%. We conservatively round up to 25% uncertainty. A total of -1.9 ± 0.5 units of DMS were lost to OH attack. Total divergence losses of DMS were -0.8 ± 0.2 units, 30% of the total loss. Photochemical oxidation by OH removed 70% of DMS.

DMS Budget Summary

Since the DMS budget imbalance of 0.3 ± 0.7 units (Table 2.2) is smaller than its uncertainty, we conclude that DMS is effectively in steady state.

2.3.2 SO_2 Processes and Budget

The SO_2 budget in the MBL is considerably more complicated (Eqn 2.11). Entrainment, surface loss, and aqueous-phase chemistry all play significant roles.

$$
\begin{aligned}
z_2 \frac{d[\mathrm{SO_2}]_{\mathrm{MBL}}}{dt} = & \\
z_1 \gamma k_{\mathrm{D}} [\mathrm{OH}]_{\mathrm{M}} [\mathrm{DMS}]_{\mathrm{M}} + (z_2 - z_1) \gamma k_{\mathrm{D}} [\mathrm{OH}]_{\mathrm{B}} [\mathrm{DMS}]_{\mathrm{B}} & \text{ (a)} \\
-z_1 k_S [\mathrm{OH}]_{\mathrm{M}} [\mathrm{SO_2}]_{\mathrm{M}} - (z_2 - z_1) k_{\mathrm{S}} [\mathrm{OH}]_{\mathrm{B}} [\mathrm{SO_2}]_{\mathrm{B}} & \text{ (b)} \\
+\omega_e [\mathrm{SO_2}]_{\mathrm{F}} - D_{\mathrm{S}} & \text{ (c)} \\
-J_{0\,\mathrm{S}} - R_{\mathrm{M\,S\,O_3}} & \text{ (d)} \\
-C_{\mathrm{M}} \xi [\mathrm{SO_2}]_{\mathrm{M}} - C_{\mathrm{B}} \xi [\mathrm{SO_2}]_{\mathrm{B}} & \text{ (e)}
\end{aligned}
\tag{2.11}
$$

Where $R_{\mathrm{M\,S\,O_3}}$ is the oxidation of SO_2 by O_3 (Eqn 2.3) in hydrated SSA particles in the ML, C is the flux of SO_2 into cloud, and ξ is the conversion efficiency of SO_2 to NSS in cloud.

SO_2 Sources (Eqn 2.11a,c)

The primary photochemical source of SO_2 is DMS oxidation (Eqn 2.11a), which contributes an average of 1.4 ± 0.4 sulfur process units (all during the daytime). Some of the photochemical uncertainty is from uncertainty in γ. Entrainment (2.11c) contributes another 0.8 ± 0.2 units of SO_2 input, for a total SO_2 source of 2.2 ± 0.4 units. While the FT is a significant SO_2 source, DMS contributes 2/3 of total SO_2. Under more polluted conditions, both entrainment and the chemical

production of SO_2 from DMS increase by about 20%. Note that FT SO_2 from LRT may include volcanic and anthropogenic sources.

Homogeneous SO_2 Oxidation (Eqn 2.11b)

The rate of homogeneous oxidation of SO_2 by OH, computed directly from measurements versus TOD (Figure 2.10b) using $k_S = 8.5 \times 10^{-13}\,cm^3$ molecule^{-1} s^{-1} (*Sander et al.*, 2006), was 0.22 ± 0.05 units. Thus, OH reaction only removes 10% of the total SO_2 source of 2.2 ± 0.4 units. Another 40% of SO_2 diverges from the sides of the box.

Heterogeneous SO_2 Oxidation by H_2O_2 in Cloud Droplets (Eqn 2.11e)

Trade-wind cumulus clouds in the lower BuL draw ML air upward. As CCN activate during cloud formation, aqueous chemistry can occur in cloud droplets. Some fraction (ξ) of the entering SO_2 will be oxidized to NSS by H_2O_2, so that upon evaporation the residual CCN will have grown larger and more easily activated. Mixing of this wet air with drier air from the FT will evaporate the cloud, cooling the mixture and driving its (aerially broader and slower) descent back into the ML.

In-cloud aqueous-phase oxidation of SO_2 by H_2O_2 to NSS might be the primary pathway by which SO_2 is oxidized to H_2SO_4. It is challenging to measure the ambient oxidation rate, however: aircraft penetrations of trade-wind cumulus clouds last at most a few seconds and most instruments can't respond quickly enough to measure much detail during a cloud penetration. Fortunately, PASE's APIMS measurements (> 1 Hz for [DMS] and [SO_2]) overcame the latter obstacle. At $\sim$1 ppbv, [H_2O_2] was always much larger than [SO_2] so was not the limiting factor in the reaction. Peroxides were measured during PASE by the Heikes group from URI (*Bandy et al.*, 2012).

During PASE, the initial intent was to avoid clouds entirely by flying BuL legs

just above cloud tops, but well below the TWI. That proved impractical, as cloud top heights changed rapidly. The net result was that we frequently flew through cloud tops. While in cloud [DMS] typically spiked, indicating ML influence, $[SO_2]$ decreased significantly, revealing in-cloud losses (Figure 2.11).

Since DMS is not lost in cloud, and average $[DMS]_M$ and $[DMS]_B$ are known, relative contributions to in-cloud air from each layer can be calculated. Once we have determined the fraction of ML air (F_M) in each cloud pass,

$$F_M = \frac{[DMS]_{Cloud} - [DMS]_B}{[DMS]_M - [DMS]_B} \tag{2.12}$$

we can solve for the loss of SO_2 in that pass:

$$\Delta[SO_2] = [SO_2]_M F_M + [SO_2]_B(1 - F_M) - [SO_2]_{Cloud} \tag{2.13}$$

If DMS mixing predicts, for example, twice as much SO_2 as we observed, then 50% of the incoming ML + BuL SO_2 must have been oxidized to NSS by cloud processing. Table 2.3 shows a selection of these calculations from various research flights.

On average, the ML contributed $35\% \pm 4\%$ (SEM, range 20% to 58%) of the air (F_M) during periods in cloud. In-cloud $[SO_2]$ should reflect the same mixture of ML and BuL air, reduced by in-cloud SO_2 oxidation. Concentrations averaged about 26% lower than mixing alone would generate. We adopt 26% as the cloud conversion efficiency ξ. As a crude parameterization of the SO_2 oxidation rate in cloud, we multiply the flux C of SO_2 into cloud by ξ (Equation 2.11e).

We have a simple approach to determining the flux of air into cloud. Since flights were during the day near the Equator and fairly close to the solstice, the sun was often nearly at zenith. Therefore, the sun was only obscured when clouds were directly overhead. Sudden drops in downwelling UV prove to be a clear

indicator of cloud (Figure 2.12). (Alternatively, we could have used MODIS cloud fraction, but *Zhao and Di Girolamo* (2006) demonstrated large overestimates when applied to trade wind cumuli.) As might be expected when BuL clouds are rooted in the ML, updrafts were stronger under cloud. Averaging across midday legs throughout PASE, the ML was under cloud 15% of the time. Vertical wind speed ω under cloud averaged $0.092\,\mathrm{m\,s^{-1}}$ during the daytime and $0.071\,\mathrm{m\,s^{-1}}$ during the nighttime, assuming that the nighttime average can be represented by the average of the earliest and latest daytime measurements. The product yields an effective exchange velocity of air from the ML into cloud $C_\mathrm{M} = 0.012\,\mathrm{m\,s^{-1}}$, which can be multiplied by $[\mathrm{SO_2}]_\mathrm{M}$ to give a flux of ML $\mathrm{SO_2}$ into cloud (the first term of Equation 2.11e).

Since clouds were 65% BuL air, $1.9C_\mathrm{M} \approx C_\mathrm{B}$, so 1.9 times as much BuL air entered cloud, yielding a total $\mathrm{SO_2}$ flux into cloud of $0.019([\mathrm{SO_2}]_\mathrm{M} + 1.9[\mathrm{SO_2}]_\mathrm{B})$.

Total in-cloud $\mathrm{SO_2}$ oxidation loss was -1.0 ± 0.5 units, about half of the 2.2 ± 0.4 unit $\mathrm{SO_2}$ source. We will revisit these numbers below.

In the clean MBL, in-cloud oxidation by peroxide represents both the largest chemical $\mathrm{SO_2}$ loss pathway and the largest local NSS formation pathway, 1.0 ± 0.5 units. The rate of cloud processing of $\mathrm{SO_2}$ is comparable to the 0.9 ± 0.3 unit loss of $\mathrm{SO_2}$ to divergence (second term of 2.11c; see Eqn 2.9).

$\mathrm{SO_2}$ Surface Deposition (Eqn 2.11d, First Term)

The predominant deposition mechanisms for gases and particles in the remote MBL are precipitation scavenging and dry deposition. $\mathrm{SO_2}$ is rapidly removed from the MBL by dry deposition upon contact with the alkaline ocean.

The rate of dry removal is controlled by turbulent transport, diffusion, solubility, and concentration. One could estimate $\mathrm{SO_2}$ dry deposition using Hicks' resistance method (*Hicks et al.*, 1987), but we elect to use direct PASE eddy flux measurements of $\mathrm{SO_2}$ dry deposition (*Faloona et al.*, 2010), except that we adjusted

the original value ($-.75 \pm 0.33$ units) to account for lower nighttime [SO_2]. Using their observed project-mean SO_2 dry deposition velocity (V_{dSO_2}) of $0.4\,\mathrm{cm\,s^{-1}}$, we calculated $J_{0\,S}$ as -0.5 ± 0.2 units.

SO_2 Oxidation by O_3 in Sea Salt (Eqn 2.11d, Second Term)

We choose not to focus on this complex topic, but leave SO_2 oxidation on sea salt as an unknown. Since we found coarse NSS to be at or near the minimum detection limit throughout the program (Figure 2.4), we assume here that little or no ozone oxidation was occurring. The one time we observed coarse NSS (RF06), it had clearly arrived by LRT with dust.

SO_2 Budget Summary

This SO_2 budget (Table 2.4) is in balance, within the uncertainty of its terms: -0.4 ± 0.8 SO_2 units, so SO_2 is effectively in steady state.

It is useful to think about the sensitivity of this imbalance to uncertainties in the terms from which it is derived. Increasing γ to 0.85 would increase the SO_2 source by 0.2 units, decreasing the imbalance to -0.2. Raising the assumed ω_e to $7\,\mathrm{mm\,s^{-1}}$ could add another 0.2 source units, again reducing the imbalance. The uncertainty of the SO_2 budget, however, prevents us from arguing for either of those changes. As noted above, *Faloona et al.* (2010) found $\gamma \approx 1$, but defined it as the ratio of total SO_2 source to DMS + OH. Using that definition, we would get $\gamma = 1.2$ due to entrainment from the FT (see Fig 2.13), but this is not directly comparable to *Faloona et al.* (2010), whose budget was for the ML only.

As it happens, most of the SO_2 sink terms could not be much smaller. Oxidation by OH is well constrained. The EC-measured dry deposition flux is already smaller than resistance models predict, although its uncertainty is large. The least well-constrained term is in-cloud oxidation. Dropping ξ, the in-cloud SO_2 conver-

sion efficiency, from 0.26 to 0.20 would reduce the in-cloud loss term by 0.2 units, a 22% change. It is also possible our cloud penetrations were not sufficiently representative of entire clouds. With so many possible sources of error, it is reassuring to find the SO_2 budget in balance within its uncertainties (Table 2.4).

This budget analysis provides no support for a significant SO_2 loss to sea salt. Budget analyses are not well posed to constrain SO_2 oxidation on coarse particles, although ours suggests it should be a small number. This is in contrast to the conclusion of *Faloona et al.* (2010), who assert that the "overwhelming majority" of their 1.6 ± 1.0 µmol m^{-2} d^{-1} SO_2 budget imbalance was oxidation by O_3 on sea salt. It is also hard to reconcile that assertion with the measured NSS size distribution in Figure 2.4.

2.3.3 NSS Aerosol Processes and Budget

The chemical sources of NSS include the three SO_2 oxidation mechanisms (Eqns 2.1 – 2.3). To this is added a significant flux of NSS aerosol from the FT. Divergence and deposition are the loss processes. Wet and dry aerosol deposition are extremely hard to constrain observationally. *Lewis and Schwartz* (2004) wisely warn that there are few or no observations supporting steady-state assumptions about coarse NSS sources and losses.

$$
\begin{aligned}
z_2 \frac{d[\mathrm{NSS}]_{\mathrm{MBL}}}{dt} = & \\
z_1 k_{\mathrm{S}} [\mathrm{OH}]_{\mathrm{M}} [\mathrm{SO_2}]_{\mathrm{M}} + (z_2 - z_1) k_{\mathrm{S}} [\mathrm{OH}]_{\mathrm{B}} [\mathrm{SO_2}]_{\mathrm{B}} & \text{ (a)} \\
+ C_{\mathrm{M}} \xi [\mathrm{SO_2}]_{\mathrm{M}} + C_{\mathrm{B}} \xi [\mathrm{SO_2}]_{\mathrm{B}} & \text{ (b)} \\
+ R_{\mathrm{M\,SO_3}} - J_{0\,\mathrm{N}} & \text{ (c)} \\
+ \omega_e [\mathrm{NSS}]_{\mathrm{F}} - D_{\mathrm{N}} & \text{ (d)}
\end{aligned}
\tag{2.14}
$$

NSS Sources (Eqn 2.14a, b, and First Term of c)

Most NSS sources have already been discussed. Homogeneous oxidation of SO_2 by OH produces 0.22 ± 0.05 NSS units, some of which condenses on the sea salt mode. This H_2SO_4 vapor source can be compared with its sink to existing aerosol: we have direct measurements of $[H_2SO_4]_{(v)}$, so that concentration, measured aerosol size distributions, and kinetic molecular theory can be used to compute the vapor loss rate. The two should agree. We used gas-phase $[H_2SO_4]_{(v)}$ measured by selected ion chemical ionization mass spectrometry (SICIMS; *Mauldin et al.* (1998)), and assumed steady state and that the only sink for $[H_2SO_4]_{(v)}$ was removal to the surface of aerosol. Derived sulfuric acid vapor condensation was 0.19 ± 0.05 budget units.

For particles with diameter d_p much larger than the mean free path of air molecules λ_{air}, vapors deposit to particles according to a formula derived by *Maxwell* (1888):

$$J = 2\pi d_p D_v (c_\infty - c_s) \tag{2.15}$$

where J is the flux, D_v is diffusivity of the vapor, and c_∞ and c_s are concentrations far from and at the surface of the particle. Note that Maxwell's formulation uses d_p to the first power, thus condensing a considerably smaller fraction of $H_2SO_{4(v)}$ onto coarse particles than if surface area ($\propto {d_p}^2$) were the relevant parameter. At 302 K and 975 hPa (typical of the PASE ML) $\lambda_{air} = 0.067\,\mu m$, so Eqn 2.15 strictly applies only to particles $\geq 0.2\,\mu m$ (*Seinfeld and Pandis*, 2006). Smaller particles cannot set up a diffusion gradient so they collect vapors even more efficiently, causing Eqn 2.15 to under-estimate the share of deposition to smaller particles when calculating H_2SO_4 deposition.

Even so, applying Eqn 2.15 to a typical size distribution leads to just ~15% of $H_2SO_{4(v)}$ depositing on super-micrometer SSA, while ~85% ends up on the accumulation mode. This is very close to the coarse and fine proportions of NSS

observed with our MOI chemical sampler (Figure 2.4, Table 2.1). If the coarse NSS source fraction equals the coarse NSS ambient concentration fraction, NSS loss has to be size-independent. This implies intermittent rainfall rather than dry deposition as the primary NSS deposition process. Or, as *Lewis and Schwartz* (2004) warn, steady state may not have been achieved for coarse aerosols.

In-cloud SO_2 oxidation by H_2O_2 produces 1.0 ± 0.5 NSS units, all of which makes existing CCN larger. Although we know of no credible way to measure the oxidation of SO_2 by O_3 in sea-salt aerosol water, we assume the rate is negligible based on Figure 2.4 and our inability to detect NSS on particles larger than a few µm. Chemical NSS sources, then, total 1.2 ± 0.5 NSS units.

Local MBL NSS sources are comparable to the other significant NSS source: entrainment from the FT. $[\mathrm{NSS}]_{\mathrm{F}}$ concentrations were about 1/3 of $[\mathrm{NSS}]_{\mathrm{MBL}}$ in clean conditions (Figure 2.9). Entrainment brings a $\sim$400 m column of FT air into the MBL every day, drawing 1.1 ± 0.3 NSS units into the MBL under clean conditions and 2.3 ± 0.7 NSS units when pollution layers reside above the inversion.

NSS Divergence (Eqn 2.14, Second Term of d)

NSS concentrations are several times larger than those of the gases, so the NSS divergence flux is several times larger as well: -2.0 ± 0.6 NSS units, whether the FT was polluted or clean. It is useful to think of divergence (see Eqn 2.9) as the export of S downwind, rather than removal from the atmosphere.

NSS Deposition (Eqn 2.14, Second Term of c)

Aerosol NSS dry deposition is hard to estimate, since there are few if any credible observations of aerosol dry deposition for testing V_d models. We estimated NSS dry deposition using V_d from *Slinn and Slinn* (1980) and our MOI-measured size distributions (Figure 2.4). The resulting fluxes were 0.03 ± 0.02 units for fine and

$< 0.07 \pm 0.05$ units for coarse particles, insignificant relative to other loss terms.

Could we have failed to measure a significant amount of super-micrometer NSS mass? It is challenging to transport coarse particles into airborne instruments with a known efficiency (*Baumgardner and Huebert*, 1993), which renders most airborne sea salt reports unreliable. In PASE, however, we used an LTI (*Wilson et al.*, 2004; *Huebert et al.*, 2004a) that minimizes losses and permits a correction for enhancement of particles up to 10 µm. [NSS] is derived by calculating the difference between analyses of [total SO_4^{2-}] and [sea-salt SO_4^{2-}], the latter derived from Na^+ and their seawater ratio. For particles larger than 6 µm or so, sea-salt-sulfate becomes so large that the difference, [NSS], becomes smaller than its analytical uncertainty. One cannot compute dry deposition fluxes for particles one cannot measure. Thus, the analytical uncertainty for NSS becomes significant at sizes above the Na^+ peak.

Marine wet deposition is episodic and virtually impossible to sample in a representative manner. There was almost no rain during PASE, although rain-shafts were occasionally visible from the C-130. It is not clear whether they reached the ocean's surface, thus becoming a sink for SO_2 and NSS. We assume wet removal was small compared to divergence as a loss process for SO_2 and NSS while PASE was in the field.

NSS Summary

As Table 2.5 shows, NSS sources ($+2.3 \pm 0.6$) essentially equal losses (-2.1 ± 0.6). The NSS budget is in balance, within 0.2 ± 0.8 units. Divergence is the only significant loss mechanism in our Eulerian study volume. Even so, this mostly fine-mode NSS budget does appear to be in steady state. On a larger scale, intermittent rainfall events will be the ultimate sink for NSS.

2.3.4 What Fraction of DMS Becomes NSS?

This question can be answered fairly simply from Figure 2.13. The production of SO_2 from DMS is 1.4 ± 0.3 units, 50% of the surface DMS source. Oxidation of SO_2 to NSS is 1.2 ± 0.5 units out of a total SO_2 loss of 2.6 ± 0.6 units. So 50% of DMS becomes SO_2, and 50% of SO_2 becomes NSS.

Hence only about 1/4 of emitted DMS (0.7 ± 0.3 units) becomes sulfate aerosol. This is similar to the *Clarke et al.* (1996) conclusion that $\sim 20\%$ of the DMS flux became accumulation mode ($< 0.3\,\mu m$) sulfate. Most of the rest of the DMS diverges (and presumably reacts downwind), while smaller amounts form organic S or are dry deposited as SO_2. Note that our DMS + OH reaction rate includes DMS from upwind, since the computation relies on measured ambient DMS, not on local emissions.

2.3.5 DMS Versus Long-Range Transport of Sulfur in MBL NSS

The relatively large contribution by the FT to the sulfur budget in this remote region naturally raises questions about the sources of SO_2 and NSS involved. Some FT-derived sulfur is certainly due to DMS in MBL air lofted by deep convection in the ITCZ (*Clarke et al.*, 1998). It has been noted that combustion-related aerosols were associated with back trajectories from South America, about 10,000 km away (*Clarke et al.*, 2013; *Freitag et al.*, 2013). While this is a long distance, there is a mechanism to facilitate rapid transport from South America to the central equatorial Pacific.

In the 1967 Line Islands Experiment, *Hastenrath* (1971) identified an easterly jet centered over Christmas Island at about 900 hPa. When the NCEP reanalysis became available, he identified it as an Equatorial Mid-Tropospheric Easterly Jet (EMTEJ), extending from South America at about 650 hPa, maintained by the

strong water temperature gradient across the equator and by the Coriolis force (*Hastenrath*, 1999a). The subsiding air suppresses cloudiness and rainfall in the region (*Hastenrath*, 1999b), thus extending aerosol lifetimes both in the FT and the MBL. The EMTEJ is strongest in April, but is present year-round. It is also stronger during the cold phase of the El Niño/Southern Oscillation, which was the case during PASE, as opposed to the 1994 ground-based Christmas Island experiment, which took place while the ENSO index was near neutral, but warm. This may account for the apparently stronger continental influence during PASE (*Clarke et al.*, 2013; *Hudson et al.*, 2011).

The EMTEJ may mean the central equatorial Pacific sulfur budget is more influenced by LRT than other remote areas of the ocean. On the other hand, enhanced productivity along the equatorial upwelling zone adds more locally produced S (*Clarke and Porter*, 1993).

When long-range transport is a significant sulfur source, it reduces the leverage of DMS as a controller of NSS and CCN concentrations. The FT is not as pristine as one might think. Airborne experiments over the Pacific frequently encounter layers and plumes of elevated ozone (*Patterson et al.*, 1980), urban/industrial pollution (*Maloney et al.*, 2001), dust (*Howell et al.*, 2006), and emissions from biomass burning (*Dibb et al.*, 1999) and volcanoes (*Carrico et al.*, 2003). Distant sources have the potential to further modify local aerosol chemistry in remote regions.

South American aerosol was observed in this region previously during the PEM-Tropics-B airborne experiment (*Dibb et al.*, 1999; *Maloney et al.*, 2001). During PASE, satellite images from CALIPSO revealed thick aerosol layers over South America as well as plumes of aerosol in the FT very close to our study site (*Simpson*, 2010). Furthermore, the PASE time frame (August and September) is the primary fire season in the Amazon Basin (*Holben et al.*, 1996).

About 36% of SO_2 was derived from entrainment (0.8 ± 0.2 SO_2 units), and 50% of this became 0.4 ± 0.2 units of NSS from LRT of SO_2. In addition, at least

1.1 ± 0.3 units of NSS were directly entrained, for a total of 1.5 ± 0.4 LRT NSS units out of the total 2.3 ± 0.6 units NSS source. Thus, long-range transport was 2/3 of the NSS source, considerably more in polluted cases. It is important to note that SO_2 and NSS can come from deep convection at the ITCZ, meaning LRT may include natural sulfur originating from a distant DMS source (*Clarke et al.*, 2013). Local DMS supplied 0.8 ± 0.3 units, only a third of the total NSS source, even with SO_2-free air above. At the extent of its error bounds, DMS could just supply half of the total 2.3 ± 0.6 units NSS source.

During PASE, we conclude that DMS was not the major source of NSS mass. More S in NSS arrived via LRT in the FT. Recall that Kiribati is 10,000 km downwind of Central and South America. In the CLAW diagram (Figure 2 in *Charlson et al.*, 1987), DMS gas is oxidized first to NSS-SO_4^{2-}. Since only a third of the ambient NSS-SO_4^{2-} was from DMS, this would reduce the sensitivity of NSS-SO_4^{2-} to the hypothesized CLAW cycle.

Quinn and Bates (2011) evaluated the next step in CLAW, the control of CCN number concentration by either DMS or NSS, in light of recent experimental work. They concluded that the number concentration of CCN is largely controlled by submicrometer primary organics, sea salt, and entrainment of continental particles and gases, rather than by local DMS emissions.

2.3.6 Context of PASE Results

We have described here data from a single month of observations in a single region in the central equatorial Pacific. Can any of our results be generalized to other parts of the world oceans? In particular, is DMS likely to be a minor source of NSS elsewhere?

First, it is important to note that our results will only be applicable to regions of subsidence, of which there are many. From the ITCZ through the descending

air of the Horse Latitudes, subsidence prevails at least in the mean. Our study site had only 15% cloudiness, though this is biased low because of our general avoidance of clouds and suppression by the EMTEJ. There was a large excess of H_2O_2, so cloudier regions should have a greater rate of in-cloud SO_2 oxidation. The PASE site had no observable rainfall; concentrations of SO_2 and NSS would be reduced in rainier regions by wet deposition. Conclusions should be adjusted accordingly.

For the large areas of the subtropics with conditions similar to those of PASE, the relative import of DMS and LRT from continental sources hinges primarily on three factors:

1. The entrainment velocity, ω_e
2. The lower-FT concentration of NSS, $[\mathrm{NSS}]_\mathrm{F}$
3. The emission flux of DMS, $J_{0\,\mathrm{D}}$

Entrainment Velocity, ω_e

Both open-ocean and western coastal stratocumulus regions can experience subsidence that generates boundary layer structures of the type we have described. The relative magnitude of NSS entrainment will depend on the product of $[\mathrm{NSS}]_\mathrm{F}$ and ω_e. We assumed $\omega_e = 5\,\mathrm{mm\,s^{-1}}$; how typical is this? Larger values would tend to increase the importance of LRT and entrainment, while a smaller ω_e would increase the relative import of DMS in producing NSS.

There have been several stratocumulus studies. From the nighttime budget analysis of DMS in the offshore VOCALS region of the SE Pacific, *Yang et al.* (2011) estimated an ω_e of $4\,\mathrm{mm\,s^{-1}}$. This matched the diel mean ω_e estimated from climatological and mixed-layer models for this region (*Wood and Bretherton*, 2004; *Caldwell et al.*, 2005). Using the Weather and Research Forecast model and

solving for the change of MBL depth over time, *Rahn and Garreaud* (2010) derived a similar mean ω_e value as a residual for VOCALS-REx.

In the eastern subtropical Atlantic *Sollazzo et al.* (2000) used both divergence and flux measurements to estimate entrainment rates of 7, 7, and 6 mm s^{-1} in three ACE-2 Lagrangian experiments. *Faloona et al.* (2005) measured values between 2 and 7 mm s^{-1} in the eastern subtropical Pacific during the DYCOMS-2 stratocumulus experiment.

There are fewer entrainment measurements to cite over the remote ocean. In the 1994 Christmas Island experiment, *Huebert et al.* (1996) used the diel variation of NSS and MS^- to estimate an entrainment velocity of 5 ± 2 mm s^{-1}. *Clarke et al.* (1996) used a similar approach with CN and CCN number to arrive at 6 ± 2 mm s^{-1}. *Ahlgrimm and Randall* (2006) diagnosed entrainment velocities throughout the Pacific with a bulk boundary layer model. Their Figure 3 shows values of 3–8 mm s^{-1} in the tropics and subtropics, with the highest values in two eastern hot spots. About 80% of the area has ω_e between 4 and 6 mm s^{-1}, centered on our 5 mm s^{-1} value. (Much smaller values are found in regions of convergence such as the ITCZ, where our analysis is not expected to apply.)

Depending on the location, ω_e can certainly deviate from our assumed 5 mm s^{-1}, but apparently not by much. ω_e alone seems unlikely to tip the balance from LRT dominance to DMS dominance in the supply of open-ocean NSS.

The Lower-FT Concentration of NSS, $[NSS]_F$

The other factor in entrainment is the NSS concentration in the air being entrained. One must question whether the PASE $[NSS]_F$ values were outside the range of values that one might find in similar marine regions. Unfortunately, the atmosphere above the Pacific has been sparsely sampled. The comparisons we describe below, therefore, should not be interpreted too rigorously. They can show whether PASE $[NSS]_F$ was unusual, but not whether is was half or twice the Pacific average, for

example.

We used the average of [NSS] from actual daily z_2 to z_2 + 1000 m for our PASE entrainment computations. For comparison, we were able to find three other airborne research programs: the Southern Hemisphere Aerosol Characterization Experiment [ACE-1] and the Global Tropospheric Experiment Pacific Exploratory Mission-Tropics A and B [PEMT-A and PEMT-B] that measured NSS in the lower FT in the Pacific tropics and subtropics. Figure 2.14a is a map showing all points from projects not affected by local sources. The locations where we found NSS data between 1250 m and 2250 m for these programs are noted on the map. The second panel (b) contains box-and-whisker plots for PASE (High- and Low-CO) and the other three programs.

Figure 2.14 suggests that PASE Low-CO was fairly typical. PEMT-B was barely higher, and PEMT-A was somewhat lower, but not by much. As an example of the caution one must use when interpreting such small data sets, the PEMT-A mean becomes identical to the PASE clean mean when the PEM data window is expanded from 1250 m to 1200 m! There just happen to be four rather high points between 1200 m and 1250 m in that range that can skew a very small dataset.

Nothing we see in Figure 2.14 suggests that the entrainment of FT NSS is likely to be significantly smaller throughout the Pacific tropics and subtropics, which would be needed to make it comparable to the DMS source. The PASE computations of entrainment in clean air seem typical for the Pacific. Episodes of pollution may increase NSS entrainment by a factor of 3 or more.

The Emission Flux of DMS, $J_{0\,\mathrm{D}}$

The measured $J_{0\,\mathrm{D}}$ is 3.0 ± 0.5 units, while the *Conley et al.* (2009) DMS flux measurements during PASE had a mean of 3.1 ± 1.5 units. For comparison, *Bates et al.* (1993) estimated 7.1 units in the equatorial Pacific during SAGA using measured $[\mathrm{DMS}]_{sw}$ and *Liss and Merlivat* (1986) k model (k in this context is the

air/water transfer velocity). *Huebert et al.* (2004b) measured DMS fluxes in the eastern equatorial Pacific (TAO cruise) of 2–4 units. On the Biocomplexity cruise in the Sargasso Sea, *Blomquist et al.* (2006) published the k values, but didn't give the measured flux numbers, which averaged 6 units. *Marandino et al.* (2007) measured an average of 8 units in the Pacific equatorial upwelling region and 2–3 units in a warm pool and mid-latitude gyre. *Marandino et al.* (2009) measured a highly variable 17 units in the east Pacific equatorial upwelling and about 6 in a mid-latitude gyre. Finally, *Yang et al.* (2011) measured an average of 4 units in the eastern South Pacific during VOCALS.

Overall, DMS emissions in the tropics and mid-latitudes range from 2–10 units, with the mean close to 3–4. The equatorial Pacific can be a hot spot which seems to average higher (5–7) and can get well over 10–15 units on occasion. See the modeled global map in Fig 2.5 of *Elliott* (2009) for a general idea.

The DMS flux we measured on PASE may be on the low side for what is normal in the equatorial Pacific. Atmospheric DMS was certainly lower than in the 1994 Christmas Island experiment (*Bandy et al.*, 1996). The PASE result may be more representative of the global mean than the equatorial Pacific mean condition with respect to the DMS contribution to MBL NSS. Since no rainfall was encountered during PASE, these results are most likely to represent similarly dry areas of subsiding air. In places where the DMS flux is larger, DMS may equal or exceed entrainment as a source of NSS.

2.4 Conclusions

Can we assume that DMS is the principle source of NSS mass in the remote MBL, especially 10,000 km downwind of the nearest continental sulfur source?

That is not a safe assumption, according to the box-model sulfur budgets developed above. The DMS emission flux (3.0 ± 0.5 units) during the PASE exper-

iment was more than 3 times larger than the formation rate of NSS from DMS (0.8 ± 0.3 units); divergence, organic sulfur production, and dry deposition (as SO_2) competed for the remaining DMS-derived sulfur. Only about 1/4 of emitted DMS becomes NSS. The NSS source from entrainment of unpolluted FT air was 1.5 ± 0.4 units, rising to 2.7 ± 0.7 units of NSS when high-CO air was present. Even though $[NSS]_F$ is usually smaller than $[NSS]_{MBL}$, subsidence at the TWI (entrainment) continually pushes FT NSS into the MBL, sometimes dominating the MBL NSS budget.

These conclusions are based on three self-consistent monthly average budgets for DMS, SO_2, and NSS. Each budget term was computed directly from ambient concentration measurements or eddy-covariance surface flux observations made from the NCAR C-130 in a month-long series of flights near Christmas Island. Each budget includes terms for surface exchange, entrainment, divergence, chemical formation, and chemical loss, each of which is evaluated directly from observations.

The DMS budget (Table 2.2) contains only one source (surface emission), since there is virtually no $[DMS]_F$ to entrain. That source is nearly equivalent to the two loss terms: divergence from the study volume (-0.8 ± 0.2 $\mu mol\, m^{-2} d^{-1}$, our budget "unit") and chemical oxidation by OH, -1.9 ± 0.3 units. The OH oxidation was derived by computing the direct product of measured OH and DMS every 10 seconds on every flight, plotting them versus TOD (Fig 2.10), and integrating under the curve. Divergence was computed separately for the mixed layer (ML) and the buffer layer (BuL), since both concentrations and divergence rates differed between these reservoirs. These two loss terms totaled -2.7 ± 0.5 units. The PASE-average eddy-covariance DMS emission flux was 3.0 ± 0.5 units.

The SO_2 budget (Table 2.4) contains 2 source terms and 4 significant loss terms. By assuming $\gamma = 0.75$, the yield of SO_2 from OH oxidation of DMS became 1.4 ± 0.4 units. Entrainment brought in approximately half that much, 0.8 ± 0.2 units, for a total SO_2 source of 2.2 ± 0.5 units. The entrainment flux increased

10–20% in the presence of pollution.

Among the SO_2 loss terms, divergence decreased SO_2 by -0.9 ± 0.3 units by dilution. This is almost twice the project-average dry deposition loss of SO_2 as calculated from diel average [SO_2] and the dry deposition velocity (*Faloona et al.*, 2010), -0.5 ± 0.2 units. The reaction rate of SO_2 and OH was computed in the same manner as DMS + OH (Fig 2.10); the resulting sulfuric acid vapor flux, -0.22 ± 0.05 units, was deposited on coarse (15%) and fine (85%) particles according to a formula derived by *Maxwell* (1888). We assume that no SO_2 was lost to ozone oxidation on sea salt particles, because we found no NSS on 2.6 µm (or larger) particles, the sea salt maximum (Figure 2.4). Almost all NSS was well below 1 µm diameter. Our observations are strongly at odds with the hypothesis that DMS forms mostly coarse-mode NSS (*Faloona et al.*, 2010).

Although cloud-cover averaged only 15%, clouds were still important chemical reactors. In-cloud oxidation of SO_2 was computed from the high-rate DMS and SO_2 data. When the aircraft punched through bits of cloud, DMS jumped and SO_2 dropped. The DMS increase allowed us to compute the relative proportions of BuL and ML air in the cloud, and thus the amount of SO_2 that it should contain. The drop in SO_2 was then attributed to in-cloud oxidation. On average 27% of SO_2 that entered these trade-wind cumulus clouds was oxidized by H_2O_2 to NSS. By measuring the average updraft velocity under these clouds, we derived a volumetric air flow rate and from that the in-cloud SO_2 oxidation rate, -1.0 ± 0.5 units.

The total SO_2 loss then was -2.6 ± 0.6 units, as compared to the SO_2 source of 2.2 ± 0.5 units. Thus, SO_2 is in steady state, within 0.4 ± 0.8 units.

The fine-particle NSS budget (Table 2.5) includes three source terms and only one loss. Two of the sources have just been discussed: in-cloud oxidation of SO_2 by H_2O_2, 1.0 ± 0.5 units, and OH + SO_2, 0.19 ± 0.05 units. The third is entrainment, 1.1 ± 0.3 units in clean conditions, and twice that when continental pollution is present. These sources total 2.3 ± 0.6 units. The principal loss is to divergence out

the sides of the box, -2.0 ± 0.6 units. Using the upper limits of uncertainties on coarse particle concentrations to compute dry deposition, that removal mechanism for all particle sizes totals slightly under -0.10 ± 0.05 unit. Wet removal is no doubt the ultimate removal method for the NSS that has diverged and moved downwind, but we neither experienced rainfall nor had the means to quantify it.

The NSS budget is therefore in balance between sources, 2.3 ± 0.6 units, and losses, -2.1 ± 0.6 units. The imbalance is 0.2 ± 0.8 units.

Under clean conditions, about 1/3 of MBL NSS originated from DMS, while 2/3 was entrained from the FT as SO_2 and NSS. While we cannot rule out uplift of DMS in the ITCZ as a source of FT SO_2 and NSS, our presumption is that most is of continental origin based on the observed frequency of continental pollution markers on several flights.

Episodes of FT pollution (sometimes significantly) increase the fractional import of LRT. They have little impact on SO_2, though, since the rise in DMS is offset by a drop in OH (the main chemical source of SO_2), the loss of SO_2 to OH is a minor term, and SO_2 entrainment goes up slightly. NSS entrainment, by contrast, increases dramatically when pollution is present.

While the PASE NSS budget falls slightly on the side of entrainment-dominance, it could just as easily have fallen on the DMS-dominance side if the DMS emission flux had been doubled or $[NSS]_F$ halved. The point is that the entrainment from LRT and DMS are surprisingly similar in magnitude; seasonality, local ocean biology, and ENSO are among many factors that could swing the balance either way. There are seawater DMS hot-spots in the eastern tropical and subtropical Pacific where DMS might be expected to dominate, for example. Do they also receive more continental SO_2 and NSS? Over what fraction of the tropical and subtropical oceans might the continents exercise control over the NSS mass?

We leave these and many other questions for future studies and models. We would welcome a discussion of better approaches to deriving budget terms than the

simple ones employed here. All the PASE data is freely available at http://data.eol.ucar.edu/master_list/?project=PASE.

Note that the budgets derived here apply only to tropical and subtropical regions of subsidence, where rainfall is relatively uncommon. They would be very different in a region of tropical convergence, where precipitation is frequent. SO_2 and NSS would have significant wet removal terms, and vertical transport would complicate attempts to describe the dynamics. Many of the measurement systems used in PASE would be compromised by water in their inlets. For these reasons we confined our study to a region of subsidence with little or no rainfall. Our budgets should not be assumed to represent wetter regions.

This budget analysis would be far more speculative if we did not have ambient observations for computing the budget terms. There is no substitute for sending instruments and aircraft (ships/towers/etc) into the field. Direct measurements provide something that models cannot: the ability to assign a meaningful analytical uncertainty and propagate it through the entire analysis.

At least in the PASE study area and time, DMS did not produce as much NSS as did entrainment from seemingly clean, "background" FT air. That was quite surprising. One must recall, however, that these conclusions are derived from a single flight program in a single month at a single location. While PASE conclusions might inform sulfur budgeting in other tropical marine locations, we look forward to similarly rigorous field evaluations of sulfur chemistry in other regions and other seasons.

Acknowledgments

The Huebert group wishes to thank the National Science Foundation for their generous support through NSF Grant #ATM06-27942 and #ATM10-36062. We could not have done this work without the rigorous analytical work of John Zhuang

and the great crew of the C-130. We would also like to thank John Merrill and the Heikes group at URI, Dan O'Sullivan, and the Campos group and Mauldin group at NCAR for providing important gas-phase measurements. We would like to express deep gratitude for the late Alan Bandy, who laid the groundwork for many atmospheric measurement methods and investigations, including PASE.

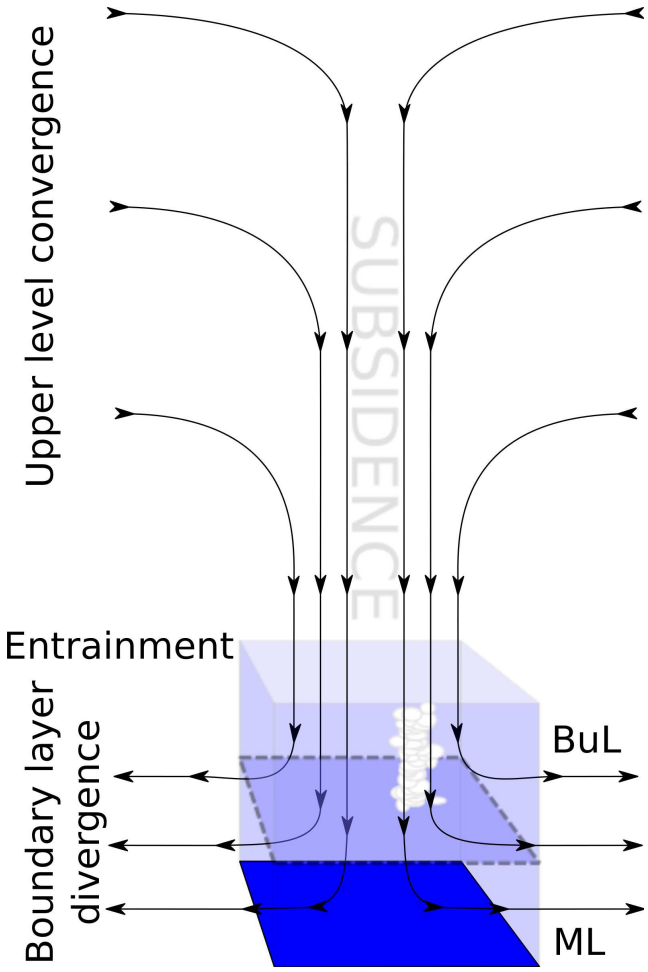

Figure 2.1: Model of subsidence, entrainment, and divergence in the central Pacific MBL and FT system. The FT resides above the MBL (light blue box), the height of which is the TWI (PASE-average z_2) at 1250 m. The dotted plane represents the boundary between the lower mixed layer and cloud layer, or buffer layer, above. An entrainment velocity of $5\,\mathrm{mm\,s^{-1}}$ brings a 430 m deep "plug" of FT air into the MBL in one day. In this region of large-scale subsidence, the entrained air displaces an equivalent volume of the new MBL air mixture. Lifetimes against divergence are therefore around 3 days.

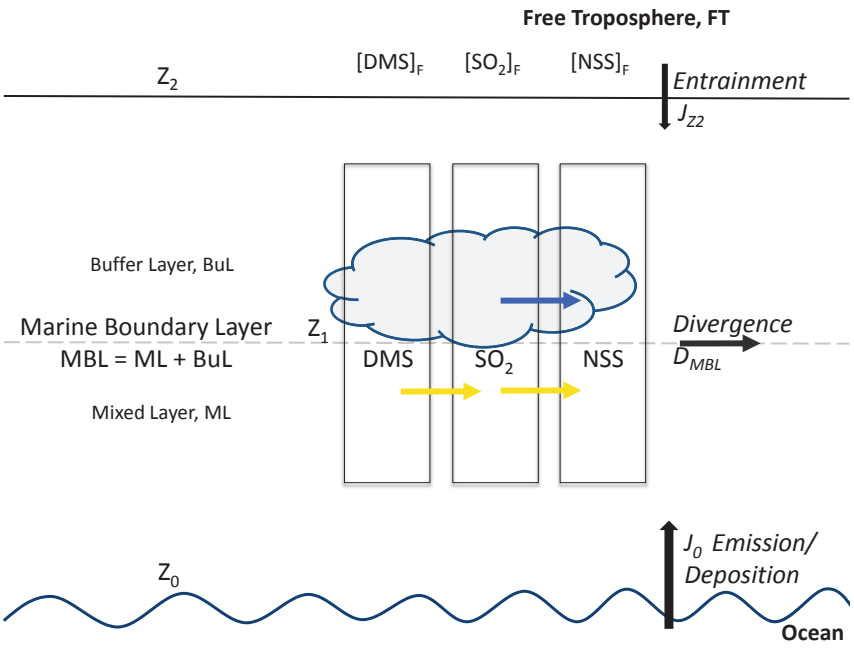

Figure 2.2: Schematic of remote marine boundary layer processes and notation used in our sulfur budget. In the text, mixed layer and buffer layer species are often denoted by "M" and "B" subscripts, respectively, similar to the free troposphere species shown in the diagram. The yellow arrows are chemical conversions out of cloud, and the blue arrow is chemical conversion in cloud.

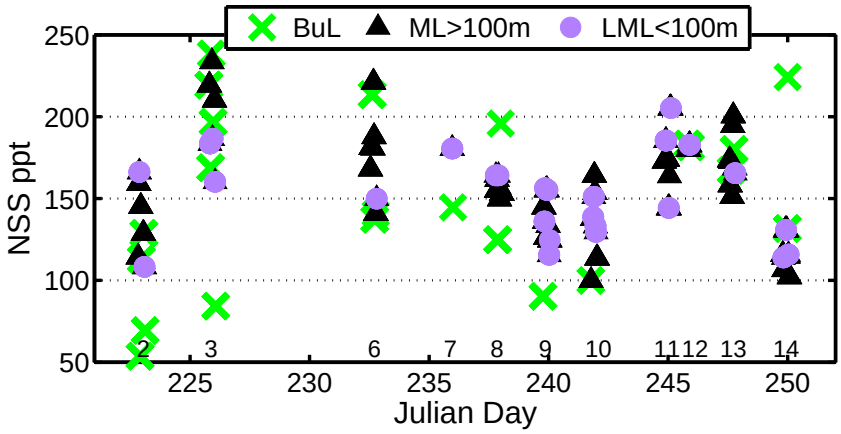

Figure 2.3: Altitude-segregated NSS during PASE flights. Numbers below the data indicate research flight number. Often [NSS] was smaller in the BuL, but not in the presence of FT pollution (as in RF14). In such cases, the FT injects continental NSS into the upper MBL. LML stands for lower mixed layer, which is the lowest altitude the C-130 was permitted to fly.

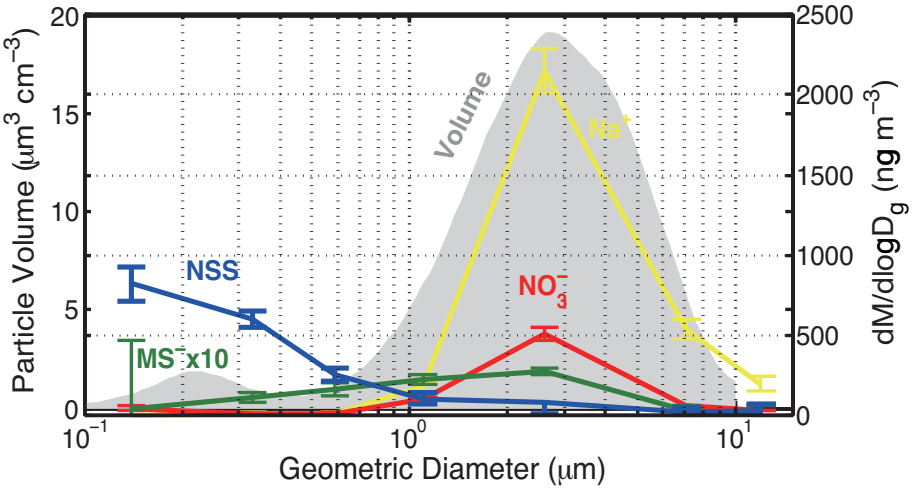

Figure 2.4: Project-average ML size distributions for NSS, MS^-, NO_3^-, and Na^+. Shaded area is the APS physical volume distribution. Every ion has its mass-peak on the same 2.6 μm impactor stage as Na^+ (SSA), except for NSS. In the ML, 89% of NSS resides in the fine mode.

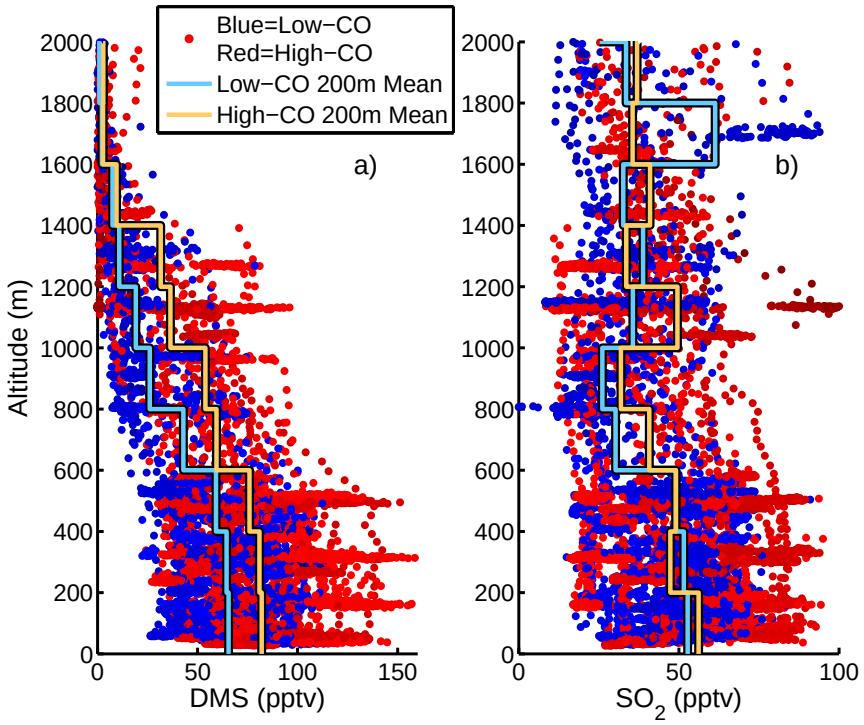

Figure 2.5: **(a)** [DMS] and **(b)** [SO_2] profiles. Points are 10-second concentrations across the entire project, segregated by simultaneous [CO] below (blue, cleaner) or above (red, more polluted) the 63 ppbv [CO] threshold. The 200 m bin averages show the difference between DMS, whose only source is at the surface, and SO_2, which comes from both above and within the study volume. In both Low-CO and High-CO cases, minimum SO_2 occurs at the altitude where clouds are most common; the FT and ML both supply the BuL, which is the primary SO_2 sink. Pollution increases [DMS] but not [SO_2].

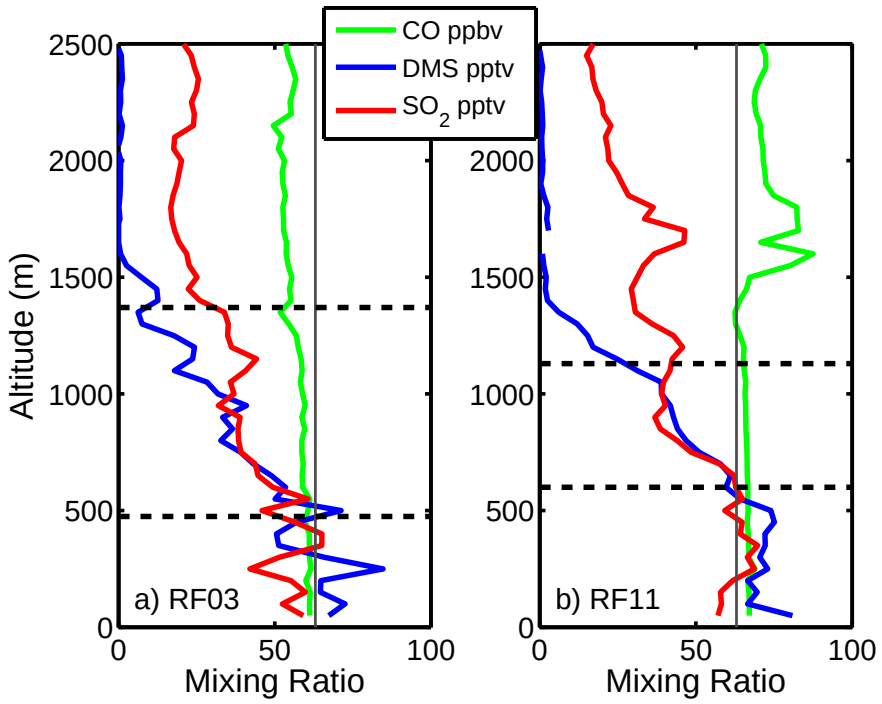

Figure 2.6: Flight-average vertical profiles of CO, DMS, and SO_2 during RF03 (Low-CO) and RF11 (High-CO). The elevated CO in RF11 is accompanied by higher SO_2 in all layers. High FT SO_2 implies a combustion source and the import of continental sulfur into the remote MBL. Horizontal dashed lines are each flight's ML height (lower line) and TWI height (upper line).

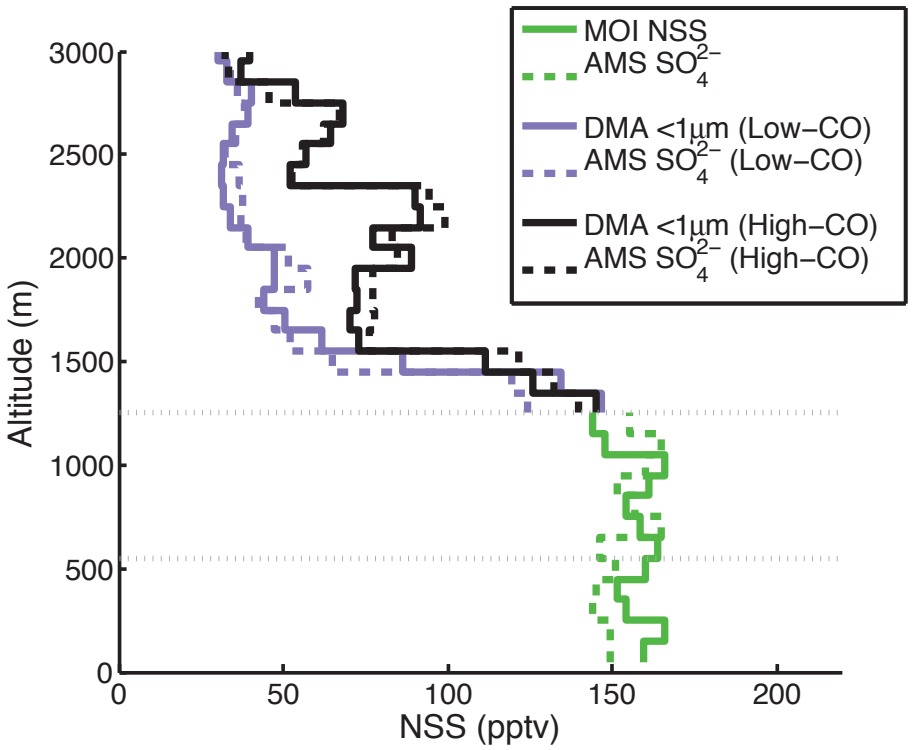

Figure 2.7: Project-average profiles of NSS from MOI, DMA mass, and AMS SO_4^{2-} in 100-m bins. AMS SO_4^{2-} was normalized to the MOI in the MBL. FT SO_4^{2-} inferred from DMA submicrometer particle volume (assuming a SO_4^{2-} density of 1.2 g cm^{-3} supports our AMS normalization. The lower FT NSS concentrations (and hence the NSS entrainment fluxes) used in our calculations come from the AMS data since there was only one MOI measurement in the FT. Dotted gray lines show the project-average ML height (lower) and TWI height (upper). Note that for budgeting purposes, we defined the lower FT as 1000 m above z_2 as measured in each flight. Those differ from the project average profile shown here, particularly in the lowest few hundred meters of the FT.

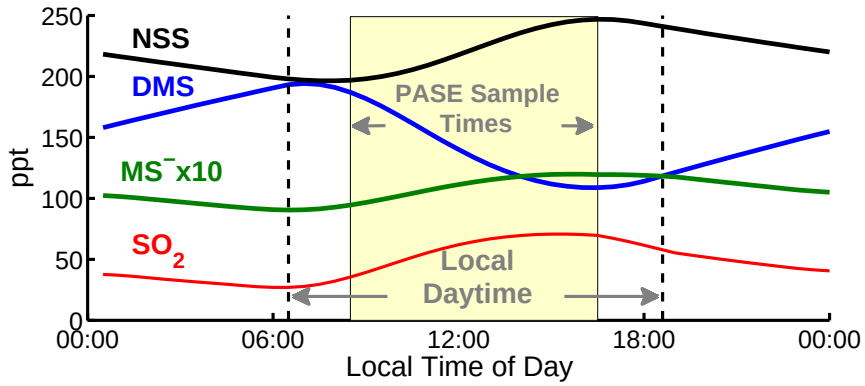

Figure 2.8: Diurnal concentrations from the 1994 experiment. [DMS] peaks at sunrise, when loss to OH turns on. By contrast [SO_2], [NSS], and [MS^-] all fall to their minima at sunrise.

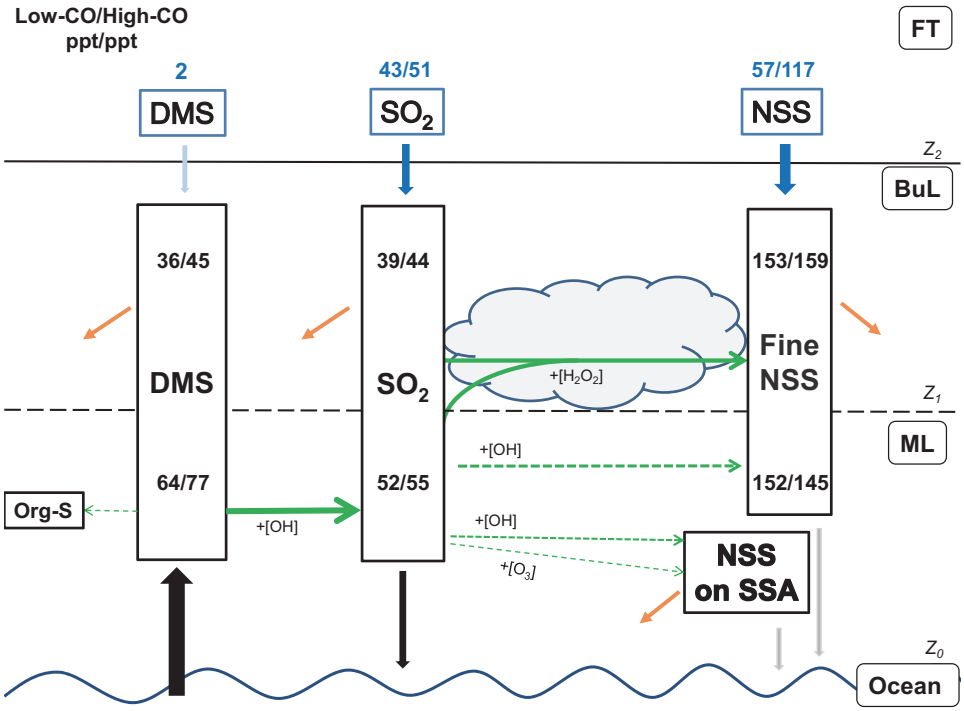

Figure 2.9: Project-mean PASE concentrations and processes. Black arrows are exchange with the ocean; blue arrows are entrainment from the FT; green arrows show chemical reactions (heavy green lines indicate dominant processes while dashed lines show less important mechanisms); and orange arrows represent divergence losses. Faintly colored arrows are used for processes so small we do not include them in the budget. Low-CO/High-CO refers to conditions where [CO] was below/above 63 ppbv.

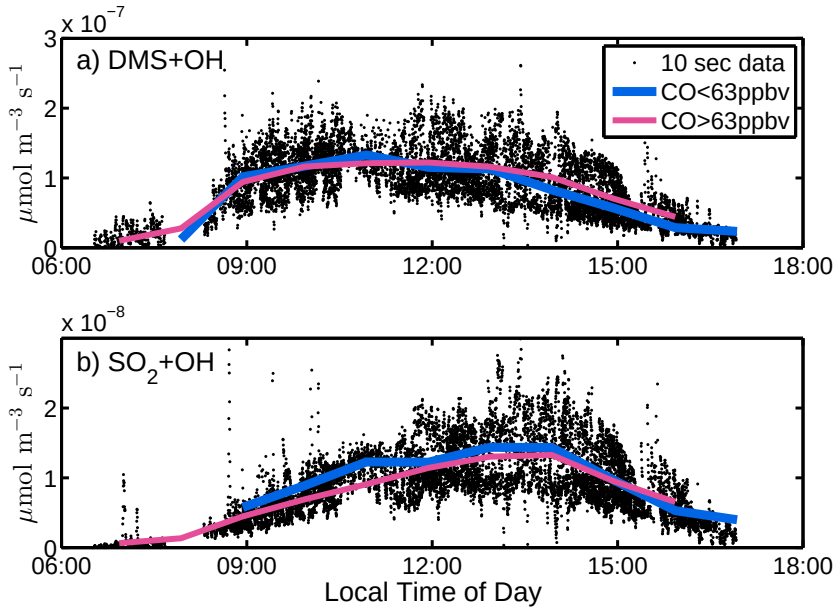

Figure 2.10: DMS-OH and SO_2-OH reaction rates versus TOD. Each point is the direct product of 10-second [OH], [DMS] or [SO_2], and the applicable rate constant. After binning by hour, the area under the curve is a direct measure of the project-average total daily DMS oxidation rate. Multiplying by z_2 yields $\mu\text{mol}\,\text{m}^{-2}\text{d}^{-1}$. **(a)** As [OH] rises through the morning, [DMS] drops from its sunrise peak. This compensation leads to a flattened reaction rate through midday. **(b)** By contrast, [SO_2] rises through the morning from a sunrise minimum (like [OH]), so the OH-SO_2 reaction rate increases through the early afternoon.

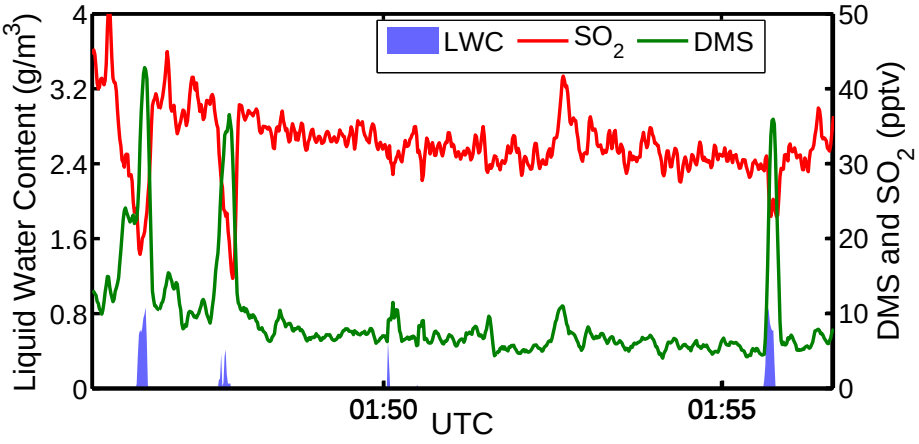

Figure 2.11: DMS, SO_2, and LWC during BuL cloud penetrations in RF03. Blue spikes are cloud water; green spikes are ML DMS; and red valleys are SO_2 (loss).

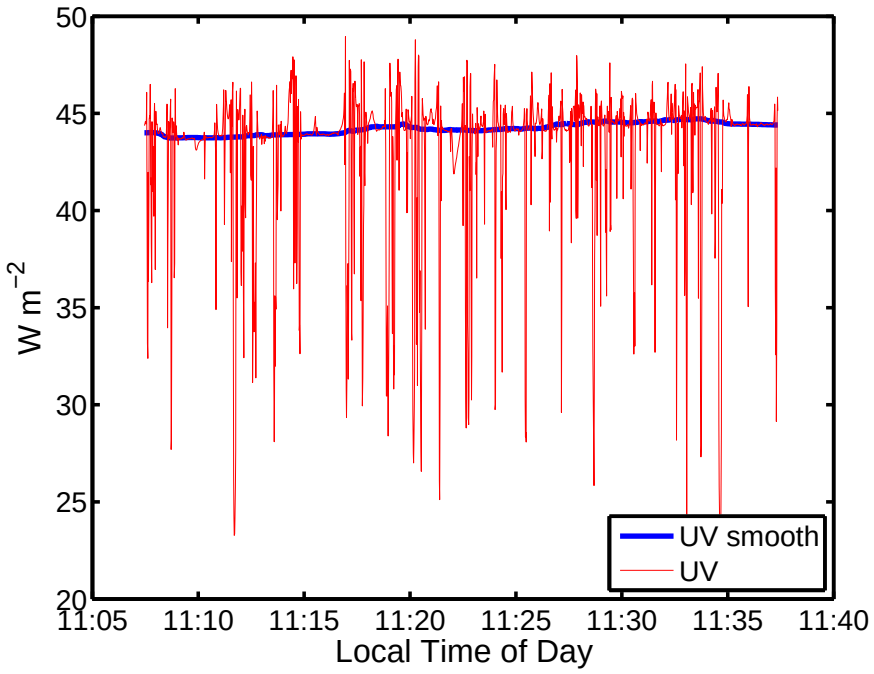

Figure 2.12: Downwelling UV irradiance versus time during upper-ML leg, just under clouds. UV smooth (blue) is a 300-point (5-minute) median filter of UV. Red traces below the blue line indicate cloud.

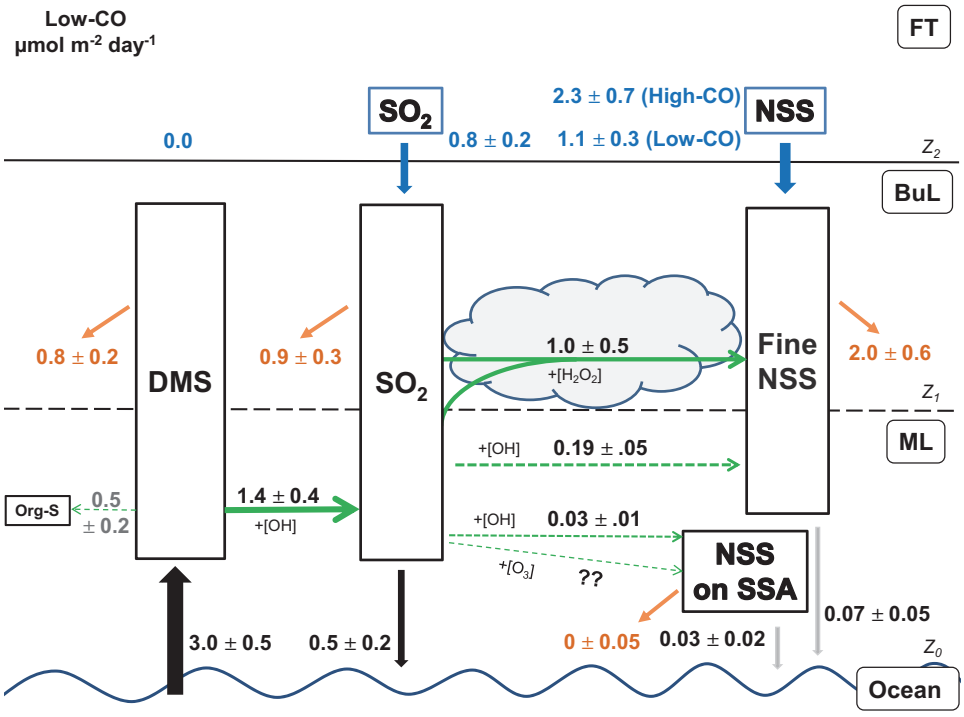

Figure 2.13: PASE process rates in $\mu\text{mol}\,\text{m}^{-2}\text{d}^{-1}$, "units," for Low-CO air. Cleaner conditions are more representative of background remote marine air. The High-CO NSS entrainment flux is included (above the Low-CO value) to emphasize the magnitude of the LRT contribution. Orange values are divergence.

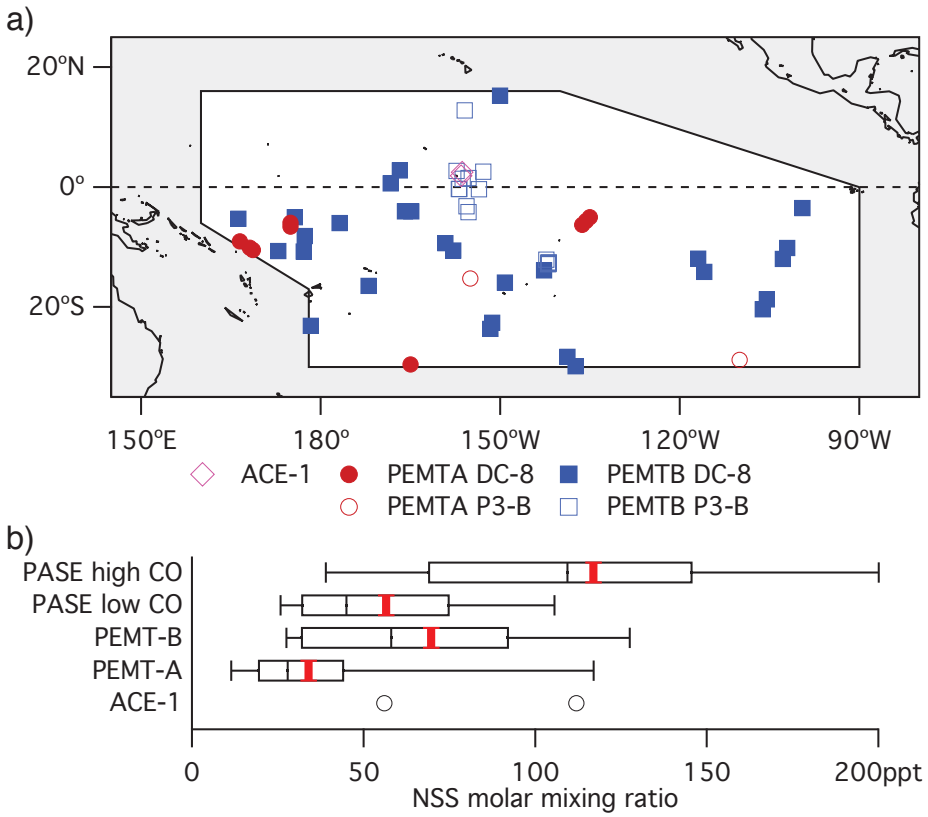

Figure 2.14: Comparison of NSS measured from aircraft campaigns in the lower FT of the remote Pacific. Panel **(a)** shows the locations of useful data from these projects. Box plots **(b)** show 95th percentile, 75th percentile, median (central black line), and mean (central red line) values in the lower 1 km of the FT for PASE and from 1.25 km to 2.25 km for PEM-Tropics A and B and ACE-1, which only has two points in this altitude range.

Table 2.1: Mixed Layer and Buffer Layer Sulfur Species in ppt.

Mixed Layer

Sulfur Species	Size[a]	Mean	Range	Analytical Uncertainty	SEM
NSS	$< 1\,\mu m$	144	41 - 210	10	3
	$\geq 1\,\mu m$	18	8 - 40[b]	8	2
MS^-	$< 1\,\mu m$[c]	2	1 - 3	5	1
	$\geq 1\,\mu m$	5	3 - 7	1	1
DMS		70	22 - 157	0.5	5
SO_2		51	13 - 176	0.5	4

Buffer Layer

Sulfur Species	Size[a]	Mean	Range	Analytical Uncertainty	SEM
NSS	$< 1\,\mu m$	140	49 - 218	10	11
	$\geq 1\,\mu m$	20	5 - 30[b]	5	4
MS^-	$< 1\,\mu m$[c]	2	0 - 3	5	1
	$\geq 1\,\mu m$	3	1 - 6	1	1
DMS		39	1 - 123	0.5	4
SO_2		40	0 - 97	0.5	4

[a] Aerodynamic diameter.

[b] Supermicrometer [NSS] in one flight, RF06, was as large as 66 ppt in the ML and 52 ppt in the BuL, but we omit this data from project averages due to its association with elevated dust and FT coarse volume.

[c] Filter mass inferred from Christmas Island 1994 experiment.

Table 2.2: DMS Budget Summary of Calculated Terms from Equation 2.10.

	flux, $\mu\text{mol}\,\text{m}^{-2}\text{d}^{-1}$
DMS Sources	
Emission, $J_{0\,\text{D}}$	3.0 ± 0.5
Entrainment	0.0
Σ DMS Sources	$\mathbf{3.0 \pm 0.5}$
DMS Losses	
OH + DMS	-1.9 ± 0.5
Divergence	-0.8 ± 0.2
Σ DMS Losses	$\mathbf{-2.7 \pm 0.5}$
DMS Budget Imbalance	$\mathbf{0.3 \pm 0.7}$

Table 2.3: Example Calculation of SO_2 in Cloud Passes.

		Full leg average		Actual in cloud pass		% MBL air	SO_2 oxidized per cloud pass
		avg DMS	avg SO_2	DMS	SO_2		SO_2(reacted)
Flight	Type	pptv	pptv	pptv	pptv	%	%
2	ML	66	50				
2	BuL	19	19	28	22	20	14
3	ML	50	67				
3	BuL	6	35	32	23	58	58
8	ML	40	48				
8	BuL	11	41	23	35	42	20

Table 2.4: SO_2 Budget Summary of Calculated Terms from Equation 2.11.

	flux, $\mu mol\, m^{-2} d^{-1}$
SO_2 Sources	
DMS + OH	$+1.4 \pm 0.4$
Entrainment	$+0.8 \pm 0.2$
Σ SO_2 Sources	$\mathbf{+2.2 \pm 0.4}$
SO_2 Losses	
SO_2 + OH	-0.22 ± 0.05
$SO_2 + H_2O_2$ in cloud	-1.0 ± 0.5
Divergence	-0.9 ± 0.3
Dry deposition	-0.5 ± 0.2
$SO_2 + O_3$ in sea salt	Assumed negligible
Σ SO_2 Losses	$\mathbf{-2.6 \pm 0.6}$
SO_2 Budget Imbalance	$\mathbf{0.4 \pm 0.8}$

Table 2.5: NSS Budget Summary of Calculated Terms from Equation 2.14.

	flux, $\mu mol\, m^{-2} d^{-1}$
NSS Sources	
Uptake of $[H_2SO_4]_{(v)}$	$+0.19 \pm 0.05$
Entrainment (Low-CO)	$+1.1 \pm 0.3$
[Entrainment (High-CO)]	$[+2.3 \pm 0.7]$
In-cloud oxidation	$+1.0 \pm 0.5$
Σ NSS Sources	$\mathbf{+2.3 \pm 0.6}$
NSS Losses	
Divergence	-2.0 ± 0.6
Dry deposition	-0.07 ± 0.05
Σ NSS Losses	$\mathbf{-2.1 \pm 0.6}$
NSS Budget Imbalance	$\mathbf{0.2 \pm 0.8}$

References

Ahlgrimm, M., and D. A. Randall (2006), Diagnosing monthly mean boundary layer properties from reanalysis data using a bulk boundary layer model, *J. Atmos. Sci.*, *63*(3), 998–1012.

Albrecht, B. A., A. K. Betts, W. H. Schubert, and S. K. Cox (1979), Model of the thermodynamic structure of the trade-wind boundary layer: Part I. Theoretical formulation and sensitivity tests, *J. Atmos. Sci.*, *36*(1), 73–89.

Bahreini, R., J. Jimenez, J. Wang, R. Flagan, J. Seinfeld, J. Jayne, and D. Worsnop (2003), Aircraft-based aerosol size and composition measurements during ACE-Asia using an Aerodyne aerosol mass spectrometer, *Journal of Geophysical Research*, *108*(D23), 8645, doi:10.1029/2002JD003226.

Bandy, A., I. C. Faloona, B. W. Blomquist, B. J. Huebert, A. D. Clarke, S. G. Howell, R. L. Mauldin, C. A. Cantrell, J. G. Hudson, and B. G. Heikes (2012), Pacific Atmospheric Sulfur Experiment (PASE): dynamics and chemistry of the south Pacific tropical trade wind regime, *J. Atmos. Chem.*, pp. 1–21.

Bandy, A. R., D. C. Thornton, B. W. Blomquist, S. Chen, T. P. Wade, J. C. Ianni, G. M. Mitchell, and W. Nadler (1996), Chemistry of dimethyl sulfide in the equatorial Pacific atmosphere, *J. Geophys. Res.*, *23*, 741–744.

Bandy, A. R., D. C. Thornton, F. H. Tu, B. W. Blomquist, W. Nadler, G. M.

Mitchell, and D. H. Lenschow (2002), Determination of the vertical flux of dimethyl sulfide by eddy correlation and atmospheric pressure ionization mass spectrometry (APIMS), *J. Geophys. Res.*, *107*, doi:10.1029/2002JD002472.

Barone, S. B., A. A. Turnipseed, and A. R. Ravishankara (1996), Reaction of OH with dimethyl sulfide (DMS). 1. Equilibrium constant for OH+DMS reaction and the kinetics of the OH-DMS+O_2 reaction, *J. Phys. Chem.*, *100*, 14,694–14,702.

Bates, T. S., B. K. Lamb, A. Guenther, J. Dignon, and R. E. Stoiber (1992), Sulfur emissions to the atmosphere from natural sources, *J. Atmos. Chem.*, *14*, 315–337, doi:10.1007/BF00115242.

Bates, T. S., K. C. Kelly, and J. E. Johnson (1993), Concentrations and fluxes of dissolved biogenic gases (DMS, CH_4, CO, CO_2) in the equatorial Pacific during the SAGA 3 experiment, *J. Geophys. Res.*, *98*(D9), 16,969–16.

Baumgardner, D., and B. Huebert (1993), The airborne aerosol inlet workshop: Meeting report, *J. Aerosol Sci.*, *24*(6), 835–846.

Betts, A. (1973), Non-precipitating cumulus convection and its parameterization, *Quarterly Journal of the Royal Meteorological Society*, *99*(419), 178–196.

Blomquist, B., B. Huebert, S. Howell, M. Litchy, C. Twohy, A. Schanot, D. Baumgardner, B. Lafleur, R. Seebaugh, and M. Laucks (2001), An evaluation of the community aerosol inlet for the NCAR C-130 research aircraft, *J. Atmos. Oceanic Technol.*, *18*(8), 1387–1397.

Blomquist, B., C. Fairall, B. Huebert, D. Kieber, and G. Westby (2006), DMS sea-air transfer velocity: Direct measurements by eddy covariance and parameterization based on the NOAA/COARE gas transfer model, *Geophys. Res. Lett.*, *33*(7), L07,601.

Blomquist, B., C. Fairall, B. Huebert, and S. Wilson (2012), Direct measurement of the oceanic carbon monoxide flux by eddy correlation, *Atmos. Meas. Tech. Discuss.*, *5*, 4809–4825.

Boucher, O., and U. Lohmann (1995), The sulfate-CCN-cloud albedo effect, *Tellus B*, *47*(3), 281–300.

Bretherton, C. S., and S. Park (2008), A new bulk shallow-cumulus model and implications for penetrative entrainment feedback on updraft buoyancy, *J. Atmos. Sci.*, *65*(7), 2174–2193.

Caldwell, P., C. S. Bretherton, and R. Wood (2005), Mixed-layer budget analysis of the diurnal cycle of entrainment in southeast Pacific stratocumulus, *J. Atmos. Sci.*, *62*(10), 3775–3791.

Carrico, C., P. Kus, M. Rood, P. Quinn, and T. Bates (2003), Mixtures of pollution, dust, sea salt, and volcanic aerosol during ACE-Asia: Radiative properties as a function of relative humidity, *J. Geophys. Res.*, *108*(D23), 8650, doi:10.1029/2003JD003405.

Chameides, W., and A. Stelson (1992), Aqueous-phase chemical processes in deliquescent sea-salt aerosols: A mechanism that couples the atmospheric cycles of S and sea salt, *J. Geophys. Res.*, *97*(D18), 20,565–20, doi:10.1029/92JD01923.

Charlson, R., I. Kami, J. Lelieveld, C. Leovy, S. Schwartz, and K. Shine (1992), Radiative forcing of climate, *Climate change 1992: the supplementary report to the IPCC scientific assessment*, p. 47.

Charlson, R., J. Langner, H. Rodhe, C. Leovy, and S. Warren (2002), Perturbation of the Northern Hemisphere radiative balance by backscattering from anthropogenic sulfate aerosols, *Tellus A*, *43*(4), 152–163, contribution no:628.

Charlson, R. J., J. E. Lovelock, M. O. Andreae, and S. G. Warren (1987), Oceanic phytoplankton, atmospheric sulphur, cloud albedo and climate, *Nature*, *326*(6114), 655–661.

Chin, M., and D. Jacob (1996), Anthropogenic and natural contributions to tropospheric sulfate: A global model analysis, *J. Geophys. Res.*, *101*, 18–18.

Chin, M., R. Rood, S. Lin, J. Muller, and A. Thompson (2000), Atmospheric sulfur cycle simulated in the global model GOCART– Model description and global properties, *J. Geophys. Res.*, *105*(D20), 24–671, doi:10.1029/2000JD900384.

Clarke, A., and V. Kapustin (2002), A Pacific aerosol survey. part I: A decade of data on particle production, transport, evolution, and mixing in the troposphere*, *J. Atmos. Sci.*, *59*(3), 363–382.

Clarke, A., N. Ahlquist, and D. Covert (1987), The Pacific marine aerosol: Evidence for natural acid sulfates, *J. Geophys. Res.*, *92*(D4), 4179–4190.

Clarke, A., Z. Li, and M. Litchy (1996), Aerosol dynamics in the equatorial Pacific marine boundary layer: Microphysics, diurnal cycles and entrainment, *Geophys. Res. Lett.*, *23*(7), 733–736.

Clarke, A., D. Davis, V. Kapustin, F. Eisele, G. Chen, I. Paluch, D. Lenschow, A. Bandy, D. Thornton, K. Moore, et al. (1998), Particle nucleation in the tropical boundary layer and its coupling to marine sulfur sources, *Science*, *282*(5386), 89–92, doi:10.1126/science.282.5386.89.

Clarke, A., S. Freitag, R. Simpson, J. Hudson, S. Howell, V. Brekhovskikh, T. Campos, V. Kapustin, and J. Zhou (2013), Free troposphere as a major source of CCN for the equatorial Pacific boundary layer: Long-range transport and teleconnections, *Atmos. Chem. Phys.*, *13*(15), 7511–7529.

Clarke, A. D., and J. N. Porter (1993), Pacific marine aerosol: 2. Equatorial gradients in chlorophyll, ammonium, and excess sulfate during SAGA 3, *J. Geophys. Res.*, *98*(D9), 16,997–17,010.

Clegg, N., and R. Toumi (1998), Non-sea-salt-sulphate formation in sea-salt aerosol, *J. Geophys. Res.*, *103*(D23), 31,095–31, doi:10.1029/98JD02595.

Conley, S., I. Faloona, D. Lenschow, T. Campos, C. Heizer, A. Weinheimer, C. Cantrell, R. Mauldin, R. Hornbrook, I. Pollack, et al. (2011), A complete dynamical ozone budget measured in the tropical marine boundary layer during PASE, *J. Atmos. Chem.*, *68*(1), 55–70, doi:10.1007/s10874-011-9195-0.

Conley, S. A., I. Faloona, G. H. Miller, B. Blomquist, D. Lenschow, and A. Bandy (2009), Closing the dimethyl sulfide budget in the tropical marine boundary layer during the Pacific Atmospheric Sulfur Experiment, *Atmos. Chem. Phys.*, *9*(22), 8745–8756.

Davis, D., G. Chen, A. Bandy, D. Thornton, F. Eisele, L. Mauldin, D. Tanner, D. Lenschow, H. Fuelberg, B. Huebert, et al. (1999), Dimethyl sulfide oxidation in the equatorial Pacific: Comparison of model simulations with field observations for DMS, SO_2, H_2SO_4(g), MSA(g), MS and NSS, *J. Geophys. Res.*, *104*(D5), 5765–5784, doi:10.1029/1998JD100002.

DeCarlo, P., J. Kimmel, A. Trimborn, M. Northway, J. Jayne, A. Aiken, M. Gonin, K. Fuhrer, T. Horvath, K. Docherty, D. R. Worsnop, and J. L. Jimenez (2006), Field-deployable, high-resolution, time-of-flight aerosol mass spectrometer, *Anal. Chem*, *78*(24), 8281–8289, doi:10.1021/ac061249n.

Dibb, J., R. Talbot, E. Scheuer, D. Blake, N. Blake, G. Gregory, G. Sachse, and D. Thornton (1999), Aerosol chemical composition and distribution during the

Pacific Exploratory Mission (PEM) Tropics, *J. Geophys. Res.*, *104*(D5), 5785–5800.

Elliott, S. (2009), Dependence of DMS global sea-air flux distribution on transfer velocity and concentration field type, *J. Geophys. Res.*, *114*(G2), G02,001.

Faloona, I. (2009), Sulfur processing in the marine atmospheric boundary layer: A review and critical assessment of modeling uncertainties, *Atmos. Environ.*, *43*(18), 2841–2854.

Faloona, I., D. Lenschow, T. Campos, B. Stevens, M. Van Zanten, B. Blomquist, D. Thornton, A. Bandy, and H. Gerber (2005), Observations of entrainment in eastern Pacific marine stratocumulus using three conserved scalars, *J. Atmos. Sci.*, *62*(9), 3268–3285.

Faloona, I., S. Conley, B. Blomquist, A. Clarke, V. Kapustin, S. Howell, D. Lenschow, and A. Bandy (2010), Sulfur dioxide in the tropical marine boundary layer: dry deposition and heterogeneous oxidation observed during the Pacific Atmospheric Sulfur Experiment, *J. Atmos. Chem.*, *63*(1), 13–32, doi: 10.1007/s10874-010-9155-0.

Freitag, S., A. Clarke, S. Howell, V. Kapustin, T. Campos, V. Brekhovskikh, and J. Zhou (2013), Assimilating airborne gas and aerosol measurements into HYSPLIT: a visualization tool for simultaneous assessment of air mass history and back trajectory reliability, *Atmos. Meas. Tech. Discuss.*, *6*, 5345–5399.

Gerbig, C., S. Schmitgen, D. Kley, A. Volz-Thomas, K. Dewey, and D. Haaks (1999), An improved fast-response vacuum-UV resonance fluorescence CO instrument, *J. Geophys. Res.*, *104*(D1), 1699–1704.

Gray, B., Y. Wang, D. Gu, A. Bandy, L. Mauldin, A. Clarke, B. Alexander, and D. Davis (2010), Sources, transport, and sinks of SO_2 over the equatorial Pacific

during the Pacific Atmospheric Sulfur Experiment, *J. Atmos. Chem.*, pp. 1–27, doi:10.1007/s10874-010-9177-7.

Gurciullo, C., B. Lerner, H. Sievering, and S. Pandis (1999), Heterogeneous sulfate production in the remote marine environment: Cloud processing and sea-salt particle contributions, *J. Geophys. Res.*, *104*(D17), 21,719–21.

Hastenrath, S. (1971), On meridional circulation and heat budget of the troposphere over the equatorial central Pacific, *Tellus*, pp. 60–73.

Hastenrath, S. (1999a), Equatorial mid-tropospheric easterly jet over the eastern Pacific, *J. Meteor. Society of Japan*, *77*(3), 701–709.

Hastenrath, S. (1999b), Dynamics of the Pacific equatorial dry zone, *Meteor. Atmos. Phys.*, *71*(3), 243–254.

Hatakeyama, S., K. Izumi, and H. Akimoto (1985), Yield of SO_2 and formation of aerosol in the photo-oxidation of DMS under atmospheric conditions, *Atmos. Environ.*, *19*(1), 135–141.

Heath, J., and B. Huebert (1999), Cloudwater deposition as a source of fixed nitrogen in a Hawaiian montane forest, *Biogeochem.*, *44*(2), 119–134.

Hegg, D. (1985), The importance of liquid-phase oxidation of SO_2 in the troposphere, *J. Geophys. Res.*, *90*(D2), 3773–3779.

Hicks, B., D. Baldocchi, T. Meyers, R. Hosker, and D. Matt (1987), A preliminary multiple resistance routine for deriving dry deposition velocities from measured quantities, *Water, Air, & Soil Pollution*, *36*(3), 311–330.

Holben, B., A. Setzer, T. Eck, A. Pereira, and I. Slutsker (1996), Effect of dry-season biomass burning on Amazon basin aerosol concentrations and optical properties, 1992–1994, *J. Geophys. Res.*, *101*(D14), 19,465–19.

Howell, S., and B. Huebert (1998), Determining marine aerosol scattering characteristics at ambient humidity from size-resolved chemical composition, *J. Geophys. Res.*, *103*(D1), 1391–1404.

Howell, S., A. Clarke, Y. Shinozuka, V. Kapustin, C. McNaughton, B. Huebert, S. Doherty, and T. Anderson (2006), Influence of relative humidity upon pollution and dust during ACE-Asia: Size distributions and implications for optical properties, *J. Geophys. Res.*, *111*(D6), D06,205, doi:10.1029/2004JD005759.

Hudson, J. G., S. Noble, and V. Jha (2011), On the relative role of sea salt cloud condensation nuclei (CCN), *J. Atmos. Chem.*, *68*(1), 71–88.

Huebert, B., G. Lee, and W. Warren (1990), Airborne aerosol inlet passing efficiency measurement, *J. Geophys. Res.*, *95*(D10), 16,369–16.

Huebert, B., D. Wylie, L. Zhuang, and J. Heath (1996), Production and loss of methanesulfonate and non-sea salt sulfate in the equatorial Pacific marine boundary layer, *Geophys. Res. Lett.*, *23*(7), 737–740.

Huebert, B., S. Howell, L. Zhuang, J. Heath, M. Litchy, D. Wylie, J. Kreidler-Moss, S. Coppicus, and J. Pfeiffer (1998), Filter and impactor measurements of anions and cations during the First Aerosol Characterization Experiment ACE-1), *J. Geophys. Res.*, *103*(D13), 16,493–16, doi:10.1029/98JD00770.

Huebert, B., S. Howell, D. Covert, T. Bertram, A. Clarke, J. Anderson, B. Lafleur, W. Seebaugh, J. Wilson, D. Gesler, et al. (2004a), PELTI: Measuring the passing efficiency of an airborne low turbulence aerosol inlet, *Aerosol Sci. Technol.*, *38*(8), 803–826.

Huebert, B. J., B. W. Blomquist, J. Hare, C. Fairall, J. E. Johnson, and T. S. Bates (2004b), Measurement of the sea-air DMS flux and transfer velocity using eddy correlation, *Geophys. Res. Lett.*, *31*(23), L23,113.

Junge, C. E. (1963), Sulfur in the atmosphere, *J. Geophys. Res.*, *68*, D02S07, doi:10.1029/2002JD003026.

Kiehl, J., and B. Briegleb (1993), The relative roles of sulfate aerosols and greenhouse gases in climate forcing, *Science*, *260*(5106), 311–314.

Kline, J., B. Huebert, S. Howell, B. Blomquist, J. Zhuang, T. Bertram, and J. Carrillo (2004), Aerosol composition and size versus altitude measured from the C-130 during ACE-Asia, *J. Geophys. Res.*, *109*(19), special Section: Characterization of Asian Aerosols and Their Radiative Impacts on Climate-D19S08.

Lenschow, D., I. Paluch, A. Bandy, R. Pearson Jr, S. Kawa, C. Weaver, B. Huebert, J. Kay, D. Thornton, and A. Driedger III (1988), Dynamics and chemistry of marine stratocumulus (DYCOMS) experiment., *Bull. Amer. Meteor. Soc.*, *69*, 1058–1067.

Lewis, R., and E. Schwartz (2004), *Sea Salt Aerosol Production: Mechanisms, Methods, Measurements and Models – A Critical Review*, vol. 152, American Geophysical Union.

Liss, P., and L. Merlivat (1986), Air-sea gas exchange rates: Introduction and synthesis, in *The Role of Air-Sea Exchange in Geochemical Cycling*, edited by P. Buat-Menard, pp. 113–127, D. Reidel.

Liu, P. S. K., R. Deng, K. A. Smith, L. R. Williams, J. T. Jayne, M. R. Canagaratna, K. Moore, T. B. Onasch, D. R. Worsnop, and T. Deshler (2007), Transmission efficiency of an aerodynamic focusing lens system: Comparison of model calculations and laboratory measurements for the aerodyne aerosol mass spectrometer, *Aerosol Sci. Technol.*, *41*(8), 721–733, doi: 10.1080/02786820701422278.

Maloney, J., H. Fuelberg, M. Avery, J. Crawford, D. Blake, B. Heikes, G. Sachse, S. Sandholm, H. Singh, and R. Talbot (2001), Chemical characteristics of air from different source regions during the second Pacific Exploratory Mission in the Tropics (PEM-Tropics B), *J. Geophys. Res.*, *106*, 32, doi:10.1029/2001JD900100.

Marandino, C., W. De Bruyn, S. Miller, and E. Saltzman (2007), Eddy correlation measurements of the air/sea flux of dimethylsulfide over the North Pacific Ocean, *J. Geophys. Res.*, *112*(D3), D03,301.

Marandino, C., W. De Bruyn, S. Miller, and E. Saltzman (2009), Open ocean DMS air/sea fluxes over the eastern South Pacific Ocean, *Atmos. Chem. Phys.*, *9*, 345–356.

Mauldin, R., G. Frost, G. Chen, D. Tanner, A. Prevot, D. Davis, and F. Eisele (1998), OH measurements during the First Aerosol Characterization Experiment (ACE 1): Observations and model comparisons, *J. Geophys. Res.*, *103*(D13), 16,713–16,729.

Maxwell, J. C. (1888), Diffusion, in *Encyclopædia Britannica*, vol. VII, edited by T. S. Baynes, 9th ed., pp. 214–221, Henry G. Allen and Company, New York.

Niki, H., P. Maker, C. Savage, and L. Breitenbach (1983), An FTIR study of the mechanism for the reaction HO+CH_3SCH_3, *Int. J. Chem. Kinet.*, *15*(7), 647–654.

Pandis, S., and J. Seinfeld (1989), Sensitivity analysis of a chemical mechanism for aqueous-phase atmospheric chemistry, *J. Geophys. Res.*, *94*(D1), 1105–1126.

Patterson, E., C. Kiang, A. Delany, A. Wartburg, A. Leslie, and B. Huebert (1980), Global measurements of aerosols in remote continental and marine regions: Concentrations, size distributions, and optical properties, *J. Geophys. Res.*, *85*(C12), 7361–7376.

Penkett, S., B. Jones, K. Brich, and A. Eggleton (1979), The importance of atmospheric ozone and hydrogen peroxide in oxidising sulphur dioxide in cloud and rainwater, *Atmos. Environ.*, *13*(1), 123–137.

Pfister, G., L. Emmons, D. Edwards, A. Arellano, G. Sachse, and T. Campos (2010), Variability of springtime transpacific pollution transport during 2000–2006: the INTEX-B mission in the context of previous years, *Atmos. Chem. Phys.*, *10*(3), 1345–1359.

Quinn, P., and T. Bates (2011), The case against climate regulation via oceanic phytoplankton sulphur emissions, *Nature*, *480*(7375), 51–56.

Rahn, D., and R. Garreaud (2010), Marine boundary layer over the subtropical southeast Pacific during VOCALS-REx–Part 1: Mean structure and diurnal cycle, *Atmos. Chem. Phys*, *10*(10), 4491–4506.

Ravishankara, A. (1997), Heterogeneous and multiphase chemistry in the troposphere, *Science*, *276*(5315), 1058–1065.

Sander, S. P., R. R. Friedl, D. M. Golden, M. J. Kurylo, G. K. Moortgat, P. H. Wine, A. R. Ravishankara, C. E. Kolb, M. J. Molina, B. J. Finlayson-Pitts, R. E. Huie, and V. L. Orkin (2006), Chemical kinetics and photochemical data for use in atmospheric studies evaluation number 15, *Tech. rep.*, Jet Propulsion Laboratory, National Aeronautics and Space Administration.

Schwartz, S. (1988), Mass-transport limitation to the rate of in-cloud oxidation of SO_2: Re-examination in the light of new data, *Atmos. Environ.*, *22*(11), 2491–2499.

Seinfeld, J. H., and S. N. Pandis (2006), *Atmospheric Chemistry and Physics: From Air Pollution to Climate Change*, 2 ed., John Wiley and Sons, Inc., New York.

Shaw, G. (1983), Bio-controlled thermostasis involving the sulfur cycle, *Climatic Change*, *5*(3), 297–303.

Sievering, H., J. Boatman, J. Galloway, W. Keene, Y. Kim, M. Luria, and J. Ray (1991), Heterogeneous sulfur conversion in sea-salt aerosol particles: the role of aerosol water content and size distribution, *Atmos. Environ. A*, *25*(8), 1479–1487.

Simpson, R. (2010), Mechanisms of sulfate formation in the equatorial Pacific marine boundary layer, M.S. thesis, Univ. Hawai'i, Mānoa, Honolulu.

Slinn, S., and W. Slinn (1980), Predictions for particle deposition on natural waters, *Atmos. Environ.*, *14*(9), 1013–1016.

Sollazzo, M. J., L. M. Russell, D. Percival, S. Osborne, R. Wood, and D. W. Johnson (2000), Entrainment rates during ACE-2 Lagrangian experiments calculated from aircraft measurements, *Tellus B*, *52*(2), 335–347.

Turnipseed, A., S. Barone, and A. Ravishankara (1996), Reaction of OH with dimethyl sulfide. 2. Products and mechanisms, *J. Phys. Chem. A*, *100*(35), 14,703–14,713.

von Glasow, R., R. Sander, A. Bott, and P. Crutzen (2002), Modeling halogen chemistry in the marine boundary layer 1. Cloud-free MBL, *J. Geophys. Res.*, *107*(D17), 4341, doi:10.1029/2001JD000942.

Weber, R., P. McMurry, R. Mauldin III, D. Tanner, F. Eisele, A. Clarke, and V. Kapustin (1999), New particle formation in the remote troposphere: A comparison of observations at various sites, *Geophys. Res. Lett.*, *26*(3), 307–310.

Wilson, J., B. Lafleur, H. Hilbert, W. Seebaugh, J. Fox, D. Gesler, C. Brock, B. Huebert, and J. Mullen (2004), Function and performance of a low turbulence

inlet for sampling supermicron particles from aircraft platforms, *Aerosol Sci. Technol.*, *38*(8), 790–802, doi:10.1080/027868290500841.

Wood, R., and C. Bretherton (2004), Boundary layer depth, entrainment, and decoupling in the cloud-capped subtropical and tropical marine boundary layer, *J. Climate*, *17*(18), 3576–3588.

Yang, M., B. Blomquist, and B. Huebert (2009), Constraining the concentration of the hydroxyl radical in a stratocumulus-topped marine boundary layer from sea-to-air eddy covariance flux measurements of dimethylsulfide, *Atmos. Chem. Phys*, *9*, 9225–9236.

Yang, M., B. Huebert, B. Blomquist, S. Howell, L. Shank, C. McNaughton, A. Clarke, L. Hawkins, L. Russell, D. Covert, et al. (2011), Atmospheric sulfur cycling in the southeastern Pacific– longitudinal distribution, vertical profile, and diel variability observed during VOCALS-REx, *Atmos. Chem. Phys*, *11*, 5079–5097.

Yin, F., D. Grosjean, and J. Seinfeld (1990), Photooxidation of dimethyl sulfide and dimethyl disulfide. I: Mechanism development, *J. Atmos. Chem.*, *11*(4), 309–364.

Zhao, G., and L. Di Girolamo (2006), Cloud fraction errors for trade wind cumuli from EOS-Terra instruments, *Geophys. Res. Lett.*, *33*(20), doi: 10.1029/2006GL027088.

Zhu, L., A. Nenes, P. Wine, and J. Nicovich (2006), Effects of aqueous organosulfur chemistry on particulate methanesulfonate to non–sea salt sulfate ratios in the marine atmosphere, *J. Geophys. Res.*, *111*(D5), D05,316, doi: 10.1029/2005JD006326.

Chapter 3

Submicrometer organic aerosol in the equatorial Pacific marine boundary layer: Links to chlorophyll *a* and entrainment from the free troposphere

Abstract

We evaluate the marine and continental contributions to submicrometer organic aerosol (OA) measured with an Aerosol Mass Spectrometer (AMS) in the equatorial Pacific marine boundary layer (MBL) during an airborne field campaign. MODIS-derived chlorophyll *a* (Chl *a*) in a 24 h fetch upwind of each flight was strongly correlated with submicrometer OA, and even more so when the Chl *a* concentration was multiplied by wind speed. This implies a marine biological source of OA. When CO was high (>63 ppbv), entrainment of free tropospheric

(FT) OA was a comparable source of OA. Under cleaner conditions (which probably represent most of the year), OA entrainment averaged $25 \pm 7\ \mu g\, m^{-2}\, d^{-1}$. Coincidentally, this is nearly equal to the non-Chl *a* source term, but we were unable to do a complete budget analysis on OA. At its most intense, the marine biological OA source represented by Chl *a* was about four times larger than FT entrainment of OA from distant sources.

3.1 Introduction

Over the global ocean, wind-generated sea spray containing organic material and condensed oxidation products of biologically emitted volatile organic compounds (VOCs) comprise the natural marine organic aerosol (mOA) reservoir. The characterization of marine aerosol is vital for quantifying and forecasting ocean-aerosol-climate feedbacks. However, mOA measurements are sparse, particularly over the open ocean, due both to the expense of remote field campaigns and to the difficulty of discriminating between marine and other OA sources. We describe here airborne submicrometer OA measurements within the central Pacific remote marine boundary layer (MBL) and explore their connection to the biologically active equatorial upwelling zone.

Aerosol and trace gases in the remote MBL have two main sources: the ocean surface below and the free troposphere (FT) above. At the ocean surface, the breaking of waves and bursting of bubbles produce the dominant MBL aerosol by mass, primary sea-spray particles. At the Trade Wind Inversion (TWI), entrainment of air from the FT is the main mechanism for non-local material to enter the MBL, often after long-range transport (LRT). OA can also be produced in the MBL from VOCs, again from the ocean's surface or remote sources.

Most wind-generated sea-spray mass is coarse (>1 µm diameter) sea salt (referred to hereafter as sea-salt aerosol, SSA) and includes other inorganic and or-

ganic compounds, depending on the biological enrichment of the sea-surface microlayer (*Aller et al.*, 2005; *Kuznetsova et al.*, 2005; *Leck and Bigg*, 2005). Submicrometer sea-spray particles are often enriched with primarily water-insoluble organic matter during periods of enhanced biological activity in the surface ocean (*Facchini et al.*, 2008; *Hawkins and Russell*, 2010). Referred to as marine primary OA (mPOA), this fine-mode organic component of nascent sea spray is thought to arise from bubble-bursting (*Tseng et al.*, 1992; *Sellegri et al.*, 2006; *Burrows et al.*, 2014). Marine secondary OA (mSOA) formed in the atmosphere from VOC oxidation may also deposit on fine and coarse sea-spray particles, forming aged sea spray.

Satellite-derived chlorophyll *a* (Chl *a*) is widely used as a proxy for primary production. However, even when measured in situ, Chl *a* cannot adequately represent the entire plankton community, including non-Chl *a* phytoplankton and heterotrophs such as bacteria that can alter ocean chemistry (*Collins et al.*, 2013; *Prather et al.*, 2013), nor can it capture the Chl *a* maximum below the surface. Many recent MBL studies have linked OA enrichment with remotely sensed Chl *a* (*O'Dowd et al.*, 2008; *Sciare et al.*, 2009; *Vignati et al.*, 2010; *Rinaldi et al.*, 2013; *Schwier et al.*, 2015), presuming submicrometer OA to be mPOA that originates from local primary productivity.

However, assumptions about mOA production have proven to be dubious – reported OA concentrations and composition often depend on the measurement method (*Frossard et al.*, 2014a) and sea spray generation method (*Collins et al.*, 2014) employed. As it stands, there is no clear consensus on what constitutes mPOA and how it varies with mixing state, ecology, season, and wind speed. Moreover, few ambient studies have the means of quantifying the fraction of non-marine OA sources.

Modeling studies attempt to compensate for the lack of in situ measurements by extrapolating poorly constrained parameterizations over large regions of the

ocean. Consequently, mOA concentration estimates vary by an order of magnitude (*Roelofs*, 2008; *Spracklen et al.*, 2008; *Gantt et al.*, 2009; *Westervelt et al.*, 2012). Insufficient knowledge about marine OA sources and physicochemical properties renders models unable to describe mOA impacts on CCN (*Albert et al.*, 2012; *Gantt et al.*, 2009; *IPCC-AR5*, 2013; *Law et al.*, 2013). Because the tropical oceans encompass a vast area, they provide the most potential for mOA production to make a significant contribution to the naturally low background CCN concentrations, despite their low Chl *a* concentrations (*Gantt et al.*, 2009; *Albert et al.*, 2012).

In this paper, we evaluate the marine and continental contributions to OA measured during an airborne field experiment, the Pacific Atmospheric Sulfur Experiment (PASE), in the equatorial Pacific MBL (Figure 3.1). We chose to work at Christmas Island because it is south of the ITCZ in summer and remote from continents (∼10 000 km downwind of South America), making it an ideal site to detect oceanic emissions.

3.2 Experimental

The measurements reported here were collected during the Pacific Atmospheric Sulfur Experiment (PASE) on board the NCAR C-130, which flew within a 4x4 degree region to the east of Christmas Island (2°N, 157°W) over the equatorial Pacific (Figure 3.1). Though 14 research flights were conducted, two flights are completely excluded from this analysis; RF01 was thoroughly contaminated with crossings of our own plume while RF04 had a unique flight plan that was not comparable to the other flights. The majority of sampling took place at constant altitudes in V patterns in the mixed layer (ML; 64% of samples), with much less in the buffer layer (BuL; 20% of samples), and rapid profiles into the free troposphere (FT; 16%). Within the ML, legs were flown at low (∼40 m), mid (∼300 m), and

upper (∼500 m) altitudes. Estimates of the MBL (MBL = ML + BuL) height are based on vertical wind measurements (breaks in turbulence). Ambient conditions in the PASE MBL were very close to 1 atm and 298 K with a relative humidity (RH) of 80%. Because of the persistent lack of precipitation during PASE (*Bandy et al.*, 2012), aerosol scavenging by wet deposition was minimal, so we treat it as negligible for the one-month time frame of PASE. (See *Bandy et al.* (2012) and *Simpson et al.* (2014) for details of the PASE MBL system.)

3.2.1 Aerosol and Gas Measurements

A High Resolution Time-of-Flight Aerosol Mass Spectrometer (AMS; Aerodyne) measured submicrometer aerosol including sulfate and OA at 10 s intervals. The AMS has been widely used to report airborne submicrometer OA measurements (*DeCarlo et al.*, 2010; *Russell et al.*, 2010; *Bates et al.*, 2012; *Shank et al.*, 2012; *Frossard et al.*, 2014b). The inlet chamber was controlled at 600 hPa, and the vaporizer temperature was set at 700 °C, which should be sufficient heat to evolve water insoluble organic carbon, WIOC, in addition to water soluble organic carbon, WSOC (*Bates et al.*, 2012; *Matsumoto et al.*, 2014). The pressure drop from the inlet to the intermediate pressure chamber reduces the sample RH below 40% prior to ionization. In the field, the AMS submicrometer size range was ∼30 nm to 600 nm geometric diameter, where the upper and lower limits are not sharp cutoffs.

PASE was the first project on which this particular AMS had been deployed, and as comparisons with impactor non-sea-salt-sulfate (NSS) revealed, the raw AMS absolute concentrations were too large, presumably due to faulty ionization efficiency calibrations. A comparison between project-average MOI NSS mass and AMS sulfate mass in the MBL showed that AMS concentrations were elevated by a factor of 5.5 (an estimate that may be biased high due to certain flights). We applied this NSS-based correction to the raw AMS data, thereby reducing the PASE

OA concentrations to levels that reassuringly agreed well with the VOCALS OA measurements (described in section 3.3.1). This correction assumes that collection and ionization efficiencies for NSS and OA are equivalent (*Middlebrook et al.*, 2012). In between research flights, build-up of organic material in the vacuum chamber required pre-flight heating that did not completely finish until an hour or two after the sampling began. The data suffering from this residual background OA was removed. This issue appears to have pervaded the majority of two flights (RF03 and RF09), degrading their signal-to-noise ratios and yielding mostly negative values. For these reasons, we exclude RF03 and RF09 from all data.

The uncertainty in individual OA values probably exceeds 30%, demonstrating the necessity for increased averaging times and altitude bins. OA values averaged for 30 min MOI sample legs have a mean error of ∼35%, whereas mean error in flight averages is 7%.

Dimethyl sulfide (DMS) concentrations were measured at 10 Hz using an Atmospheric Pressure Ionization Mass Spectrometer (APIMS; *Bandy et al.* (2002)). DMS concentrations were averaged over the level-leg sampling periods. CO was measured using a vacuum UV resonance fluorescence instrument similar to that of *Gerbig et al.* (1999). Precision is reported as ± 3 ppbv and accuracy as better than 10% for a mixing ratio of 100 ppbv (*Pfister et al.*, 2010). CNhot (non-volatile condensation nuclei (CN) > 0.01 µm) was measured using a CN counter (TSI Mod. 3010) downstream of a 360 °C heater that drives off volatile CN (*Clarke et al.*, 2013).

3.2.2 Use of CO to Differentiate between Clean Marine Air and Continentally Influenced Air

A critical question when studying the remote marine atmosphere is whether we can confidently distinguish between marine background and continentally or an-

thropogenically influenced air masses. Because its sources are predominantly continental combustion and its lifetime is up to 1 month in the tropics, CO is useful for identifying non-marine air, especially in the remote southern hemisphere where background CO concentrations are lowest (*Seinfeld and Pandis*, 2006). *Clarke et al.* (2013) demonstrated that the CO concentration is a reliable indicator of more polluted air in PASE. We will use the *Clarke et al.* (2013) threshold of 63 ppbv CO to select Low CO (LCO) and High CO (HCO) sampling intervals, the latter having greater or more recent continental influence.

3.2.3 Estimating Flight-Averaged Chlorophyll *a*

To estimate the influence of marine biological productivity on the ML, we used Chl *a* concentrations upwind of each flight from the MODIS/Aqua Level 2 daily sea-surface color OC3 algorithm product (*O'Reilly et al.* (1998); http://oceancolor.gsfc.nasa.gov/), re-gridded from 0.025° to 0.05° resolution. The retrieved Chl *a* swaths were separated by approximately two days, corresponding to the typical spacing of research flights. In this patchy high-nutrient, low-chlorophyll (HNLC) ecosystem, changes in Chl *a* are detectable over a two day period. We chose not to interpolate the missing regions in the Chl *a* swaths. The source region was defined using 24 h 3-D back trajectories generated by the HYbrid Single-Particle Lagrangian Integrated Trajectory (HYSPLIT) model (*Draxler and Rolph*, 2013) version 4 (May 2013 release) with the National Center for Environmental Prediction (NCEP) Global Data Assimilation System (GDAS) meteorological output. The back trajectories were initiated every 100 s along the ML flight track using MATLAB code developed by *Freitag et al.* (2013). The resulting trajectories, constrained to those that remained within the ML (typically ∼550 m), define the outline of the fetch region pertinent to the air we sampled (Figure 3.2). In this region of subsidence, marine influences are diluted by entrainment from the FT

(*Huebert et al.*, 1996; *Conley et al.*, 2011; *Simpson et al.*, 2014). Combined with increasing errors with time in back trajectories, 24 h is an arbitrary, but reasonable choice as a period of influence. We simply averaged chlorophyll *a* in the fetch region over the valid data points for most flights. In some cases, the Chl *a* fetches were weighted to account for the density of trajectories occurring on one side of the chevron flight pattern. Due to sparse swath coverage arising from inter-orbit gaps, RF12 and RF13 had to be omitted.

3.3 Results and Discussion

3.3.1 OA Profiles and Properties

Figure 3.3 shows PASE project-average altitude profiles of AMS OA concentrations in LCO (<63 ppbv CO) and HCO (>63 ppbv CO) air. Though the individual 10 s measurements are somewhat noisy, averaging over 200 m altitude bins for the month-long campaign results in coherent profiles. The pink dashed line includes all HCO data whereas the gray line is HCO data excluding the most polluted flight, RF14, in which CO values were the highest and a concentrated plume was encountered just above the TWI. This plume (visible near 1200 m altitude; pink dashed line) apparently enhanced submicrometer OA in the MBL and will be described in Section 3.3.5. Less-concentrated plumes were present in two other flights (∼1000 m). These FT plumes represent infusions of air measurably influenced by combustion. Removal of polluted RF14 reduces the HCO bin averages in the ML, BuL, and lower FT to the extent that LCO and HCO OA in the ML is nearly equivalent. With the exceptions of RF14, RF08, and RF11, recent entrainment of OA from the FT does not dominate the profile of OA in the ML. Indeed, the LCO OA concentrations decrease from the ML to the FT, suggesting dominance by an ocean surface source (or transport in the ML), whereas the opposite trend in HCO

OA concentrations suggests the FT is the dominant OA source.

Figure 3.4 shows a comparison of the PASE LCO OA altitude profile with the one measured in the clean remote SE Pacific during VOCALS from the NCAR C-130 in November of 2008. Using the *Shank et al.* (2012) prescribed criteria of CO<61 ppbv for cleaner air in VOCALS, we averaged VOCALS OA values west of −80° longitude in an attempt to maximize the distance from coastal sources. OA concentrations in the FT were higher in VOCALS than in PASE, no doubt a consequence of its closer proximity to South American continental outflow. Within the ML, PASE submicrometer OA is clearly enriched relative to OA above, suggesting a surface OA source. Located in the oligotrophic South Pacific Subtropical Gyre, the remote VOCALS region described here (20°S to 24°S; 80°W to 81°W) features lower surface Chl *a* concentrations than the equatorial Pacific, which could explain a weaker oceanic OA source. It should be noted, however, that removal by rain was more likely in the VOCALS ML. The overall decrease in OA with decreasing altitude in VOCALS suggests that entrainment of continental OA from the FT dominates the SE Pacific MBL (*Shank et al.*, 2012).

To investigate whether the observed submicrometer OA mass in PASE is primarily marine versus continental OA traceable to South America, we plotted AMS OA against CO in the ML and overlying BuL (Figure 3.5). CO's lifetime in the tropics is on the order of weeks to a month, making it a suitable indicator of distant combustion sources. The AMS OA was averaged within 5 ppbv CO bins and plotted as the midpoint of each bin. In the ML (turquoise), there is no coherent trend in fine OA with CO unless the most polluted flight (RF14) is included. At CO<63 ppbv, the ML OA (0.081 $\mu g\,m^{-3}$) is 40% higher than the BuL OA (0.059 $\mu g\,m^{-3}$) for corresponding CO bins, suggesting a strong surface source of ML OA. Notably, the BuL OA > ML OA only when CO>63 ppbv, indicating an OA source from above that is linked to combustion. The OA enhancement effect becomes quite significant (30-50% added OA) when RF14 (pink dashed line)

is included. RF14 is a dramatic example of the influence that LRT combustion products can have on the MBL.

Since the PASE study area is a region of subsidence, FT air was continually being entrained into the MBL (*Conley et al.*, 2011; *Clarke et al.*, 2013). This entrainment transports FT OA into the MBL, regardless of any concentration gradients; on the scale of days entrainment is essentially downward plug flow (driven by large scale subsidence), even though it is turbulent (bidirectional) on the scale of minutes to hours (*Simpson et al.*, 2014). We can compute the OA entrainment flux as:

$$J_{\mathrm{OA}} = \omega_e [\mathrm{OA}]_{\mathrm{FT}} \tag{3.1}$$

Where J_{OA} is the entrainment flux of OA, ω_e is the entrainment velocity, and $[\mathrm{OA}]_{\mathrm{FT}}$ is the mean [OA] in the lower FT. We have chosen to average only the LCO values here, since they probably represent more of a background OA entrainment rate upon which the (more polluted) HCO entrainment may be imposed, as during the peak biomass burning season in South America.

We use the PASE-average entrainment velocity of $\omega_e = 5 \pm 2\,\mathrm{mm\,s^{-1}}$ from *Simpson et al.* (2014), noting that this is a consensus value for this region (*Huebert et al.*, 1996; *Wood and Bretherton*, 2004). The mean OA in the lower FT from the TWI to 450 m above (the column entrained in 1 day) is $59\,\mathrm{ng\,m^{-3}}$ when [CO]<63 ppbv. The resulting LCO entrainment flux is $25 \pm 7\,\mathrm{\mu g_{OA}\,m^{-2}\,d^{-1}}$ into the top of the tropical MBL. Of course the HCO entrainment flux was larger, averaging $36 \pm 11\,\mathrm{\mu g_{OA}\,m^{-2}\,d^{-1}}$ and rising to a maximum during highly polluted RF14 to $82 \pm 25\,\mathrm{\mu g_{OA}\,m^{-2}\,d^{-1}}$.

In the absence of other processes, this background OA entrainment would maintain the concentration in a 1250 m-deep MBL column at about $20\,\mathrm{ng\,m^{-3}}$. As we shall see, this may help explain [OA] not related to Chl *a* variance.

Even though CO is a reliable tracer of combustion influence, to more accurately identify continental aerosol, we compare 1 min OA with CNhot, which is nonvolatile CN (condensation nuclei) that is larger than 10 nm and remains after heating to 300 °C. Since it is an aerosol (and subject to the same microphysical removal processes as OA), it might be a more suitable proxy for OA. Known to be associated with continental combustion sources (*Clarke et al.*, 2007; *Clarke and Kapustin*, 2010), CNhot in the FT tends to be aged primary aerosol (dust or soot) with sizes large enough to be CCN.2 (CCN at 0.2% supersaturation, typical of MBL clouds). Figure 3.6a shows the association between OA and CNhot in the FT that becomes more evident as CO increases. RF14 has the highest concentrations of CO, CNhot, and OA in Fig. 3.6a. The LCO average OA is $0.050 \pm 0.015\,\mu g\,m^{-3}$ in the FT whereas the HCO average is $0.057 \pm 0.02\,\mu g\,m^{-3}$. The strong linear correlation ($R^2 = 0.6$) between CNhot and OA in Figure 3.6b indicates that OA in HCO air is significantly associated with CNhot in the FT where SSA is absent, thus confirming its non-local source. This also validates the utility of CNhot as a proxy of continentally derived OA; CO does not correlate as well as CNhot with OA in the polluted FT ($R^2 = 0.4$, not shown), likely because CO is not affected by cloud processing or precipitation.

3.3.2 Wind-Driven Species Concentrations

Since mOA derives from a sea-to-air emission process, it is natural to wonder if it is controlled by wind speed (WS). In Figure 3.7, we have plotted OA versus WS measured from the aircraft (not the source region, but there probably was not much spatial variation in the trades on any given day). Surprisingly, we do not see a steady upward trend in OA with WS (Figs 3.7a & d), and in fact a correlation coefficient of only 0.2. Both sea salt (Na^+; Figs 3.7b & e) and DMS do much better (Figs 3.7c & f), with steady upward trends and R^2's of 0.48 and 0.75, respectively.

Both Na^+ and DMS have relatively stable concentrations throughout the ocean, so evidently during PASE the variation in WS was the primary controlling factor. This conforms with descriptions in the literature: ML WS controls the flux of sea spray (*Lewis and Schwartz*, 2004; *Clarke et al.*, 2006; *O'Dowd et al.*, 2008) and DMS (*Bandy et al.*, 1996; *Huebert et al.*, 2004) from the ocean to the atmosphere.

The fact that there is no significant WS trend in OA (Fig. 3.7c & f) suggests that WS alone does not control OA concentrations in this environment. We look now at variability in Chlorophyll *a* as a possible second factor.

3.3.3 OA Correlation with Chlorophyll *a*

In Figure 3.8, we compare PASE flight-averaged ML AMS OA mass with satellite-derived sea-surface Chl *a* concentrations calculated for a 24 h upwind fetch (Figure 3.2 - everything bounded by the gray lines is included in the fetch, from the upwind origin to the aircraft's chevron). In Fig. 3.8a, there is an increase in AMS OA concentrations with an increase in upwind Chl *a*, an indicator that phytoplankton biomass is an OA source. The two linear regressions represent all flights including RF14 (pink line) and flights excluding RF14 (blue line). When RF14 is excluded, the correlation coefficient improves from 0.53 to 0.75, which is consistent with previous suspicions that non-local OA from LRT entrained from the FT and infiltrated the ML during RF14 (Fig. 3.3 & Fig. 3.5). The equation for the linear regression without RF14 is:

$$OA = 0.37 \times \text{Chl } a + 0.026 \tag{3.2}$$

Where OA is in $\mu g\,m^{-3}$ and Chl *a* is in $mg\,m^{-3}$. OA's dependence on Chl *a* holds over a doubling of Chl *a* to the upper limit of surface Chl *a* typically observed in this region (*Pennington et al.*, 2006).

Chl *a*'s efficacy for predicting OA concentrations is further refined in Fig. 3.8b

as we factor in WS to account for the WS-dependent increase in air-sea transfer of species, a process which may be mediated by tangential stress and bubble bursting (*Blanchard and Syzdek*, 1982; *Huebert et al.*, 2010). In the relatively constant southeasterly trade wind regime, the WS does not vary significantly over the course of a day ($\pm 1.2\,\mathrm{m\,s^{-1}}$ on average in PASE), but to compute a more representative WS metric for each Chl *a* fetch, we averaged the WS measured in flight with that flight's average WS 12 h and 24 h upwind along its ML back trajectories. The equation for the least-squares regression is:

$$OA = 0.051 \times (\text{Chl } a \times \text{WS}) + .013 \tag{3.3}$$

Where OA is in $\mu\mathrm{g\,m^{-3}}$, Chl *a* is in $\mathrm{mg\,m^{-3}}$, and WS is in $\mathrm{m\,s^{-1}}$. ML OA is a strong function of Chl *a* multiplied by WS, supporting the hypothesis that the measured AMS OA is linked to photosynthetic biomass in the local surface waters of the equatorial upwelling zone. Again, removal of RF14 from the regression improves the fit from 0.80 to 0.91. The first power of WS may be most suitable in this range (*Liss and Merlivat*, 1986; *Huebert et al.*, 2010).

Although we can attribute most of the variance in the OA signal to changes in Chl *a*, we cannot constrain its origins to a particular class of marine organic matter. A parcel of air in the ML has a history longer than the day-long timescale that we examine in this study, resulting in marine aerosol that is heterogeneously aged; our 1-day fetches include nascent mPOA and VOCs as well as preexisting mOA (POA and SOA) and VOCs at various stages of oxidation accompanied by reaction products.

The y-intercept in equation 3.2 ($0.026 \pm 0.008\,\mu\mathrm{g\,m^{-3}}$) potentially represents ML OA that is linked to neither Chl *a* nor WS. The excess OA is about 40% of the OA at the lowest Chl *a* concentration ($0.062 \pm 0.02\,\mu\mathrm{g\,m^{-3}}$ OA), implying an important contribution to OA during periods of low local biological activity. As

hypothesized by *Quinn et al.* (2014), a portion of this excess OA may be from seawater dissolved organic carbon (DOC) sources. Other possible sources include SOA, POA not linked to Chl *a*, upwind sources, and the FT.

Perhaps coincidentally, this $0.026 \pm 0.008\,\mu g\,m^{-3}$ of excess OA agrees very closely with our calculated LCO flux of OA from the FT. Dividing the entrainment flux ($25 \pm 7\,\mu g\,m^{-2}\,d^{-1}$) by the average MBL depth (1250 m) provides the OA concentration ($0.020 \pm 0.006\,\mu g\,m^{-3}$) that could derive from LRT of continental OA to the tropical MBL in 1 day. This value's near equivalence with the intercept suggests that the majority of the excess OA is continental. Hence, when Chl *a* is low (near $0.1\,mg\,m^{-3}$), entrainment is nearly as strong an OA source as marine biology. At the upper end of Chl *a* ($0.26\,mg\,m^{-3}$), the oceanic OA source dominates the FT source by up to a factor of 4 (Figure 3.8).

Physical processes have been found to dominate the biological variability in this ecosystem, resulting in stronger interannual rather than seasonal variability (*Murray et al.*, 1994; *Landry et al.*, 1997). ENSO events drive the interannual variation in tropical marine biological productivity, which is thought to represent a significant portion of the global new carbon production (*Chavez and Barber*, 1987). When integrated over a year, the sustained primary productivity in the tropics is larger than at higher latitudes (*Hasumi and Nagata*, 2014). When PASE went to the field in August, 2007, the weak La Niña may have led to higher biological productivity due to stronger upwelling in the central Pacific. The yearly peak in Chl *a* during August-September (*Carlson and Ducklow*, 1995) further demonstrates that PASE was well timed to observe any relationship between Chl *a* and marine OA, assuming that 1) OA originates from oceanic OC that correlates with photosynthetic biomass and 2) the sampled air contains minimal amounts of OA from MBL sources farther than 1 day upwind.

As this is an HNLC region, the Chl *a* concentrations are lower than those of POA studies in more productive waters (*Sciare et al.*, 2009; *Albert et al.*, 2012;

Rinaldi et al., 2013) but higher than in oligotrophic waters. It is important to probe the marine OA link at both ends of the Chl *a* concentration spectrum as well as in diverse oceanographic regimes. Parameterizations based on productive waters may poorly represent HNLC or oligotrophic regions because ecosystem-dependent ocean chemistry likely responds differently to physical mechanisms that drive marine aerosol production (*Prather et al.*, 2013).

The link between Chl *a* and OA for this biologically active source region is on a short timescale. Until now, links between Chl *a* and ambient OA on a daily time scale have not been shown. Our Chl *a* fetches are 24 h upwind in the MBL and well defined by HYSPLIT back trajectories, whereas other studies use temporal scales of 3 days (*Spracklen et al.*, 2008; *Sciare et al.*, 2009) to 8 days (*Rinaldi et al.*, 2013), sometimes with ambiguously defined source regions.

Unfortunately, we cannot compare our OA measurements (and Chl *a*-WS fit) with the OA submicrometer fractions reported by investigators such as *O'Dowd et al.* (2008); *Vignati et al.* (2010); *Gantt et al.* (2011); *Rinaldi et al.* (2013) because such a transformation requires the dubious assumption of a stable internal mixture and thus introduces considerable uncertainty. *Spracklen et al.* (2008) relate organic carbon (OC) concentrations to Chl *a*, but they employ a fit-derived emissions factor to make up for the absence of a wind speed input. Besides, most of these studies measure OC rather than OM, which they must convert to OA by assuming the extent of OC oxidation. Compared to OC at the *Spracklen et al.* (2008) study sites (Amsterdam Island, Azores, and Mace Head), all of which are in mid-latitude regions that experience seasonal primary productivity that peaks at larger Chl *a* than that of PASE, PASE MBL OA levels ($0.081 \pm 0.02 \mu g\, m^{-3}$ in LCO air) are a bit lower than the lowest winter OC concentrations $\sim 0.1\, \mu g\, m^{-3}$, once the OC-to-OM conversion factor ($\sim$1.4 - 1.6) is applied.

Uncertainties in our 24 h HYSPLIT back trajectories and 2 km satellite products should be modest. In the stable southeasterly tropical trade wind regime,

there is little variability in WS over 1 day. Satellite Chl *a* products aim for 35% accuracy, but there is reason to believe the error is lower in the PASE region. MODIS performs better at low solar zenith angles typical of this region (*Gregg and Casey*, 2007). SeaWiFS Chl *a* (which agrees well with MODIS Chl *a* in the equatorial Pacific at this range of concentrations (*Gordon and Franz*, 2008)) averaged from 1997 - 2002 (*Gregg and Casey*, 2004) and 1997 - 2005 in the equatorial Pacific closely agrees with bottle-measured Chl *a*, remaining relatively constant throughout the year within the range of 0.15 - 0.3 $\mathrm{mg\,m^{-3}}$ with a small yearly maximum in August (*Pennington et al.*, 2006). In general, Chl *a* corresponds well with POC generated by biological processes (*Legendre and Michaud*, 1999), with a significant positive linear correlation in the central equatorial Pacific (pen). Furthermore, phytoplankton biomass is highest near the surface in the equatorial Pacific (*Wang et al.*, 2013), supporting sea-surface Chl *a* as a credible proxy for biological material available for transfer to the atmosphere.

A considerable uncertainty in our calculations is the ambiguity in airmass composition prior to arriving at the 24 h fetch boundary. Marine ML air contains a mixture of aerosol (OA, NSS, and SSA) on a continuum of physicochemical evolution depending on its airborne lifetime and interactions with other aerosol, vapors, and radicals. Hence the air we sampled has a longer ocean surface exposure and oxidation history than we explicitly consider. Our assumption is that the recent 24 h fetch submicrometer OA signal overwhelms the remnant signal, at least 30-40 % of which has already experienced dilution from entrainment. In the tropical ML where average [OH] was 4.6×10^6 molecules $\mathrm{cm^{-3}}$, peaking at 8.0×10^6 molecules $\mathrm{cm^{-3}}$ during the solar maximum, DMS is destroyed at a rate of $\sim$7.3 ppt/h, or about 10 $\%\,\mathrm{h^{-1}}$ on average (*Conley et al.*, 2009). Analogously, nascent aerosols and other VOCs in the MBL exposed to a 12 h photochemical cycle will age substantially, affecting their properties and causing transformations between the gas and particle phases. mPOA might likewise be expected to photooxidize and serve as a nucleus

for SOA and NSS accretion. This remnant signal no doubt contributes something to the intercept in Fig. 3.8a, as does OA entrainment and the oxidation of other VOCs to SOA.

3.3.4 A Note on SOA in PASE

With only one non-sulfur organic anion measured, we cannot constrain the SOA contribution to submicrometer OA nor can we identify its source as continental or oceanic. Oxalate ($C_2O_4^{2-}$; *Simpson* (2010)), is no more than 5% of OA in PASE. Further, no correlation is evident between OA and submicrometer or total MOI oxalate (not shown), suggesting that OA does not share a production mechanism with oxalate in the MBL. The SOA contribution (especially marine) to the fine mode continues to be an open question for which further careful observations are necessary.

3.3.5 Continental OA in the Remote Marine Atmosphere

As described in *Simpson et al.* (2014), enhancements in CO over the remote ocean correlate with increased entrainment into the MBL of NSS mass, probably continental in origin. The clusters of HYSPLIT back trajectories that trace from the PASE region back to South America during biomass burning season (*Clarke et al.*, 2013; *Freitag et al.*, 2013) strongly support the hypothesis that gaseous and particulate organic material were also brought to the tropical Pacific via long-range transport. We further note that studies of remotely sensed CO column concentrations combined with fire counts over South America describe considerable interannual variability in CO emissions from 2003 to 2010, with 2007 having among the highest emissions of any year with an estimated 92 Tg CO/yr biomass burning emissions (*Gloudemans et al.*, 2009; *Hooghiemstra et al.*, 2012).

Apparent in Figures 3.3 and 3.5, RF14 exhibits a deviation toward notably

higher OA concentrations than the rest of the project. Using the no-RF14 fit (Equation 3.2) in Fig. 3.8a to estimate what the "clean" RF14 OA should be, there is a surplus of $0.025 \pm 0.007\,\mu g\,m^{-3}$. Within the uncertainties (∼30%), this non-local OA is very similar to the equation 3.2 y-intercept "background" OA of $0.026 \pm 0.008\,\mu g\,m^{-3}$, which is also roughly the baseline FT OA contribution from the entrainment flux in a 1250 m deep MBL in a day.

3.4 Conclusions

We have reported AMS submicrometer OA measurements in the tropical Pacific MBL ($0.081 \pm 0.02\,\mu g\,m^{-3}$ in LCO air; $0.086 \pm 0.03\,\mu g\,m^{-3}$ in HCO air) and FT ($0.074 \pm 0.02\,\mu g\,m^{-3}$ in LCO air; $0.11 \pm 0.03\,\mu g\,m^{-3}$ in HCO air). Averaging of this data over larger temporal and spatial scales reveals 1) coherent trends that are largely consistent with a marine biological source of OA in the mixed layer (ML) and 2) entrainment of continental OA that increases with altitude above the ML, much of it apparently combustion products from Central and South America. Constraining OA concentrations in this region will aid comparisons with modeling studies (*Spracklen et al.*, 2008; *Myriokefalitakis et al.*, 2010; *Gantt et al.*, 2012).

Most of the variance in ML OA could be explained by MODIS Chl *a* under a 24 h HYSPLIT fetch, multiplied by WS. It is notable to see a significant linear relationship between OA and satellite-based Chl *a* in a relatively low-Chl *a* (0.05 - $0.35\,mg\,m^{-3}$) region. The Chl *a*-OA link could potentially be extrapolated to much of the central equatorial Pacific where mesotrophic conditions prevail (and remain relatively stable throughout the year), if it can be shown to hold for other oceanographic regimes.

Relationships between CO and OA are weak in the PASE ML, supporting our claim that the ML (below the BuL/cloud layer) is dominated by mOA but always is entraining some FT OA. However, the BuL and FT are at times heavily

influenced by continental OA, probably from LRT of biomass burning from South America. When aerosol from continental sources extensively entrain into the ML, it can nearly double the background OA concentrations ($0.03 \pm 0.01\,\mu g\,m^{-3}$), as we observed in the most polluted PASE flight, RF14. Even during the peak month for Chl *a* in this region, the MBL is highly susceptible to certain types of continental aerosol contributions (*Clarke et al.*, 2013; *Simpson et al.*, 2014), which is surprising due to the PASE region's distance ($\sim$10 000 km) from continents.

We calculated that under typical clean (CO<63 ppbv) conditions during the PASE time frame, $25 \pm 7\ \mu g\,m^{-2}\,d^{-1}$ OA entrains from the FT to the remote marine MBL. This flux matches the y-intercept of the Chl *a*-OA linear relationship, suggesting that the ML OA not linked to Chl *a* could be from LRT of continental OA. At low Chl *a* levels ($0.1\,mg\,m^{-3}$), the entrainment flux from the FT is roughly equal to the mOA flux from the ocean surface. However, if Chl *a* levels increase in the clean MBL ($0.026 \pm 0.008\,\mu g\,m^{-3}$), then the mOA source overshadows the FT source by as much as a factor of 4.

The comparison of the PASE and VOCALS remote OA profiles in clean air (low CO concentrations) suggests that the two programs measured Pacific background air, though VOCALS' proximity to South America is evident in its FT OA levels, which are considerably larger than those of the PASE FT. The more remote site of PASE had its ML OA> FT OA, supporting a dominant marine source. In contrast, combustion sources seemingly dominated VOCALS OA in the FT and MBL (*Shank et al.*, 2012).

Acknowledgments

The Huebert group wishes to thank the National Science Foundation for their generous support through NSF grants ATM06-27942 and ATM10-36062. We could not have done this work without the great crew of the C-130. We thank T. Cam-

pos for providing the PASE CO measurements and L. Mauldin for providing the MSA, H_2SO_4, and OH measurements. We would like to express deep gratitude for the late Alan Bandy, who laid the groundwork for many atmospheric measurement methods and investigations, including PASE. PASE data can be downloaded from http://data.eol.ucar.edu/master_list/?project=PASE. The authors gratefully acknowledge the NOAA Air Resources Laboratory (ARL) for the provision of the HYSPLIT transport and dispersion model used in this publication.

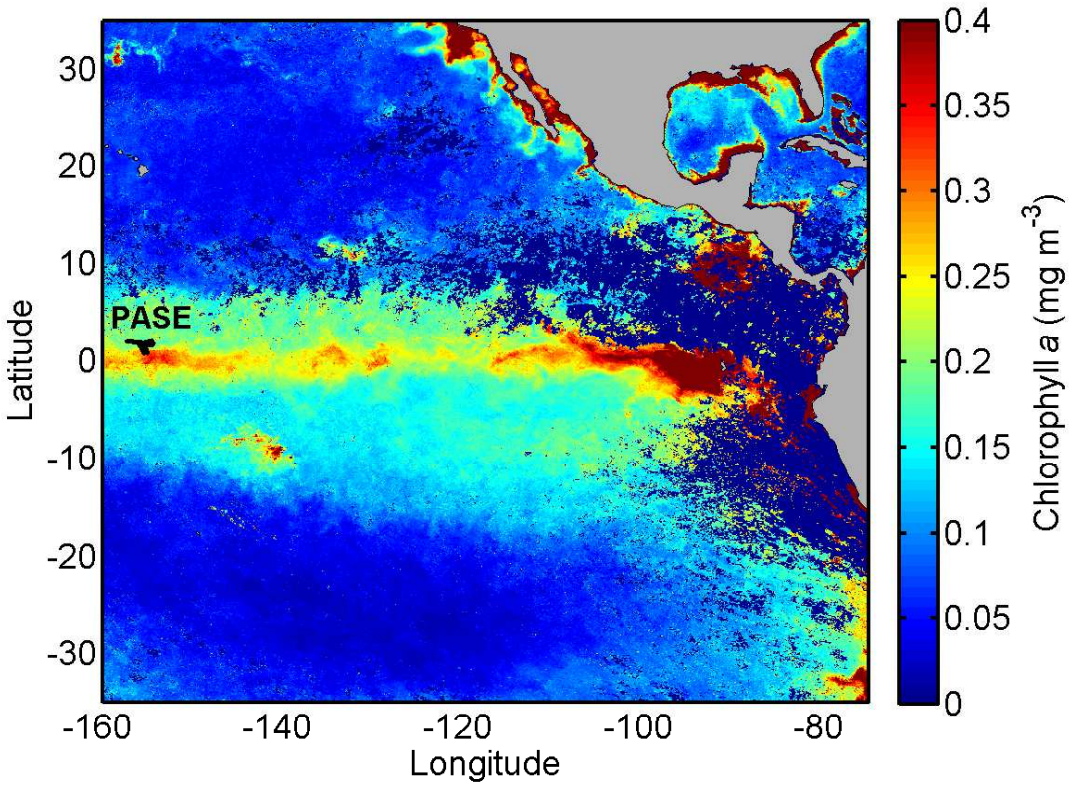

Figure 3.1: Equatorial Pacific monthly average MODIS Chl *a* for August, 2007, when PASE was in the field. A sample flight track (in black) shows the typical sampling region to the east of Kiritimati (Christmas Island).

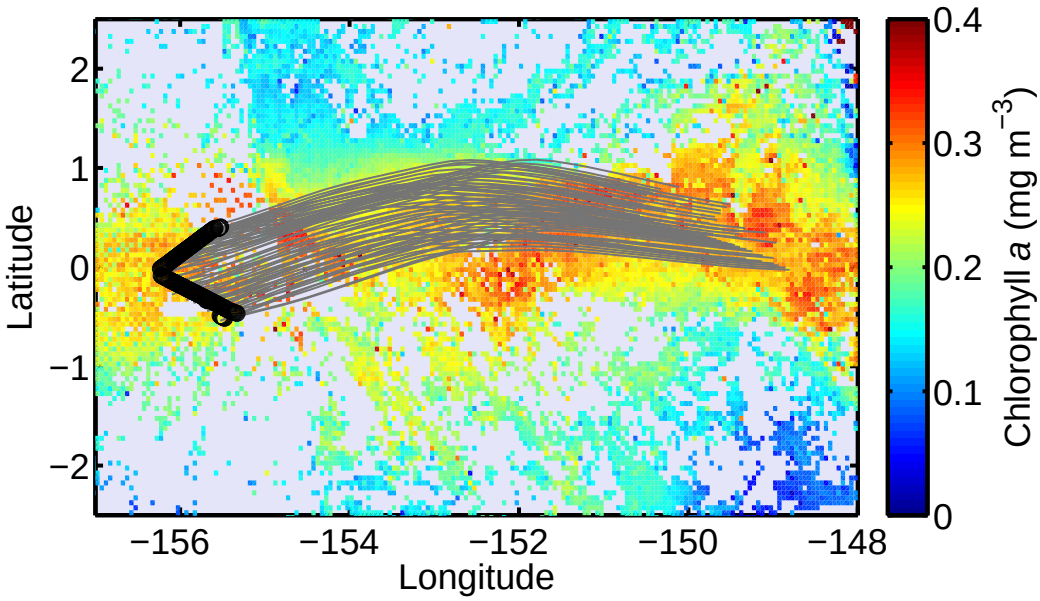

Figure 3.2: 24 h HYSPLIT back trajectories (gray lines) for Research Flight 06 (ML flight track shown in black) plotted with MODIS Chl *a*. Chl *a* data were re-gridded to a 0.05° spatial resolution. Only trajectories that remained in the ML were used.

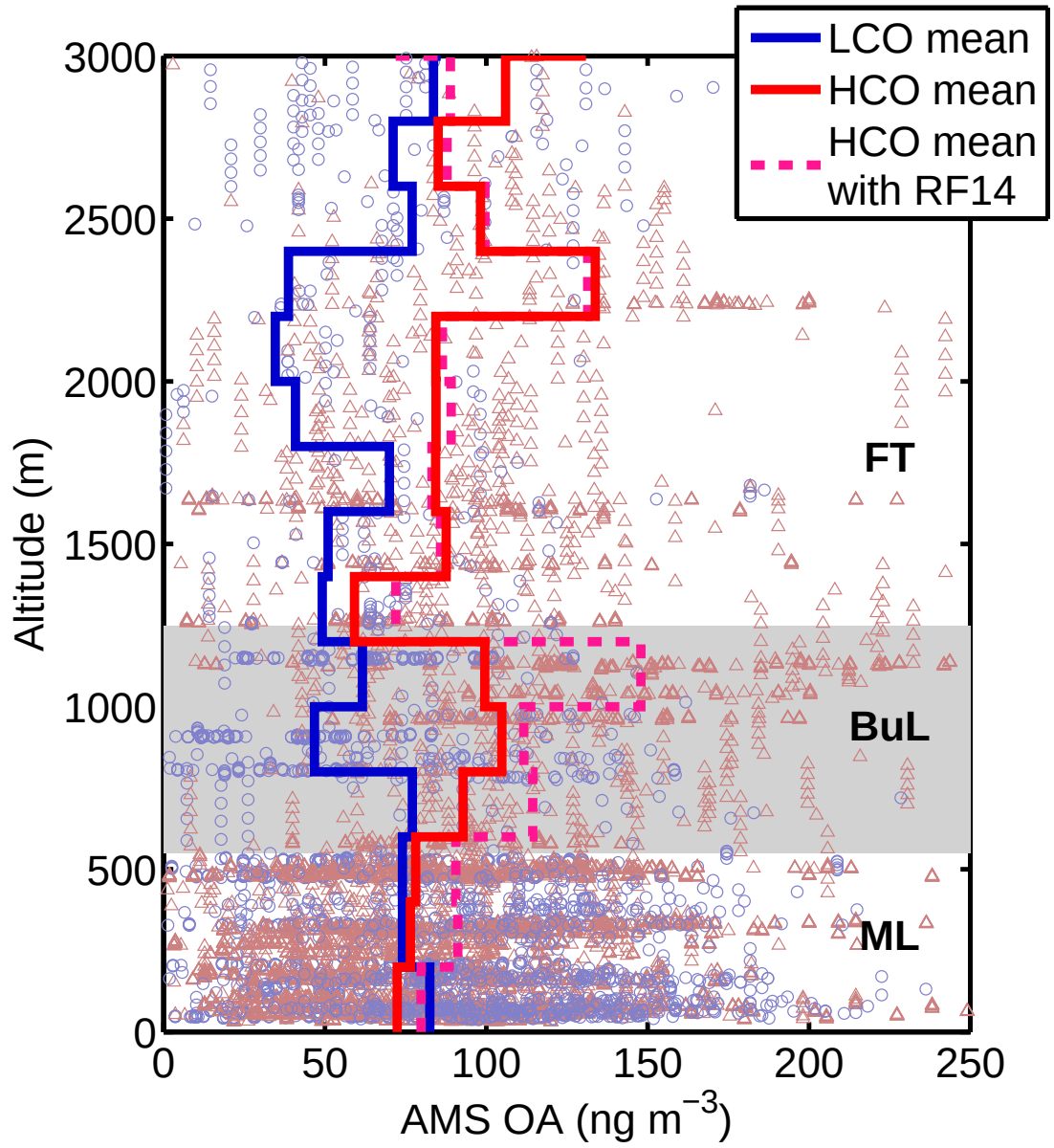

Figure 3.3: PASE altitude profiles of AMS submicrometer non-refractory OA, corrected using a factor of 5.5 derived from NSS comparisons between the AMS and impactor samples. Samples are sorted according to LCO (CO<63 ppbv, blue line) and HCO excluding RF14 (CO>63 ppbv, gray line) and averaged in 200 m bins. The HCO profile represented by the pink dashed line includes RF14, during which the highest overall CO values were measured in addition to a pollution plume in the lower FT. ML and BuL altitudes varied during PASE; average heights are shown.

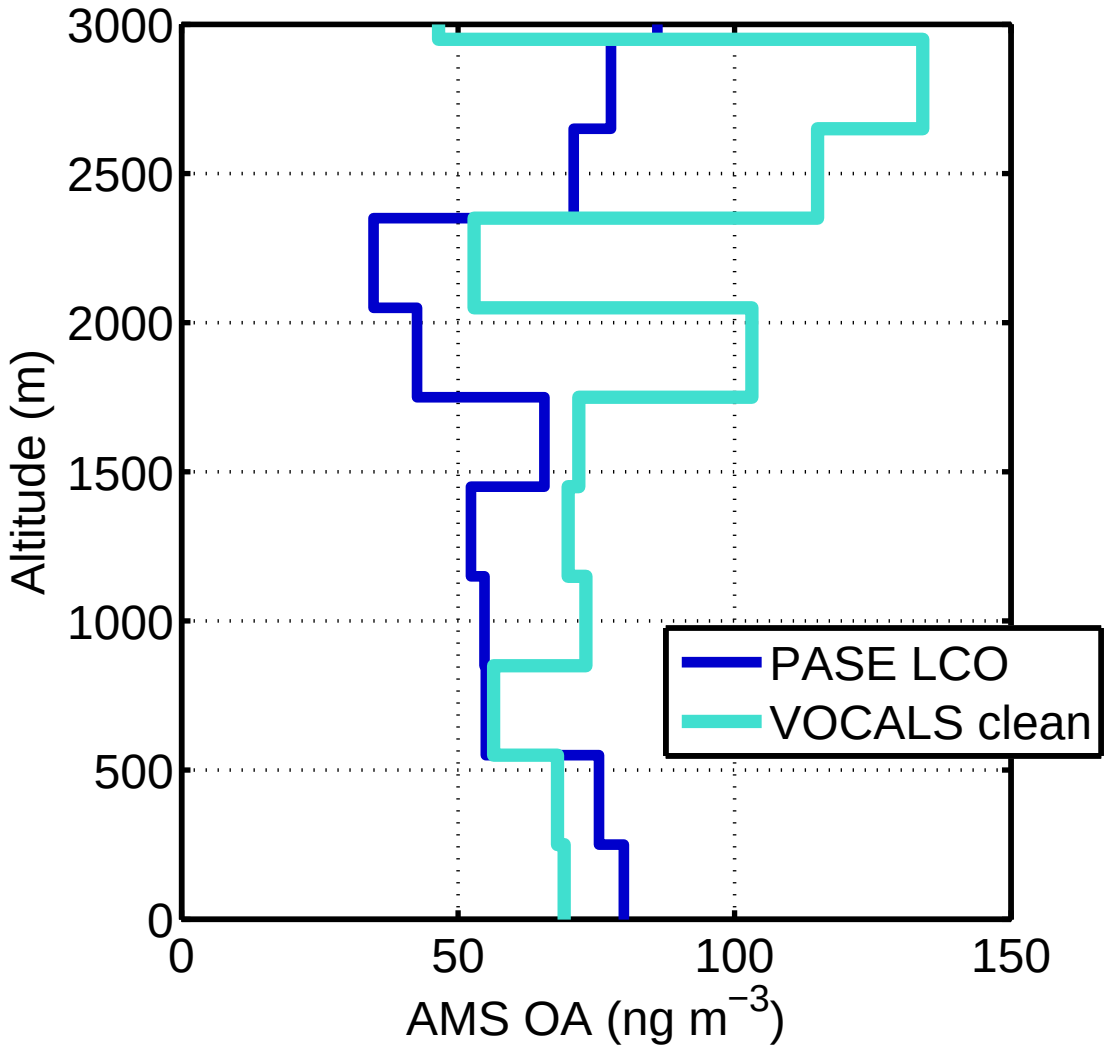

Figure 3.4: OA profiles in 300 m altitude bins for PASE and VOCALS C-130 (SE Pacific). To qualify as clean for VOCALS, CO concentrations had to fall below 61 ppbv (*Shank et al.*, 2012) and be west of 80°W Longitude to be relatively far from the South American continent.

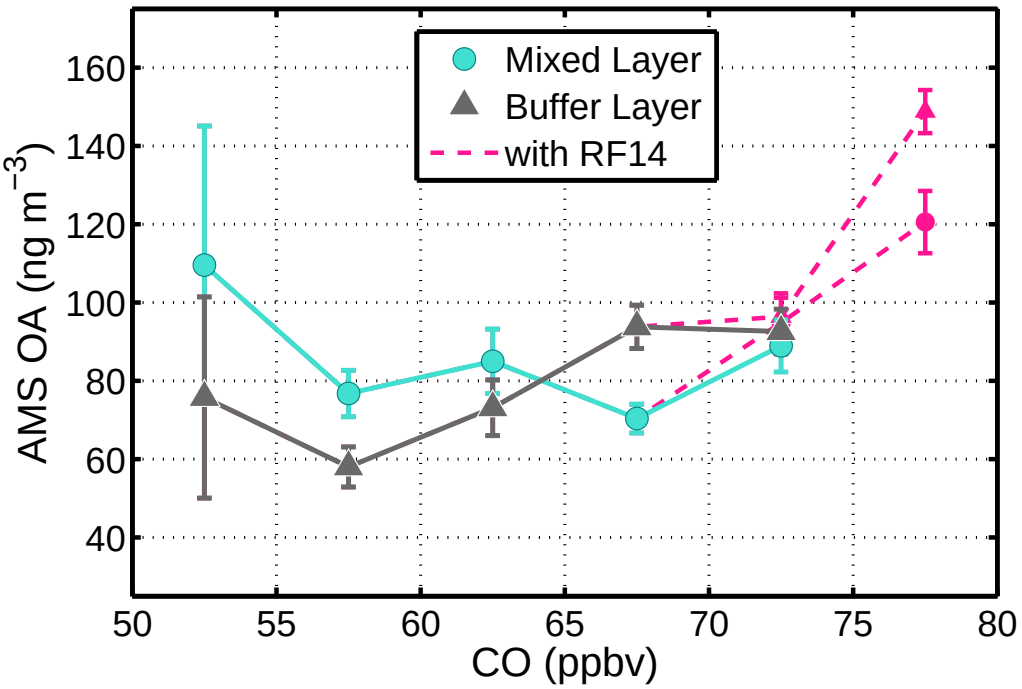

Figure 3.5: AMS OA averaged by 5 ppbv CO bins in the mixed layer (<550 m) and buffer layer (550 m - 1250 m). Error bars are standard errors of the mean.

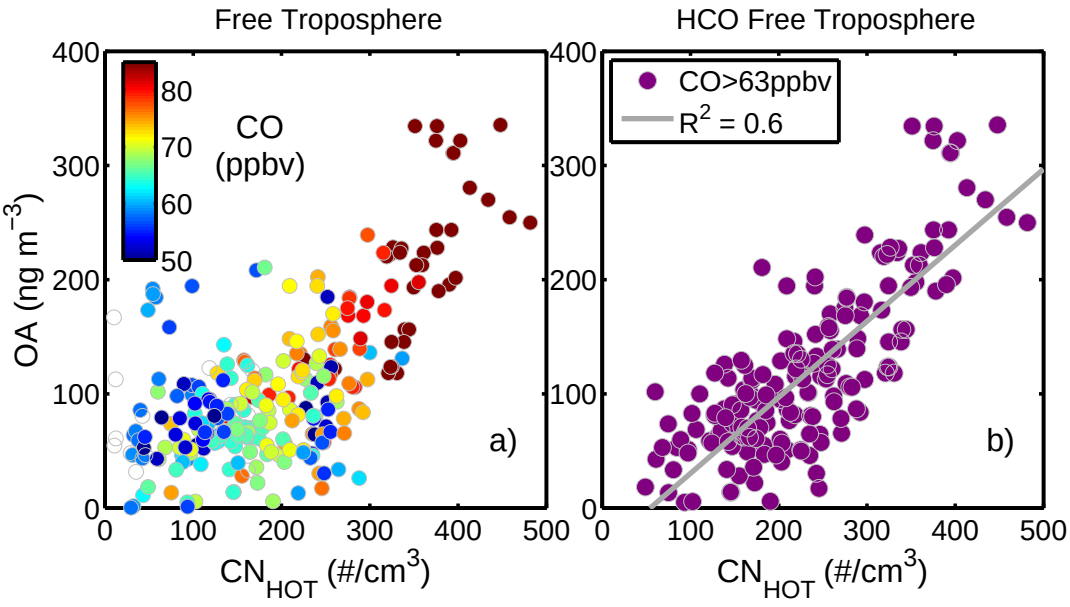

Figure 3.6: FT CNhot (refractory aerosol >10 nm after heating) versus OA (a) colored by CO ppbv and (b) fit to a linear function for only HCO air. Data points are 1 min averages of 10 s samples.

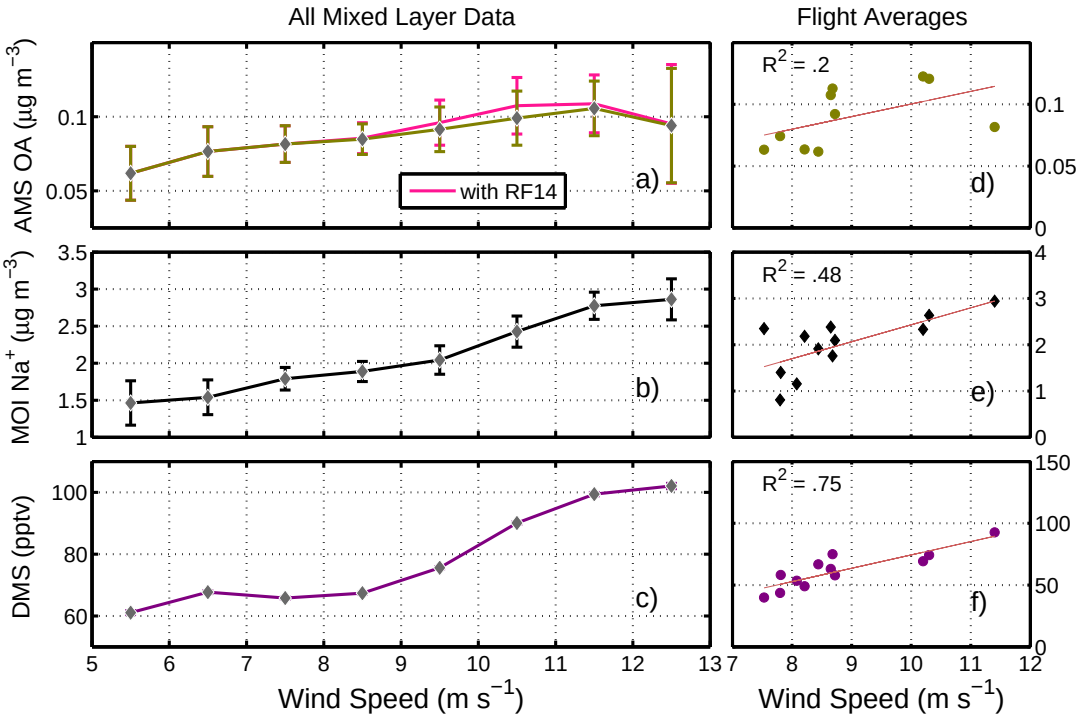

Figure 3.7: PASE OA (a), Na^+ (b), and DMS (c) averaged per $1\,m\,s^{-1}$ wind speed bins. The wind speed used here was measured in flight. Error bars signify standard errors of the mean (SEM). In (a), OA is averaged with RF14 (pink) and without RF14 (olive). OA is 10 s data, MOI Na^+ is 30 min data, and DMS is 1 s data.

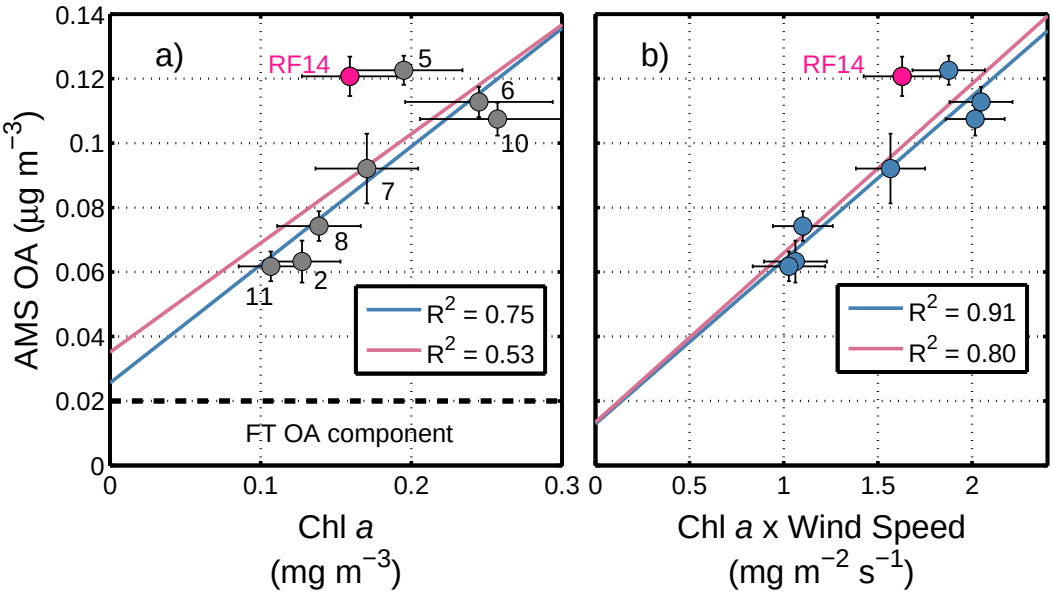

Figure 3.8: Flight-averaged AMS OA as a function of 24 h upwind MODIS Chl *a* concentrations and wind speed (WS). Numbers next to data points in (a) are research flight numbers. In (b), Chl *a* is multiplied by WS averaged from in-flight WS and 12 and 24 h upwind WS calculated from HYSPLIT back trajectories. Due to its potential for added OA from continental sources, RF14 has been excluded from the blue linear regressions. The pink regressions include RF14.

References

(), Particulate organic matter and chlorophyll in the surface layer of the equatorial Pacific Ocean along 135-degree-W., author=Pena, Angelica, journal=Mar. Ecol-Prog. Ser., volume=72, number=1, pages=179–188, year=1991.

Albert, M., M. Schaap, A. Manders, C. Scannell, C. O'Dowd, and G. de Leeuw (2012), Uncertainties in the determination of global sub-micron marine organic matter emissions, *Atmos. Environ.*, *57*, 289–300.

Aller, J. Y., M. R. Kuznetsova, C. J. Jahns, and P. F. Kemp (2005), The sea surface microlayer as a source of viral and bacterial enrichment in marine aerosols, *J. Aerosol Sci.*, *36*(5), 801–812.

Bandy, A., I. C. Faloona, B. W. Blomquist, B. J. Huebert, A. D. Clarke, S. G. Howell, R. L. Mauldin, C. A. Cantrell, J. G. Hudson, and B. G. Heikes (2012), Pacific Atmospheric Sulfur Experiment (PASE): dynamics and chemistry of the south Pacific tropical trade wind regime, *J. Atmos. Chem.*, pp. 1–21.

Bandy, A. R., D. C. Thornton, B. W. Blomquist, S. Chen, T. P. Wade, J. C. Ianni, G. M. Mitchell, and W. Nadler (1996), Chemistry of dimethyl sulfide in the equatorial Pacific atmosphere, *J. Geophys. Res.*, *23*, 741–744.

Bandy, A. R., D. C. Thornton, F. H. Tu, B. W. Blomquist, W. Nadler, G. M. Mitchell, and D. H. Lenschow (2002), Determination of the vertical flux of

dimethyl sulfide by eddy correlation and atmospheric pressure ionization mass spectrometry (APIMS), *J. Geophys. Res.*, *107*, doi:10.1029/2002JD002472.

Bates, T., P. Quinn, A. Frossard, L. Russell, J. Hakala, T. Petäjä, M. Kulmala, D. Covert, C. Cappa, S.-M. Li, et al. (2012), Measurements of ocean derived aerosol off the coast of california, *J. Geophys. Res.*, *117*(D21).

Blanchard, D. C., and L. D. Syzdek (1982), Water-to-air transfer and enrichment of bacteria in drops from bursting bubbles, *Appl. Environ. Microb.*, *43*(5), 1001–1005.

Burrows, S., O. Ogunro, A. Frossard, L. Russell, P. Rasch, and S. Elliott (2014), A physically-based framework for modelling the organic fractionation of sea spray aerosol from bubble film Langmuir equilibria, *Atmos. Chem. Phys.*, *14*, 13,601–13,629.

Carlson, C., and H. Ducklow (1995), Dissolved organic carbon in the upper ocean of the central equatorial Pacific Ocean, 1992: Daily and finescale vertical variations, *Deep Sea Res. II*, *42*(2), 639–656.

Chavez, F. P., and R. T. Barber (1987), An estimate of new production in the equatorial Pacific, *Deep Sea Res.*, *34*(7), 1229–1243.

Clarke, A., and V. Kapustin (2010), Hemispheric aerosol vertical profiles: Anthropogenic impacts on optical depth and cloud nuclei, *Science*, *329*(5998), 1488–1492.

Clarke, A., C. McNaughton, V. Kapustin, Y. Shinozuka, S. Howell, J. Dibb, J. Zhou, B. Anderson, V. Brekhovskikh, H. Turner, et al. (2007), Biomass burning and pollution aerosol over North America: Organic components and their influence on spectral optical properties and humidification response, *J. Geophys. Res.*, *112*(D12).

Clarke, A., S. Freitag, R. Simpson, J. Hudson, S. Howell, V. Brekhovskikh, T. Campos, V. Kapustin, and J. Zhou (2013), Free troposphere as a major source of CCN for the equatorial Pacific boundary layer: Long-range transport and teleconnections, *Atmos. Chem. Phys.*, *13*(15), 7511–7529.

Clarke, A. D., S. R. Owens, and J. Zhou (2006), An ultrafine sea-salt flux from breaking waves: Implications for cloud condensation nuclei in the remote marine atmosphere, *J. Geophys. Res.*, *111*(D6).

Collins, D., D. Zhao, M. Ruppel, O. Laskina, J. Grandquist, R. Modini, M. Stokes, L. Russell, T. Bertram, V. Grassian, et al. (2014), Direct aerosol chemical composition measurements to evaluate the physicochemical differences between controlled sea spray aerosol generation schemes, *Atmos. Meas. Techniques*, *7*(11), 3667–3683.

Collins, D. B., A. P. Ault, R. C. Moffet, M. J. Ruppel, L. A. Cuadra-Rodriguez, T. L. Guasco, C. E. Corrigan, B. E. Pedler, F. Azam, L. I. Aluwihare, et al. (2013), Impact of marine biogeochemistry on the chemical mixing state and cloud forming ability of nascent sea spray aerosol, *J. Geophys. Res.*, *118*(15), 8553–8565.

Conley, S., I. Faloona, D. Lenschow, T. Campos, C. Heizer, A. Weinheimer, C. Cantrell, R. Mauldin, R. Hornbrook, I. Pollack, et al. (2011), A complete dynamical ozone budget measured in the tropical marine boundary layer during PASE, *J. Atmos. Chem.*, *68*(1), 55–70, doi:10.1007/s10874-011-9195-0.

Conley, S. A., I. Faloona, G. H. Miller, B. Blomquist, D. Lenschow, and A. Bandy (2009), Closing the dimethyl sulfide budget in the tropical marine boundary layer during the Pacific Atmospheric Sulfur Experiment, *Atmos. Chem. Phys.*, *9*(22), 8745–8756.

DeCarlo, P., I. Ulbrich, J. Crounse, B. d. Foy, E. Dunlea, A. Aiken, D. Knapp, A. Weinheimer, T. Campos, P. Wennberg, et al. (2010), Investigation of the sources and processing of organic aerosol over the Central Mexican Plateau from aircraft measurements during MILAGRO, *Atmos. Chem. Phys.*, *10*(12), 5257–5280.

Draxler, R., and G. Rolph (2013), HYSPLIT (HYbrid Single-Particle Lagrangian Integrated Trajectory) Model access via NOAA ARL READY website (http://www.arl.noaa.gov/hysplit.php), *NOAA Air Resources Laboratory*.

Facchini, M. C., M. Rinaldi, S. Decesari, C. Carbone, E. Finessi, M. Mircea, S. Fuzzi, D. Ceburnis, R. Flanagan, E. D. Nilsson, et al. (2008), Primary submicron marine aerosol dominated by insoluble organic colloids and aggregates, *Geophys. Res. Lett.*, *35*(17).

Freitag, S., A. Clarke, S. Howell, V. Kapustin, T. Campos, V. Brekhovskikh, and J. Zhou (2013), Assimilating airborne gas and aerosol measurements into HYSPLIT: a visualization tool for simultaneous assessment of air mass history and back trajectory reliability, *Atmos. Meas. Tech. Discuss.*, *6*, 5345–5399.

Frossard, A. A., L. M. Russell, P. Massoli, T. S. Bates, and P. K. Quinn (2014a), Side-by-side comparison of four techniques explains the apparent differences in the organic composition of generated and ambient marine aerosol particles, *Aerosol Sci. Tech.*, *48*(3), v–x.

Frossard, A. A., L. M. Russell, S. M. Burrows, S. M. Elliott, T. S. Bates, and P. K. Quinn (2014b), Sources and composition of submicron organic mass in marine aerosol particles, *J. Geophys. Res.*, *119*(22), 12–977.

Gantt, B., N. Meskhidze, and D. Kamykowski (2009), A new physically-based

quantification of marine isoprene and primary organic aerosol emissions, *Atmos. Chem. Phys.*, *9*(14), 4915–4927.

Gantt, B., N. Meskhidze, M. Facchini, M. Rinaldi, D. Ceburnis, and C. O'Dowd (2011), Wind speed dependent size-resolved parameterization for the organic mass fraction of sea spray aerosol, *Atmos. Chem. Phys.*, *11*(16), 8777–8790.

Gantt, B., M. Johnson, N. Meskhidze, J. Sciare, J. Ovadnevaite, D. Ceburnis, and C. O'Dowd (2012), Model evaluation of marine primary organic aerosol emission schemes, *Atmos. Chem. Phys.*, *12*(18), 8553–8566.

Gerbig, C., S. Schmitgen, D. Kley, A. Volz-Thomas, K. Dewey, and D. Haaks (1999), An improved fast-response vacuum-UV resonance fluorescence CO instrument, *J. Geophys. Res.*, *104*(D1), 1699–1704.

Gloudemans, A., A. De Laat, H. Schrijver, I. Aben, J. Meirink, and G. van der Werf (2009), SCIAMACHY CO over land and oceans: 2003–2007 interannual variability, *Atmos. Chem. Phys.*, *9*(11), 3799–3813.

Gordon, H. R., and B. A. Franz (2008), Remote sensing of ocean color: Assessment of the water-leaving radiance bidirectional effects on the atmospheric diffuse transmittance for SeaWiFS and MODIS intercomparisons, *Remote Sens. Environ.*, *112*(5), 2677–2685.

Gregg, W. W., and N. W. Casey (2004), Global and regional evaluation of the SeaWiFS chlorophyll data set, *Remote Sens. Environ.*, *93*(4), 463–479.

Gregg, W. W., and N. W. Casey (2007), Sampling biases in MODIS and SeaWiFS ocean chlorophyll data, *Remote Sens. Environ.*, *111*(1), 25–35.

Hasumi, H., and T. Nagata (2014), Modeling the global cycle of marine dissolved organic matter and its influence on marine productivity, *Ecological Modelling*, *288*, 9–24.

Hawkins, L. N., and L. M. Russell (2010), Polysaccharides, proteins, and phytoplankton fragments: four chemically distinct types of marine primary organic aerosol classified by single particle spectromicroscopy, *Adv. Meteorol.*, *2010*.

Hooghiemstra, P., M. Krol, v. T. Leeuwen, v. d. G. Werf, P. Novelli, M. Deeter, I. Aben, and T. Röckmann (2012), Interannual variability of carbon monoxide emission estimates over South America from 2006 to 2010, *J. Geophys. Res.*, *117*(D15).

Huebert, B., D. Wylie, L. Zhuang, and J. Heath (1996), Production and loss of methanesulfonate and non-sea salt sulfate in the equatorial Pacific marine boundary layer, *Geophys. Res. Lett.*, *23*(7), 737–740.

Huebert, B., B. Blomquist, M. Yang, S. Archer, P. Nightingale, M. Yelland, J. Stephens, R. Pascal, and B. Moat (2010), Linearity of DMS transfer coefficient with both friction velocity and wind speed in the moderate wind speed range, *Geophys. Res. Lett.*, *37*(1).

Huebert, B. J., B. W. Blomquist, J. Hare, C. Fairall, J. E. Johnson, and T. S. Bates (2004), Measurement of the sea-air DMS flux and transfer velocity using eddy correlation, *Geophys. Res. Lett.*, *31*(23), L23,113.

IPCC-AR5 (2013), *Climate Change 2013: The Physical Science Basis. Contribution of Working Group I to the Fifth Assessment Report of the Intergovernmental Panel on Climate Change*, 1535 pp., Cambridge University Press, Cambridge, United Kingdom and New York, NY, USA, doi:10.1017/CBO9781107415324.

Kuznetsova, M., C. Lee, and J. Aller (2005), Characterization of the proteinaceous matter in marine aerosols, *Marine Chem.*, *96*(3), 359–377.

Landry, M., R. Barber, R. Bidigare, F. Chai, K. Coale, H. Dam, M. Lewis, S. Lindley, J. McCarthy, and M. Roman (1997), Iron and grazing constraints on pri-

mary production in the central equatorial Pacific: An EqPac synthesis, *Limnol. Oceanogr*, *42*(3), 405–418.

Law, C. S., E. Brévière, G. de Leeuw, V. Garçon, C. Guieu, D. J. Kieber, S. Kontradowitz, A. Paulmier, P. K. Quinn, E. S. Saltzman, et al. (2013), Evolving research directions in Surface Ocean–Lower Atmosphere (SOLAS) science, *Environ. Chem.*, *10*(1), 1–16.

Leck, C., and E. K. Bigg (2005), Biogenic particles in the surface microlayer and overlaying atmosphere in the central Arctic Ocean during summer, *Tellus B*, *57*(4), 305–316.

Legendre, L., and J. Michaud (1999), Chlorophyll a to estimate the particulate organic carbon available as food to large zooplankton in the euphotic zone of oceans, *J. Plankton Res.*, *21*(11), 2067–2083.

Lewis, R., and E. Schwartz (2004), *Sea Salt Aerosol Production: Mechanisms, Methods, Measurements and Models – A Critical Review*, vol. 152, American Geophysical Union.

Liss, P., and L. Merlivat (1986), Air-sea gas exchange rates: Introduction and synthesis, in *The Role of Air-Sea Exchange in Geochemical Cycling*, edited by P. Buat-Menard, pp. 113–127, D. Reidel.

Matsumoto, K., Y. Ishii, S. Kim, N. Kaneyasu, and H. Kobayashi (2014), Volatility of water-soluble organic carbon in ambient aerosols, *J. Aerosol Sci.*, *67*, 38–47.

Middlebrook, A. M., R. Bahreini, J. L. Jimenez, and M. R. Canagaratna (2012), Evaluation of composition-dependent collection efficiencies for the Aerodyne aerosol mass spectrometer using field data, *Aerosol Sci. Tech.*, *46*(3), 258–271.

Murray, J. W., R. T. Barber, M. R. Roman, M. P. Bacon, and R. A. Feely (1994), Physical and biological controls on carbon cycling in the equatorial pacific, *Science*, *266*(5182), 58–65.

Myriokefalitakis, S., E. Vignati, K. Tsigaridis, C. Papadimas, J. Sciare, N. Mihalopoulos, M. C. Facchini, M. Rinaldi, F. J. Dentener, D. Ceburnis, et al. (2010), Global modeling of the oceanic source of organic aerosols, *Adv. Meteorol.*, *2010*.

O'Dowd, C. D., B. Langmann, S. Varghese, C. Scannell, D. Ceburnis, and M. C. Facchini (2008), A combined organic-inorganic sea-spray source function, *Geophys. Res. Lett.*, *35*(1).

O'Reilly, J. E., S. Maritorena, B. G. Mitchell, D. A. Siegel, K. L. Carder, S. A. Garver, M. Kahru, and C. McClain (1998), Ocean color chlorophyll algorithms for SeaWiFS, *J. Geophys. Res.*, *103*(C11), 24,937–24,953.

Pennington, J. T., K. L. Mahoney, V. S. Kuwahara, D. D. Kolber, R. Calienes, and F. P. Chavez (2006), Primary production in the eastern tropical Pacific: A review, *Prog. Oceanogr.*, *69*(2), 285–317.

Pfister, G., L. Emmons, D. Edwards, A. Arellano, G. Sachse, and T. Campos (2010), Variability of springtime transpacific pollution transport during 2000–2006: the INTEX-B mission in the context of previous years, *Atmos. Chem. Phys.*, *10*(3), 1345–1359.

Prather, K. A., T. H. Bertram, V. H. Grassian, G. B. Deane, M. D. Stokes, P. J. DeMott, L. I. Aluwihare, B. P. Palenik, F. Azam, J. H. Seinfeld, et al. (2013), Bringing the ocean into the laboratory to probe the chemical complexity of sea spray aerosol, *P. Natl. Acad. Sci.*, *110*(19), 7550–7555.

Quinn, P. K., T. S. Bates, K. S. Schulz, D. Coffman, A. Frossard, L. Russell, W. Keene, and D. Kieber (2014), Contribution of sea surface carbon pool to organic matter enrichment in sea spray aerosol, *Nature Geosci.*, *7*(3), 228–232.

Rinaldi, M., S. Fuzzi, S. Decesari, S. Marullo, R. Santoleri, A. Provenzale, J. Hardenberg, D. Ceburnis, A. Vaishya, C. D. O'Dowd, et al. (2013), Is chlorophyll-a the best surrogate for organic matter enrichment in submicron primary marine aerosol?, *J. Geophys. Res.*, *118*, doi:10.1002/jgrd.50417.

Roelofs, G. (2008), A gcm study of organic matter in marine aerosol and its potential contribution to cloud drop activation, *Atmos. Chem. Phys.*, *8*(3), 709–719.

Russell, L. M., L. N. Hawkins, A. A. Frossard, P. K. Quinn, and T. S. Bates (2010), Carbohydrate-like composition of submicron atmospheric particles and their production from ocean bubble bursting, *Proc. Natl Acad. Sci.*, *107*(15), 6652–6657.

Schwier, A., C. Rose, E. Asmi, A. Ebling, W. Landing, S. Marro, M.-L. Pedrotti, A. Sallon, F. Iuculano, S. Agusti, et al. (2015), Primary marine aerosol emissions from the Mediterranean Sea during pre-bloom and oligotrophic conditions: correlations to seawater chlorophyll *a* from a mesocosm study, *Atmos. Chem. Phys.*, *15*(14), 7961–7976.

Sciare, J., O. Favez, R. Sarda-Estève, K. Oikonomou, H. Cachier, and V. Kazan (2009), Long-term observations of carbonaceous aerosols in the austral ocean atmosphere: Evidence of a biogenic marine organic source, *J. Geophys. Res.*, *114*(D15).

Seinfeld, J. H., and S. N. Pandis (2006), *Atmospheric Chemistry and Physics: From Air Pollution to Climate Change*, 2 ed., John Wiley and Sons, Inc., New York.

Sellegri, K., C. O'Dowd, Y. Yoon, S. Jennings, and G. de Leeuw (2006), Surfactants and submicron sea spray generation, *J. Geophys. Res.*, *111*(D22).

Shank, L., S. Howell, A. Clarke, S. Freitag, V. Brekhovskikh, V. Kapustin, C. McNaughton, T. Campos, and R. Wood (2012), Organic matter and non-refractory aerosol over the remote southeast Pacific: oceanic and combustion sources, *Atmos. Chem. Phys.*, *12*(1), 557–576.

Simpson, R. (2010), Mechanisms of sulfate formation in the equatorial Pacific marine boundary layer, M.S. thesis, Univ. Hawai'i, Mānoa, Honolulu.

Simpson, R. M., S. G. Howell, B. W. Blomquist, A. D. Clarke, and B. J. Huebert (2014), Dimethyl sulfide: Less important than long-range transport as a source of sulfate to the remote tropical Pacific marine boundary layer, *J. Geophys. Res.*, *119*(14), 9142–9167.

Spracklen, D. V., S. R. Arnold, J. Sciare, K. S. Carslaw, and C. Pio (2008), Globally significant oceanic source of organic carbon aerosol, *Geophys. Res. Lett.*, *35*(12).

Tseng, R.-S., J. T. Viechnicki, R. A. Skop, and J. W. Brown (1992), Sea-to-air transfer of surface-active organic compounds by bursting bubbles, *J. Geophys. Res.*, *97*(C4), 5201–5206.

Vignati, E., M. Facchini, M. Rinaldi, C. Scannell, D. Ceburnis, J. Sciare, M. Kanakidou, S. Myriokefalitakis, F. Dentener, and C. O'Dowd (2010), Global scale emission and distribution of sea-spray aerosol: Sea-salt and organic enrichment, *Atmos. Environ.*, *44*(5), 670–677.

Wang, X., R. Murtugudde, E. Hackert, and E. Marañón (2013), Phytoplankton carbon and chlorophyll distributions in the equatorial Pacific and Atlantic: a basin-scale comparative study, *J. Marine Syst.*, *109*, 138–148.

Westervelt, D., R. Moore, A. Nenes, and P. Adams (2012), Effect of primary organic sea spray emissions on cloud condensation nuclei concentrations, *Atmos. Chem. Phys.*, *12*(1), 89–101.

Wood, R., and C. Bretherton (2004), Boundary layer depth, entrainment, and decoupling in the cloud-capped subtropical and tropical marine boundary layer, *J. Climate*, *17*(18), 3576–3588.

Chapter 4

Revising concepts of methanesulfonic acid (MSA) formation in the remote tropical Pacific marine boundary layer using high-resolution measurements and a thermodynamic model of aerosol chemistry

Abstract

We report and interpret high-resolution MSA and MS^- measurements collected during a field campaign in the tropical Pacific marine boundary layer (MBL). An

earlier study noted vapor-phase MSA was twice as concentrated near the ocean surface as at the top of the mixed layer. We use aerosol composition measurements and the online Extended AIM Aerosol Thermodynamics Model (*E-AIM*; *Clegg et al.* (1998)) to demonstrate that this pattern is due to evaporation of particulate MSA from sulfuric acid-dominated particles. We cannot rule out the possibility of a small homogeneous production source.

Up to 99 % of the MS^- in aerosol forms in the aqueous phase after DMSO/MSIA vapor is wet-scavenged and oxidized to MS^- in aerosol water and cloud droplets. More alkaline coarse-mode aerosol generates MS^- by this mechanism and gathers MSA evading from fine particles. It is not clear which of these paths is more important. The lower FT is a source of MSA to the buffer layer (BuL) (entrainment flux: 9.9×10^{11} molecules/cm^2/d), probably dissolving in cloud droplets and emerging below cloud as find-mode MS^-. Most fine-mode MS^-, however, is formed in cloud from DMSO/MSIA, while coarse-mode MS^- is formed on sea salt particles that have greater alkalinity.

4.1 Introduction

Over remote ocean environments, dimethyl sulfide (DMS) and its main oxidation products such as SO_2, SO_4^{2-}, dimethyl sulfoxide (DMSO), and methane sulfonic acid (MSA) have been the subjects of much study and debate concerning the sources of natural aerosol and cloud condensation nuclei (CCN). The paucity of measurements in isolated marine regions has hindered our understanding of the chemical processes that influence marine aerosol. MSA vapor in the marine boundary layer (MBL) is a product of the OH radical-initiated oxidation of DMS emitted from the ocean. MSA and its condensed-phase anion, methane sulfonate (MS^-), are two natural organo-sulfur compounds that are often measured but are inadequately characterized.

Throughout this paper, MSA always refers to the vapor while MS^- always refers to the aerosol species due to its high degree of dissociation once in solution (on wetted particles). As MSA and MS^- are thought to be exclusively of marine biological origin, they are often used to estimate the oceanic source strength among sulfur products (*Saltzman et al.*, 1986; *Savoie and Prospero*, 1989; *Ayers et al.*, 1996; *Gondwe et al.*, 2004). However, our inadequate understanding of the processes connecting MSA and MS^- obscures the nature of their interrelatedness and their influence on marine aerosol properties.

OH can react with DMS by either addition or by extraction of an H atom. The latter yields SO_2 and ultimately H_2SO_4 after several steps; only the addition pathway is thought to produce MSA (Fig. 4.1). In the low-NO_x MBL (Figure 4.1), the addition channel of the DMS-OH reaction is the pathway presumed capable of producing the majority of MSA and its condensed-phase anion, methanesulfonate (MS^-), by way of intermediate species dimethyl sulfoxide (DMSO) and methane sulfinic acid (MSIA) (*Davis et al.*, 1999; *Urbanski et al.*, 1998; *Arsene et al.*, 2002). However, whether this reaction pathway largely proceeds through the gas phase or the aqueous phase is at issue. In the tropics, the temperature-dependent addition channel is less favorable than in high-latitude regions and represents $\sim$25 % of the DMS-OH reaction. The other $\sim$75 % is the abstraction channel, which yields SO_2 and H_2SO_4 (*Yin et al.*, 1990; *Turnipseed and Ravishankara*, 1993; *Turnipseed et al.*, 1996). However, the bifurcation of the DMS-OH reaction mechanisms is not complete; recent lab (*Arsene et al.*, 2002; *Kukui et al.*, 2003) and theoretical (*Tian et al.*, 2007; *González-García et al.*, 2007) studies have revealed that the main gas-phase product of MSIA is SO_2.

Although the only reported MSA formed in lab studies required high NO_x concentrations (e.g. *Hatakeyama and Akimoto*, 1983; *Yin et al.*, 1990), there is clearly at least one pathway to form MSA in the tropical MBL without NO_x. Despite not being directly observed as a product in artificially simulated clean MBL

conditions (*Berndt and Richters*, 2012), the homogeneous pathway that *Davis et al.* (1998) thought could form MSA in the MBL is OH oxidation of DMSO to MSIA followed by OH oxidation of MSIA to MSA (dashed black arrow in Fig. 4.1). Yet recent laboratory studies indicate that this reaction yields primarily SO_2 and $\leq$1 % of MSA (*Arsene et al.*, 2002; *Kukui et al.*, 2003). Despite the established (abstraction channel) mechanism's requirement for multiple steps of elevated O_3 and/or NO_x typical of more coastal regions (*Yin et al.*, 1990), many still assume that all MSA vapor is homogeneously produced in the remote MBL (e.g., *Zhang et al.*, 2014).

As for particulate MS^-, condensation of MSA vapor onto aerosol was thought to be its production mechanism. However, improved measurements of MSA and MS^- in the field consistently reveal a large disparity: aerosol MS^- is larger than MSA vapor by at least 2 orders of magnitude. According to numerous combined field and model studies, computed vapor condensation rates are much too small to explain particulate MS^- MBL measurements unless an unrealistically long aerosol lifetime of 10 days (or in Antarctic cases, much longer) is assumed (*Jefferson et al.*, 1998; *Davis et al.*, 1998; *Chen et al.*, 2000; *Mihalopoulos et al.*, 2007). This casts serious doubt upon the viability of an exclusively gas-phase MSA production mechanism to sustain ambient particulate MS^- levels in any MBL environment.

Recent literature consensus supports aqueous-phase production of MS^- through uptake and oxidation of the soluble addition-channel compound DMSO and/or its oxidation product MSIA (Figure 4.1). [DMSO] is $\sim$ 4 orders of magnitude higher than [MSA], so its uptake rate by particles will be correspondingly larger. It is now thought that at most, MS^- accreted from homogeneously produced MSA contributes $\sim$3 % of MS^- (*Zhu et al.*, 2006; *Davis et al.*, 1998; *Glasow and Crutzen*, 2004). Despite lacking in situ empirical evidence that particulate MS^- forms via aqueous production, multiphase chemistry is kinetically favored to form the observed sulfur product distribution. Many authors regard the heterogeneous path-

way as the main contributor to MS^- production/DMSO loss (*Falbe-Hansen et al.*, 2000; *Sciare et al.*, 2000; *Campolongo et al.*, 1999; *Legrand et al.*, 2001; *Kerminen and Leck*, 2001; *Zhu et al.*, 2006), and lab studies have shown this reaction to be very rapid at 298 K, tropical MBL temperature (*Bardouki et al.*, 2002; *Zhu et al.*, 2003a).

As the substantial variability in aqueous DMSO-OH yields across lab studies (*Arsene et al.*, 2001) and DMSO concentrations across field studies (*Bandy et al.*, 1996; *Sciare et al.*, 2000) attest, this intermediate is not well understood and is sensitive to ambient conditions such as relative humidity, temperature, and NO_x (*Davis et al.*, 1998; *Arsene et al.*, 2001). In the typically NO_x-free conditions of the remote MBL, the gas-phase DMS-OH mechanisms may produce MSA only in trace amounts (*Albu et al.*, 2006) if at all (*Berndt and Richters*, 2012). (Notably, $[NO_x]$-free means <1 ppbv for many of the cited lab studies, whereas in the remote oceanic atmosphere it means <10 pptv.)

Because it is a highly soluble strong acid, MSA in the MBL largely partitions into the condensed phase (to MS^-), which may include hydrated particles and cloud droplets. Indeed, its Henry's Law constant at 298 K is so high that its presence in the gas phase is only possible at low relative humidity (RH) or low pH. Though undoubtedly high, MSA's actual K_H value is not well known and estimates span a few orders of magnitude ($1 \times 10^9\,\mathrm{M\,atm^{-1}}$: *Campolongo et al.* (1999); $\sim 1 \times 10^{13}\,\mathrm{M\,atm^{-1}}$: *Clegg and Brimblecombe* (1985)) depending on the method. Particulate pHs around -1 or below would (a) prevent MSA vapor from significantly adsorbing to submicrometer particles or (b) cause MSA to "salt out" of MS^- solution, as its $pK_a < -1$ ($K_a = 73$). Such a low pH is possible in fine-mode particles that are predominantly composed of cloud-generated sulfate (with little NH_4^+) and are thus highly concentrated sulfuric acid solutions.

In the remote tropics, the lack of other aerosol components that are typical of continental particles (especially alkaline cations like NH_4^+) limits the submicrom-

eter alkalinity. This scenario is likely in PASE, as we will demonstrate, and may lead to evasion of MSA from MS^--containing fine particles in the ML (green arrow in Figure 4.1). As far as we know, this has not been suggested as a mechanism of MSA vapor formation in the ML. But to complete the mechanism, viable avenues for aerosol MS^- formation are needed.

Even though we focus on evasion of MSA from the fine mode, most MS^- mass is actually on the coarse mode in the tropics (*Huebert et al.*, 1996). At higher latitudes, most MS^- is fine (*Quinn et al.*, 1996; *Jefferson et al.*, 1998; *Legrand et al.*, 2001; *Kerminen and Leck*, 2001). Possible coarse MS^- production routes include 1) uptake of DMSO (or its oxidation products) with subsequent liquid-phase oxidation and 2) cloud processing of DMSO/MSIA in the BuL. Thus far, there have not been any mechanisms developed that can both resolve the MS^- observations and unify them with MSA vapor concentrations.

Hindered by the complexity of studying DMS oxidation's many mechanisms in the ambient MBL, we still do not fully understand the formation of MSA and MS^- (*Lucas and Prinn*, 2005; *Barnes et al.*, 2006), nor do we understand their relationship to each other. The story of MSA and MS^- depends on quantifying very poorly understood intermediate species and their role in multiphase chemistry. Lab studies provide insight into gas-phase reactions but are unable to integrate them with the complicated condensed-phase chemistry of aerosol particles and cloud droplets. Depending on the conditions, methods, and instruments used to generate and measure gases, sulfur oxidation studies often yield different results for the same principal reactions (e.g., *Arsene et al.*, 2001; *Barnes et al.*, 2006; *Jensen et al.*, 1992; *Sørensen et al.*, 1996; *Kukui et al.*, 2003; *Berndt and Richters*, 2012).

We now have a more complete suite of observations for a well-posed study of ambient MSA formation. Our study aims to reconstruct the likely pathways that lead to observed MSA and MS^- concentrations in the remote tropical MBL. The sulfur cycle species available to us include gas-phase (DMS, SO_2, MSA, H_2SO_4,

OH, O_3) and aerosol-phase (MS^-, NSS, Na^+) airborne measurements made in the equatorial Pacific MBL. Featuring impactor-measured, size-resolved particulate MS^- in concert with MSA vapor measurements in 30 min level legs, we have a unique data set that enables a more comprehensive interpretation of MSA's origins in the MBL.

In a previous study, *Zhang et al.* (2014), took a 1-D model approach to constructing an MSA budget in the PASE MBL using PASE MSA concentrations and a limited selection of other available measurements. Though our two studies were inspired to explain the same exceptional feature in the MSA data, we view the question through the lens of physical chemistry whereas *Zhang et al.* (2014) view it through the lens of a 1-D dynamic model. Consequently, we develop decidedly different hypotheses to explain the MSA observations.

4.2 Measurements and Calculations

4.2.1 PASE

The Pacific Atmospheric Sulfur Experiment (PASE) was conducted in the meteorological Southern Hemisphere tropical trade-wind regime of the central Pacific Ocean (*Bandy et al.*, 2012). The NCAR C-130 research aircraft was based at Christmas Island (2° N, 156° W) and flew to the east over the equatorial Pacific upwelling regime. During each flight, a series of 30 min legs were flown in chevron patterns at varying altitudes: in the lower mixed layer (LML; ∼40 m to 200 m), the top of the mixed layer (TML; 200 m to 550 m), and the buffer layer (BuL; 550 m to 1250 m), which is also the cloud layer. A typical flight consisted of 3 of these stacks with a profile in-between stacks to sample the free troposphere (FT). Figure 4.2a shows the project-average boundaries for these vertical layers. The mixed layer (ML) = LML + TML, while the MBL = ML + BuL. The FT is thermally sepa-

rated from the MBL, and its undulating boundary may vary in altitude throughout the day in response to entrainment (*Simpson et al.*, 2014) and convection, though it did not change significantly during the four week PASE deployment due to the stable trade wind system. The southeasterly winds in the ML averaged $\sim$8 m s^{-1}. More information can be found in *Simpson et al.* (2014); meteorological conditions are further described in *Freitag et al.* (2013).

All but two flights were flown during daylight hours, generally from 0900 to 1700 local. The two early morning flights (RF6 and RF13) that spanned sunrise took off at 0200 and landed at 1000 local time. Highly convective regions were avoided by design. PASE observations reported in this study draw from flights 2, 3, and 5 through 14. We included RF09 and RF10, whereas *Zhang et al.* (2014) excluded them in their analysis of PASE MSA.

The PASE region is located in a region of large-scale subsidence with shallow trade-wind cumulus clouds populating the BuL. The mixed layer averaged $\sim$550 m, and the BuL above extended to the trade wind inversion (TWI) near 1250 m separating the BuL from the FT. The FT above the TWI never had any clouds or signs of recent convective activity.

4.2.2 Aerosol and Gas Measurements

PASE featured impactor-measured aerosol chemistry in concert with gas-phase measurements in 30 min level legs. A multi-orifice impactor (MOI) downstream of a well-characterized low-turbulence inlet (LTI; *Huebert et al.* (2004)) measured size-resolved aerosol chemistry on six stages and a backup filter; ions such as methane sulfonate (MS^-), oxalate, Na^+, Cl-, NO_3^-, NH_4^+, and non-sea-salt sulfate (NSS) were extracted and assayed by ion chromatography (IC). Details can be found in *Simpson* (2010). We could not quantify MS^- on the backup filter stage due to an analytical interference on the Teflon. Extensive MS^- measurements from this

region made in 1994 with similar impactors found that the filter only comprised 5 % of the total MS^- (*Huebert et al.*, 1996).

In addition to impactor NSS measurements, we also have high time-resolution submicrometer SO_4^{2-}, NH_4^+, and NO_3^- measured with a time-of-flight aerosol mass spectrometer (AMS) (*DeCarlo et al.*, 2006). The AMS is capable of measuring volatile particles from 0.03 µm to 0.6 µm. For further information on this instrument, see *Shank et al.* (2012); the same AMS was later deployed on VOCALS behind the same inlet system in the C-130.

Submicrometer number was measured with the optical particle counter (OPC, *Clarke et al.* (2013)) behind the solid diffuser inlet (SDI, *McNaughton et al.* (2007)), the same inlet used by the AMS. Submicrometer number distributions were measured by a long differential mobility analyzer (LDMA) also behind the same inlet. A TSI Model 3321 aerodynamic particle sizer (APS) measured detailed supermicrometer physical size distributions every minute. The APS (0.8 µm to 20 µm) and LDMA (∼0.01 µm to 0.5 µm) number distributions were converted to ambient distributions by assuming humidity-dependent diameters and densities for sea-salt and $(NH_4)_2H_2SO_4$, respectively.

DMS and SO_2 mixing ratios were measured with two atmospheric pressure ionization mass spectrometers (APIMS) (*Bandy et al.*, 2002) at 10 Hz with an internal standard.

MSA, OH radical, and H_2SO_4 vapors were measured using selected ion chemical ionization mass spectrometry (SICIMS) adapted for aircraft and capable of making 30 s measurements (*Mauldin et al.*, 1999). There were two nighttime sampling periods, but the SICIMS was only operational during one (RF13).

CO was measured using a vacuum UV resonance fluorescence instrument similar to that of *Gerbig et al.* (1999). Precision is reported as ±3 ppbv and accuracy as better than 10 % for a mixing ratio of 100 ppbv (*Pfister et al.*, 2010).

4.2.3 Aerosol Property Model: *E-AIM*

Particles remain liquid at the relative humidities (RH) in the tropical MBL. Because RH determines the volume of water associated with the condensed ions in particles, changes in RH instantly impact the aerosol water content. For example, a decrease in RH causes an increase in ion concentration and thus the ionic strength of the solution. To describe the ion interactions and gas-particle partitioning in these non-ideal solutions, it is necessary to include ion and solvent activities, osmotic coefficients, and relevant equilibrium constants (e.g., Henry's Law) as a function of temperature. Fortunately, there is an available model that calculates these parameters.

To obtain the requisite aerosol properties such as pH, volume, density, and $[SO_4^{2-}]$ molality, we inserted our project-average submicrometer AMS and supermicrometer MOI ion concentrations into the online Extended AIM Aerosol Thermodynamics Model (*E-AIM*; http://www.aim.env.uea.ac.uk/aim/aim.php). For fine-mode calculations, we used the average AMS SO_4^{2-}, NO_3^-, and NH_4^+ with Inorganic Model II (H^+, NH_4^+, SO_4^{2-}, NO_3^-, H_2O) at 298 K (*Clegg and Toumi*, 1998; *Carslaw et al.*, 1995; *Massucci et al.*, 1999; *Clegg and Brimblecombe*, 2005). For coarse-mode calculations, we used the average coarse MOI NSS, NO_3^-, NH_4^+, Na^+, and Cl^- as inputs to Inorganic Model III (H^+, NH_4^+, Na^+, SO_4^{2-}, NO_3^-, Cl^-, H_2O) at 298 K (*Clegg and Toumi*, 1998). H^+ was inferred as the difference between the anion and cation equivalent concentrations (the model requires a charge balance). Table 4.1 shows the ion concentrations and %RH used for calculations. Undoubtedly, other species such as organic compounds are present in the aerosol, but they have a negligible effect on the activities of other ions (supported by *E-AIM* calculations performed with addition of organic acids similar to those in PASE) and thus no effect on the aerosol pH.

MS^- is not included in the current version of *E-AIM*, but its concentration is so

low relative to NSS ($MS^-/NSS \approx 0.02$), NH_4^+, and NO_3^- that it would not impact the activities of the major ions. Its exclusion, however, means that it will be a challenge to determine a suitable activity coefficient for MS^-.

4.3 Results

4.3.1 MSA Vapor Observations

Figure 4.2 shows the PASE MSA concentration profiles as a) molecules/cm^3 and b) nmol/m^3 from the MBL into the lower FT up to 3 km. The majority of sampling time was spent in the ML (below ∼600 m). The overlain solid lines are 200 m-bin means. MSA is 2.1×10^6 molecules/cm^3 $\pm$ 4×10^4 molecules/cm^3 near the ocean surface in the LML (<200 m), decreases by half to 9.2×10^5 molecules/cm^3 throughout the upper ML, and then begins to increase in the BuL (∼600 m to 1250 m), reaching $\sim 20 \times 10^6$ molecules/cm^3 above the TWI (Table 4.2). It is evident with the log scale in Fig. 4.2b that MSA increases towards the ocean surface, particularly below ∼200 m. This unique feature of the MSA measurements occurs in each and every flight (regardless of time or spatial gradient) and contrasts with all other gas-phase concentrations, which remain constant throughout the ML. Indeed, MSA contradicts the defining characteristic of the ML, which is that it is well mixed. PASE total MS^-, which is well mixed in the ML, is plotted next to MSA in Figure 4.2b to demonstrate the disparity in their concentrations; MSA is on average only ∼1 % of the particulate MS^-.

Zhang et al. (2014) discussed the negative MSA gradient, assigning it a value of 2.5×10^6 molecules/cm^3 km^{-1}. Employing the one-dimensional version of the Regional chemical transport Model (1-D REAM) used in a PASE DMS oxidation study (*Gray et al.*, 2011), *Zhang et al.* (2014) found that the model could not account for the enhanced MSA concentrations in the LML, leading them to pos-

tulate the existence of a missing MSA source (4.0×10^7 molecules/cm^3 s^{-1}) that strengthens near the ocean surface and is larger than their calculated rate of gas-phase MSA production. On this we agree. We will discuss their interpretations of the data and an alternate hypothesis for the missing MSA source in the Discussion section.

4.3.2 Particulate MS^- Observations

MS^- in the ML averaged 0.31 nmol/m^3 (Table 4.2, Figure 4.3a). In contrast to the MSA vapor concentrations (Figure 4.2), there is no significant difference between concentrations in the LML (<200 m) and TML (>200 m), nor do there appear to be large differences in the size distributions within the ML (though there are a few differences between flights). Total MS^- decreases by $\sim 1/4$ in the BuL entirely due to a reduction in the coarse mode MS^-. BuL air is a mixture of ML and FT air, the latter being devoid of sea salt aerosol. Whereas the overall coarse aerosol (SSA) mass decreases from the ML to the BuL, the fine aerosol mass remains essentially constant due to the production of NSS aerosol by reactions in cloud droplets (*Clarke et al.*, 2013; *Simpson et al.*, 2014). Figure 4.3a shows the consistent fine and coarse MS^- profiles throughout the ML, with fine MS^- maintaining its relatively small level of 0.10 nmol/m^3 (compared to NSS' ~5.5 nmol/m^3). Figure 4.3b depicts the MS^- mole ratio relative to the dominant fine (NSS) and coarse (Na^+) mass constituents. The MS^-/Na^+ ratio remains approximately constant throughout the ML and into the BuL, indicating that coarse MS^- is always associated with SSA and thus mostly forms in the ML.

4.3.3 MS^- Size Distributions

The PASE MS^- mass distributions measured by the MOI are bimodal (Figure 4.4). In the ML and BuL, the majority of the MS^- mass occurs in the supermicrometer

range, peaking on the Na^+ mass peak (Figure 4.4b). A smaller peak occurs in the submicrometer range at a larger stage than the NSS peak. The larger supermicrometer peak is consistent with the few other MS^- size distributions from the tropical Pacific MBL (*Huebert et al.*, 1996; *Quinn et al.*, 1996), though it differs from the MS^- size distributions measured in colder regions like the Arctic (*Leck and Persson*, 1996).

4.4 Discussion

We will infer the sources of MSA vapor and MS^- aerosol in the equatorial Pacific MBL by exploring the notable LML MSA gradient in the context of the diverse PASE measurements available. Though *Zhang et al.* (2014) proposed hypotheses for the sources of MSA (in the MBL and FT) from a dynamic modeling approach, we revisit this issue from the perspective of modeling with physical chemistry.

4.4.1 LML Sources of MSA

To explain the enhancement in MSA in the lower 200 m above the ocean surface, there are three main possibilities that could sustain an increase toward the surface:

- **Hypothesis 1**: A surface source from air-sea gas exchange explains the enhancement in MSA in the lower 200 m above the ocean surface.

  Zhang et al. (2014) suggest this can account for their model's estimated missing MSA source of 4.0×10^7 molecules/cm^2/s in the LML. After ruling out BrO as an extra oxidant and DMSO as a stronger-than-expected source, they recommend the ocean surface as the only viable source strong enough to both produce the missing MSA (BrO could not) and maintain the vertical gradient in MSA (extra DMSO could not).

- **Hypothesis 2**: A slower LML loss rate – whereby residual MSA produced by homogeneous oxidation has not had sufficient time to encounter and adsorb to or react with particles – explains the enhancement in MSA in the lower 200 m above the ocean surface.

  This applies prevailing notions of MSA homogeneous formation to the PASE ML observations. We consider this hypothesis essentially to be the default position.

- **Hypothesis 3**: Vaporization from extensively acidified submicrometer particles – (pH < 0) aided by lower RHs and increased temperatures – explains the enhancement in MSA in the lower 200 m above the ocean surface.

  We advance hypothesis 3 to explain not only the enhanced LML MSA concentrations but to some extent also the observed MS^- aerosol concentrations and mass distributions.

H1: Surface source suggestion

We will first address the *Zhang et al.* (2014) suggestion that MSA is emitted from the ocean. To our knowledge, no other author has suggested this as a viable mechanism. The alkaline ocean surface is surely under-saturated in MSA (which has a pK_a of <-1 (*Covington and Thompson*, 1974) and would completely dissociate $MSA_{(aq)}$ to non-volatile MS^-), even in the sea surface microlayer. MSA and its aqueous precursors (DMSO and MSIA) are extremely soluble, with Henry's Law constants exceeding $1 \times 10^9\,\mathrm{M\,atm^{-1}}$ at 298 K. Given its properties, net loss of MSA to the ocean via dry deposition is common, but emission is virtually impossible. Emission of MSA vapor or even a vapor-phase MSA precursor (like DMSO) from the ocean surface that leads to such a linear gradient in MSA is physically unrealistic, so we will dismiss it.

The only support that *Zhang et al.* (2014) present for this argument is a purported positive correlation between MSA and wind speed (*Zhang et al.* (2014) supplemental information; Figure 4.5a) in the lowest 200 m. However, their entire correlation depends on one flight, RF05, in which there is clearly a MSA gradient with latitude (not shown) as well as mixing of entrained air from the FT (*Clarke et al.*, 2013). If this single flight is removed as in Fig. 4.5b, there is no correlation whatsoever between LML MSA and wind speed. There is no support for H1.

H2: Residual MSA

One could argue that the MSA vapor seen in the LML is residual from the proposed homogeneous DMSO (to MSIA) oxidation pathway that has not yet encountered aerosol. For this argument, two initial assumptions are necessary: 1) MSA is homogeneously produced in the MBL, and 2) once MS^- is adsorbed, it cannot evaporate under typical MBL conditions (80 % RH).

According to the prevailing addition channel blueprint, OH converts ∼25 % (1 - PASE's γ) of DMS to DMSO, which then yields MSIA upon further reaction with OH, and finally (for those hypothesizing homogeneous MSA production such as *Urbanski et al.* (1998); *Arsene et al.* (2002)) MSA after another homogeneous OH oxidation step (also see Fig. 4.1):

$$\mathrm{DMS + OH \xrightarrow{1-\gamma} DMSO} \tag{4.1}$$

$$\mathrm{DMSO + OH \longrightarrow MSIA} \tag{4.2}$$

$$\mathrm{MSIA + OH \xrightarrow{?} MSA} \tag{4.3}$$

The scavenging of DMSO by the aqueous phase competes with this chain of reactions, but we will discuss that later. The remaining ∼75 % of DMS reacts with OH in the abstraction route to become SO_2, some of which is oxidized to H_2SO_4

by OH.

$$\mathrm{DMS + OH \xrightarrow{\gamma} SO_2} \tag{4.4}$$

$$\mathrm{SO_2 + OH \longrightarrow H_2SO_4} \tag{4.5}$$

Along with MSA, we measured DMS, OH, SO_2, and H_2SO_4, all of which remained well mixed and constant with altitude throughout the ML (*Simpson et al.*, 2014). Moreover, the ambient temperature in the LML is only ∼2 °C higher than the TML, not enough to significantly affect the reaction rates or branching ratios. Because there is no support for a $\sim 2\times$ faster rate of homogeneous MSA production with increasing proximity to the ocean, the basis of the residual MSA argument would have to be that the vapor's lifetime against loss to aerosol is longer in the LML than the TML.

In order to test this hypothesis, it is useful to compare MSA with H_2SO_4, a vapor known to a) be produced in situ via OH oxidation of SO_2 (reaction 4.5) – a sort of analogue to DMSO/MSIA as possible DMS oxidation products (reaction 4.3) – and b) adsorb to hydrated aerosol rapidly and almost irreversibly. For both these gases, uptake to the aqueous phase is the dominant sink as it is much faster than further gas-phase reaction. As a strong acid with a K_H that's even higher than that of MSA (and thus difficult to actually define), H_2SO_4 can be expected to have a shorter lifetime than MSA against loss to aerosol. This is borne out in their diurnal variations; H_2SO_4 increases dramatically during daytime and drops by two orders of magnitude during nighttime whereas MSA remains relatively constant (within a layer) and is only slightly lower at night, similar to the lowest daytime MSA values.

Even though this is apparently consistent with the residual MSA premise, it does not explain the strong altitude variation whereby the loss process presumably becomes $\sim 2\times$ slower in the LML. Despite sharing the same reactant as MSA (OH),

H_2SO_4 maintains a more constant profile in Figure 4.6 – and the same aerosol sink – that averages 6.5×10^6 molecules/cm^3 throughout the ML with no significant LML gradient. In the context of the residual gas-phase MSA hypothesis with its required assumptions, a suppressed LML loss rate/increased TML loss rate to the aqueous phase for MSA, then, is demonstrably unlikely.

As a matter of fact, the marked difference in the shapes of the MSA and H_2SO_4 curves in Figure 4.6 calls into question the assumptions made at the beginning of this H2 section. First, the assumption that MSA is produced homogeneously in the MBL lacks empirical support. As we outlined earlier, it is now widely thought that heterogeneous processing of DMSO – instead of MSA vapor uptake – is the pathway to particulate MS^-. Meanwhile, *Zhang et al.* (2014) still argue that the observed MBL MSA is formed in the gas phase. Under the proposed MSA mechanism (equation 4.3), MSA should increase with OH unless MSA has a rapid loss mechanism, which we have established is not likely. Finally, measured MSA does not appear to have any direct relationship with OH (Figure 4.7a) in either the LML or TML, whereas H_2SO_4 clearly increases with increasing OH (Figure 4.7b, equation 4.5). Unless MSA reacts with an alternate oxidant, gas-phase chemistry cannot produce a significant amount of MSA.

As it stands in the literature, the assumption of an addition channel homogeneous production pathway for MSA is indeed dubious. Even though multiple studies have reported varying product distributions, there is strong consensus that DMSO-OH at 298 K produces large yields (up to 99 %) of MSIA (*Arsene et al.*, 2002; *Urbanski et al.*, 1998; *Barnes et al.*, 2006). The most uncertainty surrounds the route to MSA from MSIA. In a lab study at 298 K, *Kukui et al.* (2003) found that (reaction 4.2) formed MSIA, and MSIA-OH subsequently generated SO_2 at a 90(20) % yield for each step. The correct mechanism for MSIA-OH is unknown, but *Barnes et al.* (2006) speculate that the MSIA-OH adduct could lead to MSA if it could react with O_2 before it undergoes decomposition reactions. Until further

studies can evaluate whether this alternative loss route is viable, we remain skeptical that measurable amounts of MSA can originate purely in the gas phase in the remote tropical MBL, though we acknowledge it is a possibility for the addition and even perhaps the abstraction channels.

Now that we have refuted the first assumption, we can examine the second assumption concerning the adsorption of MSA to aerosol. Prior tropical Pacific MSA observations (*Mauldin et al.*, 1999) have noted that MSA vapor concentrations are much larger in the dry FT than in the humid MBL, leading to the conclusion that MSA is taken up by aerosol and/or cloud drops due to its high solubility, and the implication was that this is an irreversible process. As Figure 4.7c shows, MSA exhibits a strong inverse relationship with %RH even within the ML. The relative locations of the LML and TML samples in this plot may explain the enhanced MSA in the LML. Sulfuric acid, on the other hand, does not vary with %RH (Figure 4.7d). If RH controls the variation of MSA, it follows that aqueous-phase chemistry (which is mostly aerosol in ML) controls the MSA burden. Still, there seems to be a low background value in Fig. 4.7 that may be from homogeneous processes or even another source.

H3: MSA emission from fine particulates

Having ruled out the first two hypotheses, we hypothesize that the enhanced LML MSA volatilizes from fine-mode particles that have been acidified to the point that they are saturated with respect to MS^-/MSA (or any acid weaker than H_2SO_4 such as HNO_3, organic acids, and HSO_4^-). This requires pretty extreme conditions. $MSA_{(aq)}$ is a very strong acid, requiring a pH < 0 to exist in an associated form at all. However, H_2SO_4 is an even stronger acid, and there is little NH_4^+ to neutralize it in this region (Fig. 4.8), so that low of a pH is plausible. This is particularly true as an air parcel descends in the LML, with 1) increasing temperature, 2) decreasing RH, 3) decreasing $[H_2O]p$, and consequent 4) increase in $[H^+]$. MSA evasion is

plausible at least in a laboratory setting: *Allen et al.* (2001) used vibrational sum frequency analysis to probe MSA's structure once adsorbed to the aqueous phase, detecting displacement of MSA by H_2SO_4 at an aqueous surface.

Due to adiabatic compression, ambient air temperature increases linearly toward the ocean surface at $\sim 0.8^{\circ}/100\,\mathrm{m}$, causing a corresponding decrease in RH at the bottom of the ML (Fig. 4.2c). This apparently small trend has significant ramifications for chemical processes. Indeed, the driving force behind aerosol pH change is RH change, which potentially concentrates the mostly sulfate fine mode, forcing some $MSA_{(aq)}$ (and any other acid weaker than H_2SO_4) to partition back to the gas phase in the LML by concentrating the newly reduced solution volume with H^+, thereby preventing complete acid dissociation at the surface or in the bulk phase. The MSA degassing flux from small particles increases as temperature increases and RH decreases. Additionally, evasion of vapor at the particle surface is further promoted by the Kelvin effect (increase in pressure inside droplet) of an increasingly curved surface.

Approach 1: Model with *E-AIM* and mass transfer

Our first approach to test our hypothesis considers whether the chemical composition of the LML fine mode has achieved a pH that is sufficiently low to induce vaporization of MSA. Furthermore, by integrating what is known about MSA's Henry's Law coefficient and theoretical mass transfer, we attempt to quantify the hypothetical MSA fluxes to/from the fine and coarse modes in the LML and TML. Though remaining uncertainties in certain fundamental physical parameters (mainly K_H and pH) prevent a definitive confirmation of the hypothesis, comparison with experimental data will provide the additional validation.

A notoriously difficult parameter to measure in ambient samples, aerosol pH is nonetheless important for understanding processes like gas-particle partitioning. In the case of a strong acid such as MSA that will dissociate completely in water, it

is critical to know the pH to gauge solubility. However, aerosol pH is inextricably linked to ambient RH since RH controls the volume of aerosol water and thus the concentrations of ions in the aerosol aqueous phase. Consider the equilibria of MSA, beginning with its condensed anion:

$$[\mathrm{MS^-}]_{(\mathrm{aq})} + [\mathrm{H^+}]_{(\mathrm{aq})} \overset{K_a}{\underset{\mathrm{H_2O}}{\rightleftharpoons}} [\mathrm{MSA}]_{(\mathrm{aq})} \overset{K_H}{\underset{\text{aerosol}}{\rightleftharpoons}} p\mathrm{MSA}_{(\mathrm{g})} \tag{4.6}$$

Where the aqueous phase is the aerosol liquid water content, aqueous concentrations are molalities ($\mathrm{mol\,kg^{-1}}$), and pMSA is in atm. A decrease in ambient RH increases $[\mathrm{H^+}]_{(aq)}$, diminishing the extent to which $\mathrm{MSA}_{(aq)}$ is dissociated; the acid-base equilibrium (K_a at 298 K) requires a shift toward $\mathrm{MSA}_{(aq)}$ to compensate for more $\mathrm{H^+}$ in solution (Equation 4.6). When pH = pK_a = −1.9, $[\mathrm{MSA}]_{(aq)}$ is 50 % dissociated. Though the aerosol pH is unlikely to decline below −1, only a small portion of $\mathrm{MS^-}$ needs to convert back to the volatile form, $\mathrm{MSA}_{(aq)}$, and thus facilitate degassing of MSA. As MSA is ∼1 % of $\mathrm{MS^-}$, the pH needs to decrease to at least zero for this mechanism to be viable.

Once there is sufficient $\mathrm{MSA}_{(aq)}$, the Henry's Law constant (K_H) describing the equilibrium between $\mathrm{MSA}_{(aq)}$ and its vapor, MSA, is important for determining the vapor pressure of MSA (RHS of equation 4.6) at the surface of the aerosol particle. For degassing to occur, there must be a gradient in MSA vapor concentrations: the vapor pressure of MSA at the surface, controlled by $K_H = [MSA]_{(aq)}/p\mathrm{MSA}$, must exceed the partial pressure of MSA far away from the particle. Otherwise, ambient MSA will adsorb to the particle.

Clegg and Brimblecombe (1985) recommend modifying the Henry's Law equilibrium expression to include the acid/base equilibrium of $\mathrm{MSA}_{(aq)}$:

$$K_H = \frac{\gamma_{\mathrm{MS^-}}[\mathrm{MS^-}] \times \gamma_{H^+}[H^+]}{(K_a \times p\mathrm{MSA})} \tag{4.7}$$

γ_i are the activity coefficients of the ions in solution; activities are critical when modeling such highly concentrated ionic solutions. The only well-known variables are K_a (73), and pMSA (Table 4.2). We measured MS^-, but we need the volume and density (which vary with composition and RH) of the submicrometer aerosol solution to infer its molality. K_H is known to be quite large, but there is considerable disagreement in the literature on the exact value. Estimates range from $1 \times 10^9\,\mathrm{M\,atm^{-1}}$ (*Campolongo et al.*, 1999) to $8.9 \times 10^{11}\,\mathrm{M\,atm^{-1}}$ (*Clegg and Brimblecombe*, 1985) at 298 K. We will incorporate the range of K_H values into our calculations to assess the most realistic (consistent with empirical evidence).

These extremely concentrated solutions are difficult to model, as activity coefficients can have large effects, and data at very high ionic strengths are sparse. Fortunately, a model has been built for precisely this situation and been made easily available on the world wide web.

To obtain the $[H^+]$ in addition to the aqueous volume and density parameters, we turn to the *E-AIM* Model, details of which are in Measurements and Calculations (section 4.2). Running the *E-AIM* Model II (*Clegg et al.*, 1998) with our fine-mode NH_4^+, NSS, NO_3^-, and inferred H^+ (to achieve charge balance) as inputs (Table 4.1), we obtained the $[H^+]$ and H^+ activity coefficient in both the LML and TML at their characteristic %RH and temperature (LML: 76 %; TML: 84 %). Hence, the outputs from the model are only as good as thermodynamic aerosol theory and our simplified chemistry, but their collective uncertainty is probably not larger than that of K_H.

After obtaining the *E-AIM* outputs (Table 4.1) and re-arranging equation 4.7, we can solve for pMSA at the surface of an aerosol particle. This parameter determines the direction and magnitude of the mass transfer flux of MSA to/from ML particles. The *Maxwell* (1888) formulation for vapor diffusing to particles in the continuum regime where particle diameter, d_p, is much larger than the mean

free path of the vapor, λ, is:

$$J_c = 2\pi \times d_p \times D_{\mathrm{MSA}} \times (C_\infty - C_s) \tag{4.8}$$

Where J_c is the continuum flux in $\mathrm{nmol/m^3\,h^{-1}}$; D_{MSA} is the diffusivity of MSA, $0.066\,\mathrm{cm^2\,s^{-1}}$ (*De Bruyn et al.*, 1994); C_∞ is the concentration of MSA far from the particle, i.e. the ambient MSA concentration; and C_s (also pMSA) is the concentration of MSA at the particle surface.

As mentioned, J_c only applies for $\mathrm{d}_p >> \lambda$, which is true for the coarse mode, but not generally for the submicrometer mode, except for the upper end of the submicrometer mode where particle number is low. Hence, we need appropriate equations to compute the fine-mode flux for our hypothesis. Dubbed the kinetic (or free molecular) regime, the small end of the size distribution where $\mathrm{d}_p << \lambda$ follows:

$$J_k = \pi \times (\frac{d_p}{2})^2 \times C_{\mathrm{MSA}} \times \alpha \times (C_\infty - C_s) \tag{4.9}$$

Where C_{MSA} is the mean speed of MSA molecules, and α is the accommodation or sticking coefficient. We calculated C_{MSA} from a simple formula to be $256\,\mathrm{m\,s^{-1}}$. Although α is another parameter that must be determined in the laboratory with diverse methods that lead to diverse results (*Davidovits et al.*, 2006), its value in the kinetic regime is of little importance because this regime contributes an insignificant portion of the total MSA flux.

When $\mathrm{d}_p \approx \lambda$ (at $\sim$0.1 µm to 0.5 µm), neither the continuum nor the kinetic regime is an adequate approximation of the gas-particle interactions. There are various proposed correction factors that can be applied to J_c depending on the properties of the gas in question. For MSA, which has a molecular weight much

larger than that of air, the best available treatment comes from *Dahneke* (1983):

$$J_t = J_c \times \frac{(Kn+1)}{(1+2\times Kn\times(1+Kn)/\alpha)}\; Kn = \frac{2\times\lambda}{d_p} \tag{4.10}$$

Where Kn is the Knudsen number, a dimensionless number that in practice determines the cutoffs for each dynamical regime. Note that α appears in the J_t correction factor. *De Bruyn et al.* (1994) determined α to be ~ 0.1 at 273 K and a pH range of 1 to 14, whereas *Hanson* (2005) found it to be close to 1 (0.86 ± 0.3) at 296 K. Having surveyed multiple kinetic studies, *Kolb et al.* (2010) contend that $\alpha = 1$ for all hydrophilic gases. We assume $\alpha = 1$, noting that decreasing α from 1 to 0.1 will not decrease the resulting fine-mode MSA flux to the particles in the TML by much more than 10 %.

Applying the range of K_H values in these calculations to the ambient RH-corrected LDMA number distributions yields the fluxes in Table 4.3. J_t accounts for most of the fine-mode flux, and J_c accounts for the coarse-mode flux. Our fine-mode results from the theoretical calculations are quite sensitive to the value chosen for MSA's Henry's Law constant, as it is the single largest source of uncertainty. If the upper limit of reported K_H's, $8.9 \times 10^{11}\,\mathrm{M\,atm^{-1}}$ (*Clegg and Brimblecombe*, 1985) were correct, we would see a flux of MSA to the accumulation mode of $0.3\,\mathrm{nmol/m^3\,d^{-1}}$ to $0.7\,\mathrm{nmol/m^3\,d^{-1}}$, $\sim 5\times$ what the MOI measurements (Table 4.2) can support, leaving no room for MS^- formation in cloud. If the lower-limit K_H were correct ($1 \times 10^9\,\mathrm{M\,atm^{-1}}$, *Campolongo et al.* (1999)), it would lead to a large negative flux of MSA, indicating that up to 9× the fine-mode MS^- concentration is vaporizing per hour! This lower K_H even leads to a negative flux from the coarse mode. Neither of these possibilities is realistic.

To obtain closer agreement with ambient observations, we choose to use $K_H = 3 \times 10^{10}\,\mathrm{M\,atm^{-1}}$, a value in between the lower and higher K_H's from the literature. We do this in part because to date no studies have measured K_H with

aerosol in relevant conditions – and furthermore, it is often measured with respect to idealized/homogeneous solutions in a laboratory. Given the complexity of atmospheric heterogeneous reactions, K_H may not be sufficient for describing gas-particle interactions in the humid MBL.

Generated using $K_H = 3 \times 10^{10}\,\mathrm{M\,atm^{-1}}$, Figure 4.9 displays the modeled diameter-dependent MSA flux in the fine and coarse modes. Remarkably, we observe a negative fine-mode flux in the LML, consistent with our hypothesis that MSA evaporates from LML fine MSA. On the other hand, the TML fine MSA flux is positive and 20 % smaller than the total LML fine flux, suggesting that some MSA re-adsorbs to the accumulation mode higher in the ML. Keep in mind, these hourly fluxes make imperceptible changes to the much larger particulate MS^- concentrations, even though they have a large effect on LML MSA. Moreover, the hourly fluxes (Table 4.3) agree reasonably well with the mean MSA observations (Table 4.2), particularly in the TML; removing the lowest-RH, highest-temperature RF05 from the LML brings it into closer agreement.

As for the coarse mode continuum regime MSA fluxes, we computed 0.08 and $0.05\,\mathrm{nmol/m^3\,d^{-1}}$ in the LML and TML, respectively (Table 4.3 and Figure 4.9). These fluxes are larger than their corresponding fine-mode fluxes (Table 4.3). According to our total coarse MS^- data, the daily fluxes are probably not enough to accumulate the observed MS^- on the SSA mode, taking 3 or more days to make the entirety of the observed mass. Depending on the lifetime of SSA against deposition or divergence, MS^- accumulation likely takes longer than the time that the particle spends suspended in the ML. (There is a caveat that the calculated daily fluxes may be smaller than reported in Table 4.3 due to diurnal variations in temperature and RH; the large increase in RH at night would suppress evaporation of MSA, and this is supported by the night flight points at ~ 0 [OH] in Fig. 4.7a that maintain at about half MSA's daytime concentration (versus H_2SO_4's drop to about 5 % of its daytime concentration) and Fig. 4.7c showing these lower MSA

points associated with highest RHs). Supermicrometer SSA particles in the ML may not last more than 2 days due to divergence and wet and dry removal *Simpson* (2010). Although uptake of MSA that first evaporated from the acidic fine mode is a means of adding MS^- mass to coarse SSA, our analysis suggests that it can only contribute a small fraction of observed coarse MS^- (Figure 4.10), requiring an additional mechanism to explain the remainder. This mechanism entails the uptake of DMSO/MSIA, which is rapidly converted to MS^- by OH radical in the liquid water phase of large SSA particles. We will revisit DMSO's role in MS^- formation in section 4.4.2.

Approach 2: Empirical observations of MSA vapor increasing with increasing submicrometer acidity

While we find the chemical modeling compelling, the large uncertainties in K_H, α, and γ_{MS^-} render it inconclusive. The second approach to testing our hypothesis is an investigation of MSA's link to the sulfate content of the fine mode – essentially a proxy for aerosol acidity – that integrates our in situ data with some of the *E-AIM* output parameters. Our aim is to provide evidence from our aerosol measurements that support both our hypothesis (Hypothesis 3) and our Approach 1 with the *E-AIM* model. Moreover, these aerosol measurements derive from a variety of techniques including the AMS, optical particle counter (OPC), and MOI.

An important facet of our explanation for driving MSA off of the fine mode is the low pH that must be achieved to trigger the process. As we alluded to earlier, we could not directly measure pH, but in the remote MBL, the bulk of the H^+ ions come from dissolved S(IV), which we did measure and whose molality in the submicrometer aerosol liquid water should directly relate to $[H^+]_{(aq)}$ (we have shown in Fig. 4.8 that NH_4^+ is under-saturated even relative to HSO_4^-). In reality, $S(IV)_{(aq)}$ in particles is a mixture of $SO_4^{2-}{}_{(aq)}$ and $HSO_{4(aq)}^-$; in practice, the AMS measures both as SO_4^{2-}.

The simultaneous submicrometer aerosol volume was measured with the OPC. We applied a correction factor to the submicrometer aerosol volume to account for the difference between sampling and ambient RH. To convert the submicrometer volume to mass, we derived a density from the linear correlation between the *E-AIM* RH and density. The OPC volume is not exclusively volatile, so it likely includes a small amount of submicrometer SSA volume present at the upper end of the fine mode that should not interfere with the acidity of the smaller particles of interest here.

To make a credible comparison between our empirical data and the $[SO_4^{2-}]_{(aq)}$ (our pH proxy) generated by the *E-AIM* model, we plotted $\log_{10}$[MSA] from Fig. 4.7c versus the *E-AIM* $[SO_4^{2-}]_{(aq)}$ + $[HSO_4^-]_{(aq)}$ output. Figure 4.11 presents this *E-AIM* linear relationship (solid purple line) between MSA and $[SO_4^{2-}]_{(aq)}$ alongside the PASE data from the LML (navy) and TML (gold) and their linear fits. The scatter in the observational data is expected since we do not account for the non-NSS composition (varying amounts of NH_4^+, organics, NO_3^-, HCO_3^-), making $[SO_4^{2-}]_{(aq)}$ a less precise approximation of pH. Additionally, $[SO_4^{2-}]_{(aq)}$ may have a low bias because of the OPC submicrometer volume's inclusion of non-volatile volume. The correlation coefficients of the field data are not very strong: $R^2 = 0.25$ in the TML and $R^2 = 0.53$ in the LML. Still, the fits of the TML and *E-AIM* model agree quite well, having similar slopes and y-intercepts. The LML slope also agrees well with the others, though the LML's y-intercept is larger than the TML's by $\sim 3 \times 10^5$ molecules/cm^3, which is nearly the difference between the calculated LML (-1×10^6 molecules/cm^3 h^{-1} and TML (7×10^5 molecules/cm^3 h^{-1}) hourly fine-mode MSA fluxes.

According to our flux calculations (Table 4.3), MSA does not remain in the vapor phase for long (1 h to 2 h) in the ML, diffusing to the more alkaline coarse-mode SSA. In order to maintain a LML gradient with a highly soluble gas such as MSA, the gas must be longer-lived than the ML mixing time. In a $\sim$0.5 km

ML with mean wind speed of $10\,\mathrm{m\,s^{-1}}$, the ML mixing time is $\sim$1 h (*Lewis and Schwartz*, 2004). As the PASE mean wind speed was $\sim 8\,\mathrm{m\,s^{-1}}$, we expect the mixing time to be slightly longer than 1 h, which is approximately in accordance with our calculated MSA lifetimes. In the ML, a steady state is established at each altitude:

$$\frac{d\,\langle[\mathrm{MSA}]\rangle}{dt} = Production - Loss = Production(alt) - [\mathrm{MSA}] \times k_{loss}(alt) \approx 0$$
$$[\mathrm{MSA}](alt) = \frac{Production(alt)}{k_{loss}(alt)} \tag{4.11}$$

where k_{loss} is MSA's loss rate to aerosol, and *alt* denotes altitude. As air descends from the bottom of the BuL to the LML, it warms, and the resulting decrease in RH decreases the volume of sulfuric acid solution of the fine particles subsiding from the cloud layer. The parameters of k_{loss} do not change much with altitude. MSA vapor evades rapidly (Production increases toward the surface), establishing steady state vapor concentrations that increase towards the surface.

The approach laid out in this section lends a great deal of confidence to our first model approach, which is admittedly hampered by the large uncertainty in K_H. However, this large uncertainty is more a function of the difficulty in quantitatively describing gas-particle interactions since the influence of other parameters (e.g. surface tension and reactions) surely increases as particle diameter decreases. Further studies are needed to refine theory and to develop lab experiments with realistic conditions. The poor understanding of gas-particle partitioning in remote marine environments leads to inadequate model descriptions of natural aerosol properties (e.g. size distribution, hygroscopicity) and how their effects on climate evolve in response to local chemistry and dynamics.

4.4.2 MBL Particulate MS^- Measurements Support Hypothesized MSA Processes

The total daily MSA fluxes depicted in Figure 4.10 reveal that driving MSA off of small, acidic particles is a means of re-distributing small amounts of MSA to larger particles. However, our calculations indicate that the full coarse-mode MS^- cannot be made from evaporated fine-mode MSA unless a 3+ day lifetime is assumed for large particles (Table 4.3, last column). The question of the origin of coarse MS^- also begs the question of how the fine-mode MS^- forms in the first place. We argue that the majority of particulate MS^- is initially formed in cloud (fine MS^-) and hydrated aerosol (coarse MS^-). We assess these pathways with the aid of our synchronous MSA and MS^- measurements.

DMSO

In addition to this study, other field experiments (*Davis et al.*, 1998; *Jefferson et al.*, 1998; *Nowak et al.*, 2001; *Mihalopoulos et al.*, 2007) have deduced that ambient MS^- concentrations were too large to originate by the uptake of MSA gas alone, leading investigators to favor heterogeneous formation of MS^-. Laboratory kinetics (*Bardouki et al.*, 2003) and sparse field evidence corroborate the presence of ample DMSO concentrations to yield MS^-. Model results also support the large role hypothesized for DMSO in multiphase chemistry (*Campolongo et al.*, 1999; *Zhu et al.*, 2003a, 2006). Even still, a large gap remains in our understanding of this DMSO-to-MS^- route due to a lack of empirical evidence.

Once it is formed in the addition channel, DMSO's fate rests on competing reactions: a) destruction by OH in the gas phase and b) uptake to the aqueous phase followed by conversion to MSI^- and MS^- by $OH_{(aq)}$ and possibly $Cl^{2-}{}_{(aq)}$ and $SO^-_{4(aq)}$ radicals (*Bardouki et al.*, 2002; *Zhu et al.*, 2003b, 2006). The rates and yields for these reactions come solely from lab studies performed in either the gas

(e.g., *Falbe-Hansen et al.*, 2000; *Arsene et al.*, 2002) or the aqueous phase (e.g., *Bardouki et al.*, 2002), so there is inevitably much uncertainty in how these reactions proceed in the MBL. Nevertheless, these important parameters determine the partitioning of the DMS addition channel sulfur products, and thus it is valuable to compare model output with our field observations.

Some authors found the homogeneous and heterogeneous DMSO sinks to be roughly equal (*Sciare et al.*, 2000), but *Zhu et al.* (2006) contend in their model study that heterogeneous loss represents 90 % of the total DMSO loss. The split between the sinks likely depends on local dynamics and conditions. In completely dry lab studies, DMSO's lifetime against homogeneous reaction with OH is expected to be around 5 h (*Urbanski et al.*, 1998; *Falbe-Hansen et al.*, 2000). Completely neglecting the real-life scenario of scavenging by the aqueous phase, DMSO reacts $\sim 15\times$ faster with OH than DMS does, but the products and yields of the homogeneous DMSO reaction are far from settled. Current consensus is that when DMSO is oxidized in the gas phase, MSIA is the primary product at high yields (80 % to 90 %; *Arsene et al.* (2002); *Tian et al.* (2007); *González-García et al.* (2007)). As mentioned in an earlier section, MSIA, which has a high solubility on par with DMSO, may react further with OH in the gas phase to produce SO_2 at nearly 100 % yield in a laboratory setting with an excess of OH and DMSO (*Kukui et al.*, 2003). These reactions need to be evaluated in the field.

In the humid MBL, physical removal to the aqueous phase (wetted aerosol and cloud droplets) is an important sink for soluble products of DMS oxidation. For example, $\sim$50 % of SO_2 is converted in cloud to fine NSS (*Simpson et al.*, 2014). Using a published accommodation coefficient (0.1; *De Bruyn et al.* (1994)) and assuming an aerosol surface area in their model, *Chen et al.* (2000) calculated a DMSO lifetime of 70 min at night and 20 min during the day (43 min diel average) for the tropical Pacific. The cloud DMSO sink in the BuL depends on the vapor's diffusivity, and in the ML, the sink relates to the frequency of collisions between

DMSO and large SSA particles. We reason that the extremely low pH of fine-mode aerosol will preclude uptake of DMSO; therefore, fine-mode MS^- must be produced by cloud processing in the BuL. This scenario agrees well with our MOI observations of a constant fine MS^-/NSS molar ratio throughout the ML and BuL (Figure 4.3b).

Once in solution, DMSO reacts rapidly with aqueous OH radicals (*Scaduto*, 1995; *Zhu et al.*, 2003a). *Bardouki et al.* (2002) determined that MS^- was the major product of both DMSO and MSI^- reactions with $OH_{(aq)}$, both with a yield >95 %. Therefore, whether $DMSO_{(g)}$ or $MSIA_{(g)}$ are scavenged into the liquid phase, both can produce MS^- in ∼4 min at 300 K with $[OH]_{(aq)} = 6 \times 10^{-13}$ M (*Zhu et al.*, 2003a), if there are no competing reactions to deplete $[OH]_{(aq)}$. Interestingly, *Zhu et al.* (2006) computed that $Cl^{2-}{}_{(aq)}$ radical's oxidation of $MSI^-{}_{(aq)}$ was responsible for the largest fraction of MS^- production (∼65 %) whereas $OH_{(aq)}$ contributed ∼25 %. Though their results are heavily dependent on parameterization choices in their model simulations, they point to intriguing possibilities for other radical species, many of which are largely unobserved in the remote MBL.

Notably, the conversion rate of DMSO/MSI^- to MS^- in cloud droplets may be contingent upon the time spent in cloud. If the lifetime of small cloud droplets against evaporation is shorter than the reaction time of $DMSO_{(aq)}$ (∼4 min to 6 min; *Zhu et al.* (2003a)), multiple cloud cycles would be needed to convert most DMSO/MSI^- to fine MS^-. In the trade-wind cumulus clouds of PASE, we estimated that an air parcel would spend a maximum of 7 min in cloud, which is very close to the estimated reaction time, assuming an $[OH]_{(aq)} = 6 \times 10^{-13}$ M (*Herrmann et al.*, 1999). But in the case of always-wet SSA particles, their lifetime of 1 d to 2 d removes the time limit on MS^- formation from aqueous reaction. Supermicrometer MS^- formation depends on the flux of DMSO/MSIA (and MSA mobilized from fine particles) to SSA and their condensed-phase chemistry.

Our inclusion of DMSO lifetime in the discussion is unavoidable when assessing

MS^- formation, but it is not our goal to directly quantify this species' budget. We can roughly estimate that DMSO was ∼15 pptv by scaling the ∼25 % higher-than-PASE DMS and DMSO observations reported in 1994 by *Bandy et al.* (1996) from a tower on Christmas Island (PASE base). In PEM-Tropics, *Nowak et al.* (2001) measured 5 pptv DMSO in the central Pacific, though their model could not account for that much, prompting the authors to propose an additional DMSO source in the remote MBL, perhaps involving BrO. Hopefully future measurements of remote DMSO will be more successful as this intermediate in the DMS oxidation scheme may be the key to understanding multiphase mechanisms and their impact on marine aerosol properties.

Using our estimate of 15 pptv $DMSO_{(g)}$ in both the LML and TML, we performed a similar calculation as in section H3 for the coarse-mode mass transfer flux to evaluate whether condensation of DMSO/MSIA and aqueous-phase conversion to MS^- could produce the observed coarse MS^- in PASE. As mentioned, we will neglect the DMSO flux to fine-mode particles. DMSO has a reported Henry's Law constant of $1.0 \times 10^7\,\mathrm{M\,atm^{-1}}$ (*Campolongo et al.*, 1999) and an accommodation coefficient of 0.1 (*De Bruyn et al.*, 1994). Because we do not have measurements of DMSO in aerosol nor its vapor pressure at the particle surface, we assume it is 0, acknowledging that this will maximize the vapor concentration gradient and the resulting DMSO coarse flux. From equation 4.8 and assuming a constant DMSO concentration, we compute that $\sim 27\,\mathrm{nmol\,m^{-3}\,d^{-1}}$ DMSO adsorbs to SSA as an upper limit.

Conversion to MS^- requires $[OH]_{(aq)}$ radical (and/or $[Cl_2^-]_{(aq)}$), which we can calculate using the average daytime [OH] and its K_H. As there is a range of reported values for OH's K_H ($25\,\mathrm{M\,atm^{-1}}$ to $1 \times 10^5\,\mathrm{M\,atm^{-1}}$, *Lelieveld and Crutzen* (1991)), we will use a conservative value of $100\,\mathrm{M\,atm^{-1}}$, noting that 1) the final calculated yield of MS^- formed in SSA is sensitive to the concentration of radical oxidant and 2) OH, a hydrophilic gas, may be concentrated at the aqueous surface

by up to 8× the bulk concentration (*Vácha et al.*, 2004), and 3) $OH_{(aq)}$ can be photochemically generated in particles at rates comparable to gas uptake (*Zhou et al.*, 2008). If $OH_{(aq)}$ is the oxidant, the aqueous phase reactions and rates at 298 K are:

$$DMSO + OH \longrightarrow MSIA + CH_3 \qquad k = 6.6 \times 10^9\,M^{-1}\,s^{-1} \qquad (4.12)$$

$$MSI^- + OH \longrightarrow MS^- \qquad k = 7.7 \times 10^9\,M^{-1}\,s^{-1} \qquad (4.13)$$

Given the large amount of SSA mass in the marine atmosphere and that SSA contains a high molar concentration of Cl^- anion, Cl or Cl_2^- radicals are potentially important aqueous oxidants in the remote MBL. These reactions are:

$$DMSO + Cl \longrightarrow MSI^- \qquad k = 6.3 \times 10^9\,M^{-1}\,s^{-1} \qquad (4.14)$$

$$DMSO + Cl_2 \longrightarrow MSI^- \qquad k = 1.6 \times 10^7\,M^{-1}\,s^{-1} \qquad (4.15)$$

$$MSI^- + Cl_2^- \longrightarrow MS^- \qquad k = 8 \times 10^8\,M^{-1}\,s^{-1} \qquad (4.16)$$

If we assume only reactions 4.12 and 4.13 are relevant (with $[OH]_{(aq)} = 2 \times 10^{-11}$ M) and convert the calculated DMSO-to-SSA flux of 27 nmol/m^3 d^{-1} to MS^-, DMSO uptake can account for 0.1 nmol/m^3 d^{-1} in the ML, where this process is only active during the ∼12 h photochemical cycle. Whether in the LML or TML, DMSO combined with MSA evaporated from the fine mode (Fig. 4.10) can account for the total coarse MS^- in 1.5 d to 2 d. Our calculated DMSO flux (applying 4.8 to the assumed [DMSO]) suggest DMSO's lifetime against uptake to the aqueous phase is only 1.3 h, though this may be the lower limit. As the gas-phase DMSO sink is thought to be 3 h to 5 h, aqueous loss – including cloud chemistry – may indeed be the dominant DMSO sink in the remote MBL.

At the reported literature value of 1×10^{-11} M (*Herrmann et al.*, 1999), $[Cl^-_{2(aq)}]$ does not appear to be sufficient to produce the coarse MS^- through reactions 4.15

and 4.16, but there are reasonable possibilities that 1) $[Cl_2^-]_{(aq)}$ is higher in PASE than the reported literature value and 2) $[OH]_{(aq)}$ is consumed in SSA by competing reactions such as the oxidation of organic acids, which is supported by MOI data. Moreover, $Cl^-_{2(aq)}$ may be important for in-cloud oxidation of DMSO. *Zhu et al.* (2006) found $Cl^-_{2(aq)}$ to be more important in oxidizing $MSI^-_{(aq)}$ to MS^- in their model simulations that included clouds.

Fine-mode MS^-

The aqueous conversion of DMSO to MS^- in cloud through reactions 4.12 through 4.16 can support the 0.1 nmol/m^3 fine MS^- burden (Table 4.2) in PASE. Aqueous oxidation of DMSO/MSIA precursors is not as rapid as the formation of NSS from oxidation of SO_2 by H_2O_2 in the BuL (*Barnes et al.*, 2006), requiring multiple cycles through cloud and perhaps in larger cloud droplets. Additionally, the in-cloud reaction pathways for MS^- production may be pH-sensitive, which could potentially hinder these pathways in the somewhat acidic (pH $\approx$ 4) cloudwater. The MS^- shift to submicrometer sizes that are larger than the NSS peak (Fig. 4.4b) is compatible with such processes.

Further evidence for fine MS^- formation in the BuL is provided in the profiles of fine MS^-, NSS, and their constant MS^-/NSS ratio (Fig. 4.3) throughout the BuL and ML. As the majority of the NSS is formed in cloud (*Simpson et al.*, 2014), their constant ratio indicates their shared origin in the BuL. The fine MS^- size distribution (Fig. 4.4a) supports our MSA volatilization hypothesis; the increasing acidity and vapor pressure of MSA as fine particles decrease in size tends to deplete the smallest sizes of MS^-.

Coarse-mode MS^-

We have presented two possible coarse MS^- formation mechanisms that are consistent with flux calculations and empirical data, but we lack enough information (e.g., SSA lifetime, [DMSO], aqueous oxidants) that we cannot confirm or quantify the mechanisms. Figure 4.12a supports the conjecture that SSA, represented by coarse Na^+ mass, takes up MSA throughout the ML.

We reason that MS^- is more likely made by DMSO/MSIA precursor, which is up to 200× more concentrated in the ML. Figure 4.12b is consistent with the possibility of reactions 4.15 and 4.16 taking place in the aqueous SSA solution where the high concentration of $Cl^-_{(aq)}$ is a potentially large $Cl^{2-}_{(aq)}$ source, particularly in the tropics.

4.4.3 Gas-phase MSA production

We are only able to detect the evaporation-induced MSA gradient (Fig. 4.2b) because the homogeneous routes to MSA are so insignificant in the ML. However, we do not completely discount the possibility of homogeneous MSA formation. After all, we did not measure every possible oxidant such as halogens.

From simply comparing the MSA vapor and MS^- concentrations (Table 4.2), MSA is approximately 1 % of MS^-. Because we contend that the majority of the ML MSA vapor was formed initially as MS^- through aqueous chemistry, our estimate of the direct homogeneous route to MSA will be even smaller. The TML y-intercept of Figure 4.11 is 3.2×10^5 molecules/cm^3, which may be a mixture of MSA from MBL homogeneous oxidation and entrainment from the FT. This background MSA vapor is 1/3 of the average ML MSA (Table 4.2) and ∼0.2 % of the total MS^-. *Zhu et al.* (2006) found this pathway to contribute 3 % to the total MS^- while *Davis et al.* (1998) estimated its contribution to be ∼1 %.

4.4.4 FT Sources of MSA

Figure 4.2 and Table 4.2 show that PASE MSA concentrations were highest in the FT with an average of 7.7×10^6 molecules/cm^3 in the lower FT (LFT: 450 m column available to entrain in 1 d), 3.5× the ML concentrations. This pattern of higher MSA concentrations in the FT was observed in PEM-Tropics as well (*Mauldin et al.*, 1999). In their study, *Mauldin et al.* (1999) attributed the FT MSA concentrations to complete volatilization of particulate MS^- due to the absence of MS^- in the FT. This argument rests on the assumptions that MSA vapor and MS^- aerosol concentrations are always interdependent, locally produced, and that MBL particles could penetrate significant distances up into the FT.

With the PASE FT data, *Zhang et al.* (2014) favor a similar interpretation as *Mauldin et al.* (1999), citing the need for a LFT MSA source in their model and the possibility of MSA evaporating off of aerosol due to the dry air in the FT. Presumably, the MS^--rich aerosol that loses MSA to the FT originates in the local MBL, though *Zhang et al.* (2014) do not mention their origin or reference any of the publicly available PASE aerosol measurements. At 3× the chemical production term in the LFT, the authors propose that degassing of aerosol to the LFT makes up most of the MSA source that then entrains into the BuL.

Although we cannot completely rule out degassing of MSA into the FT from local aerosol (since, after all, we have a similar hypothesis in the LML), it is very unlikely. There is subsidence and entrainment of LFT air into the MBL (confirmed and calculated using PASE O_3 budget by *Conley et al.* (2011)) that occurs in regions of large-scale subsidence where PASE is located. Our high-resolution measurements revealed virtually no DMS in the FT (except in a single instance of mixing visible in Fig. 4.13), demonstrating that MBL gases and therefore, particles, do not penetrate upward into the LFT in the PASE region.

To explore whether there is MBL influence in the LFT, we show the PASE po-

tential temperature (θ) profiles colored by MSA and DMS (Figure 4.13). Samples in the PASE FT were largely taken during rapid ascents and descents ($\sim$5 m s^{-1}), and the small variations in instrument response time could become significant enough under such conditions to prevent accurate comparisons of measurements from different instruments. However, MSA and DMS are fast (>1 Hz).

MSA is more concentrated in the FT (Fig. 4.13a) while DMS is largely confined to the MBL (Fig. 4.13b). Even when traces of DMS mix into the LFT, the corresponding points in the MSA profile appear to be diluted. The mixing at the TWI boundary between upper BuL and LFT air, respectively represented by DMS and MSA, is shown in Figure 4.14. The driest FT air with the least DMS lacks any signature of MBL air yet is the most enriched in MSA, suggesting that FT MSA is transported in the FT from elsewhere, likely the Inter Tropical Convection Zone (ITCZ).

Zhang et al. (2014) considered transport of MSA in the FT from distant sources, but they dismissed its possibility based on a flawed assumption – that any FT material not from the local MBL would be associated with the continental long-range transport (LRT) sources documented in other PASE publications (*Gray et al.*, 2011; *Clarke et al.*, 2013). These continental plumes often had large enrichments of refractory particles, CO, and SO_2 (*Clarke et al.*, 2013; *Simpson et al.*, 2014). *Zhang et al.* (2014) found that FT SO_2 was unrelated to MSA, leading them to rule out non-local MSA sources.

As *Clarke et al.* (2013) have argued, the clean FT air sampled in PASE originated from ITCZ outflow, strongly suggesting that the FT MSA has advected from this nearby ($\sim$8° North) source. Airmass back trajectory analysis of the PASE sampling window strongly supports the influence of ITCZ outflow (*Freitag et al.*, 2013). Though we suspected that MSA could arrive in LRT of biomass-burning-type continental air, comparisons of CO and submicrometer volume with MSA (not shown) suggest that mixing with air recently transported from the ITCZ

causes any apparent MSA association in the FT. Deep convection in the ITCZ is capable of injecting the DMS (least soluble) emitted from the ocean surface into the FT where it has days to react to form $DMSO_{(}g)$ (more favorable than SO_2 at low temperatures) and eventually MSA, which is long-lived with respect to oxidation by OH (*Barnes et al.*, 2006). The MSIA-OH reaction to form MSA is more favorable in the colder FT because of reduced competition from thermal decomposition of the MSIA-OH adduct (*Barnes et al.*, 2006). *Marandino et al.* (2013) postulate that this lifting of DMS in the highly convective tropical western Pacific may even penetrate the lower stratosphere.

Using the PASE-average entrainment velocity of $5\,\mathrm{mm\,s^{-1}}$ (*Simpson et al.*, 2014; *Huebert et al.*, 1996), the depth of the MBL ($\sim$1250 m), and the MSA concentration in the LFT, we calculate that entrainment of MSA from the FT could contribute 3.5×10^6 molecules/cm^2/d to 5.5×10^6 molecules/cm^2/d of MSA to the MBL. Our entrainment rate is comparable to that of *Zhang et al.* (2014), though their estimate of $\sim 1.1 \times 10^7$ molecules/cm^3 d is slightly higher, probably because their LFT MSA average concentration is based on a larger altitude range. Due to its high solubility, a significant fraction of this entrained MSA is probably scavenged by clouds, becoming MS^-.

After an analysis of the proposed DMS oxidation mechanisms, *Capaldo and Pandis* (1997) pointed to the uncertainty and variability in FT-MBL interactions as sources of differing results between models and observations. As we have shown elsewhere (*Huebert et al.*, 1996; *Clarke et al.*, 2013; *Simpson et al.*, 2014), the extent of communication between the MBL and FT is a significant factor in remote marine atmospheric chemistry where background concentrations tend to be sensitive to all inputs.

4.5 Conclusions

In terms of average concentrations, PASE MSA vapor and MS^- aerosol concentrations agree well with previous measurements made in the central Pacific (PEM-T, RITS, 1994 Christmas Island project). We observed, however, an unexpected and previously unobserved enhancement of MSA in the lower 200 m of the ML: the MSA vapor concentrations doubled from the upper ML to the ocean's surface. While *Zhang et al.* (2014) believed this feature to be an unidentified source of MSA from the ocean, thermodynamic theory led us to the conclusion that MSA evades from SO_4^{2-}-rich fine-mode particles as the RH decrease in the lower ML suppresses pH to ~ -0.8.

We presented model and observational evidence that the main source of MSA vapor in the ML is desorption of MSA from fine MS^- aerosol rather than the oft-cited homogeneous formation pathway. In the tropical MBL, gaseous MSA's precursor is predominantly made in the aqueous phase (99 %) after DMSO/MSIA vapor is wet-scavenged, not in the gas phase. Our study upholds the suspected multiphase route to MS^- through DMSO as outlined by *Davis et al.* (1998); *Zhu et al.* (2006) and others.

The especially large coarse-mode MS^- (unique to the tropics) is another signature of our hypothesis' prediction. The fine mode is too acidic to accommodate significant DMSO uptake, leaving a) large SSA particles as an important DMSO sink in the ML and b) clouds as a primary sink in the BuL.

We find that the FT MSA vapor is not from the local MBL, contrary to the finding of *Zhang et al.* (2014) that degassing of locally produced MS^- aerosol contributes the majority of the FT MSA. In a tropical southern hemisphere subsidence region, FT MSA likely derives from ITCZ outflow of DMS that homogeneously oxidizes to MSA; the homogeneous pathway is much more favorable in the cold, stable, low-aerosol conditions of the FT rather than the wet MBL. We calculate

that entrainment of MSA from the FT could contribute 3.5×10^6 molecules/cm^2/d to 5.5×10^6 molecules/cm^2/d of MS^- to the MBL, via the evaporation of cloud droplets.

Comparison with *Zhang et al.* (2014) demonstrates that validating models with data can be problematic without viable chemical and physical processes. MSA simply cannot evaporate from an alkaline ocean surface, for example. It will all be in the form of non-volatile MS^-. To have plausible, testable hypotheses for atmospheric processes, one must thoroughly elucidate the theory underpinning said processes.

Multiphase chemistry in the remote tropical atmosphere has great potential for modifying the aerosol size distribution and physicochemical properties. Although accurate Henry's Law constants, rate constants, and activities could not be simulated well enough to rigorously quantify our proposed mechanism, in situ field measurements of gases and aerosols helped us assemble a plausible scenario.

About 25 % of DMS in the ML is oxidized to DMSO. Some of this diffuses to the surface of coarse particles where it is oxidized to MS^-. In BuL cloud droplets, both MS^- and NSS are produced from oxidation; fine as well as coarse particles will result from the evaporation of those particles upon their return to the ML. Little MSA vapor is produced homogeneously. Most is derived from the fine particles, which warm as they subside near the surface, dry a bit, concentrate their sulfuric acid, and drive some (a few %) MS^- to the neutralized form, MSA. It is the evaporation of this fine-particle MSA that provides most of the gas-phase MSA in the MBL, although a few other mechanisms cannot be completely ruled out.

Since convecting air is hottest at its lowest point, the RH is lowest there, and MSA vaporization is highest there. Absent a faster sink near the surface, the MSA concentration rises close to the surface. The smallest particles are depleted of MS^- relative to larger ones, due to the Kelvin effect causing higher MSA vapor pressure. This appears to be a mechanism for distributing MS^- to larger particle diameters.

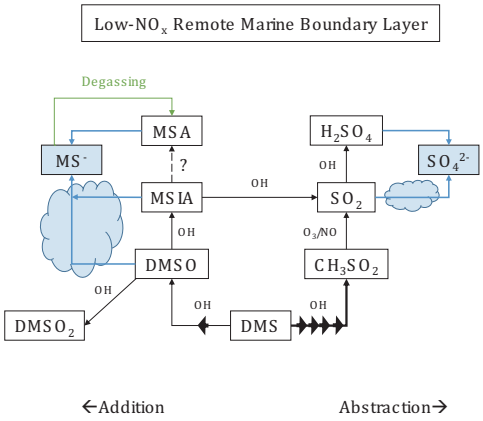

Figure 4.1: Simple DMS oxidation scheme in the remote tropical marine boundary layer (∼25 °C, 80 % RH, 8 m s^{-1} winds) where NO_x concentrations are low (∼4 pptv: *Conley et al.* (2011)). Black boxes are gases while black with blue backgrounds are hydrated aerosol species (MS^- on fine and coarse particles, SO_4^{2-} on fine particles). Black arrows represent gas-phase reactions known to occur in low-NO_x conditions. Multiple consecutive arrows signify multiple intermediate steps. Blue arrows are uptake of gases to aqueous phase sea salt aerosol (coarse particles) and cloud droplets (producing fine particles). The hypothesized mechanism illustrated by the green arrow generates MSA vapor in the MBL and is the heart of our investigation.

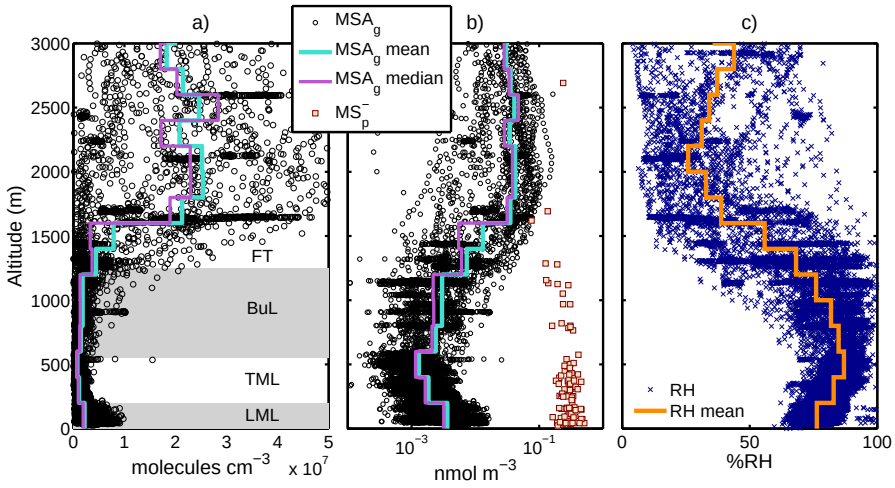

Figure 4.2: a) PASE MSA gas profile (CIMS 10 s data) with 200 m-bin mean and median traces. In b), total particulate MS^- (MOI 30 min data) is plotted with MSA on a logarithmic x-scale. Typically expressed in units of molecules/cm^3, MSA concentrations in b) are in nmol/m^3 to compare with particulate concentrations. The % Relative Humidity (RH) profile appears in c).

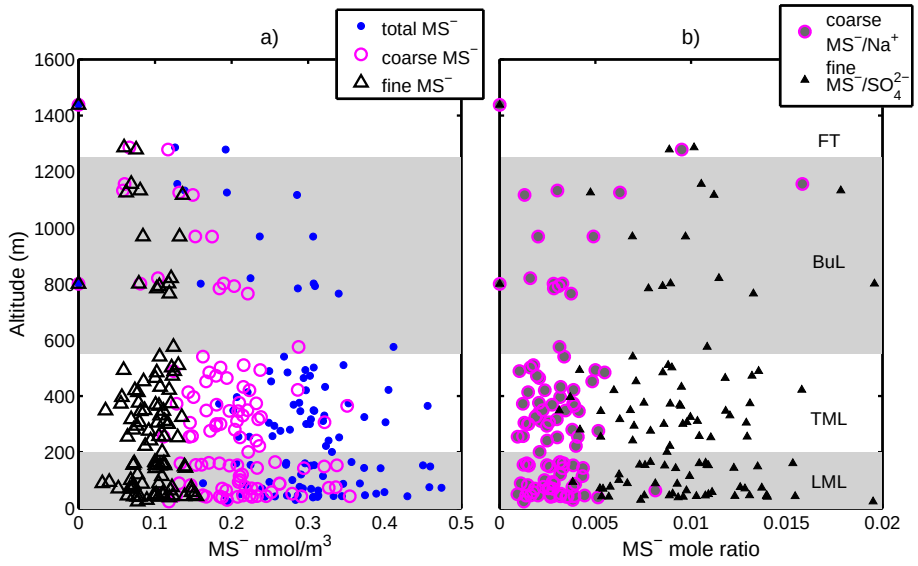

Figure 4.3: PASE MS^- aerosol profile showing total, coarse-mode (>1um), and fine-mode (<1 µm) concentrations (a) measured by the MOI. MS^- concentrations on the backup filter (<0.14 µm) could not be measured and so were estimated to be 5 % of the total MS^-, derived from *Huebert et al.* (1996). In b), we show the mole ratios of coarse MS^- to Na^+ and fine MS^- to NSS (SO_4^{2-}).

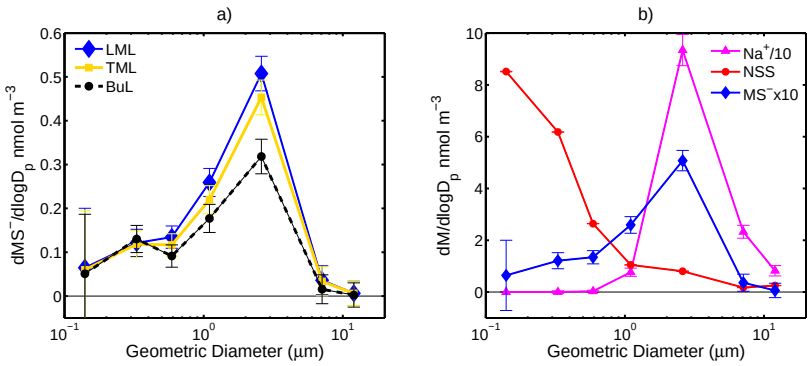

Figure 4.4: a) PASE MS^- mean mass distribution in the LML, TML, and BuL and b) ML $Na^+/10$, NSS, and $MS^-\times 10$ mass distributions. RF05 is excluded as it was an outlier. Note that most of the MS^- mass is supermicrometer, peaking on the primary SSA mass peak. The error in the smallest MS^- stage is large because we could not analytically quantify the concentrations, hence we used mass distributions from the 1994 experiment (*Huebert et al.*, 1996) and the RITS cruises (*Quinn et al.*, 1996) to estimate the MS^- at the smallest diameters. There are no other measurements with which to constrain the MS^- on this stage in the BuL, so its error is largest.

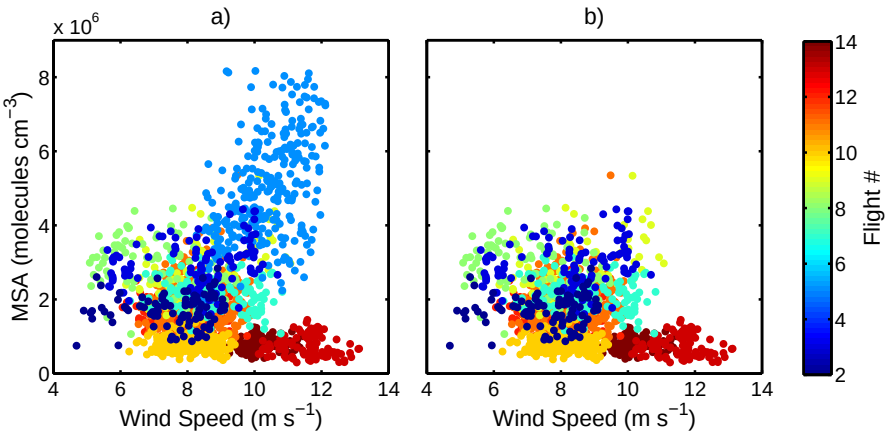

Figure 4.5: MSA versus simultaneous wind speed measured from the plane in the PASE LML. The 1 min data are color-coded by research flight number. A) displays all flights while b) excludes RF05.

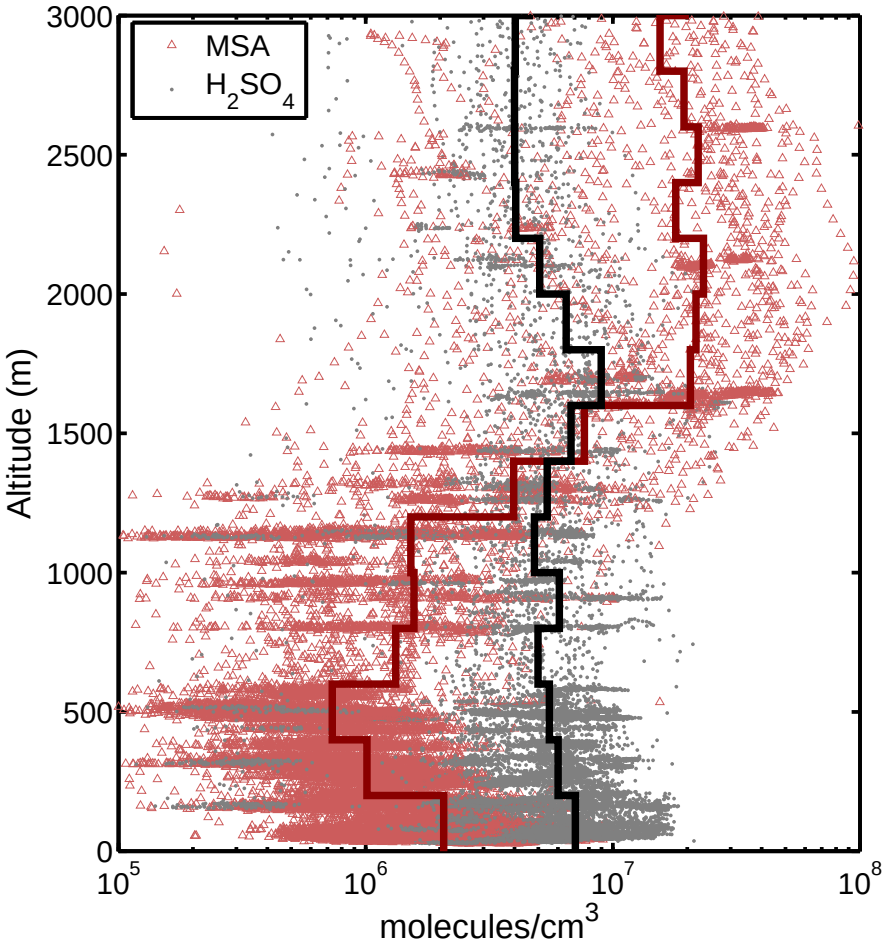

Figure 4.6: MSA and H_2SO_4 profiles and 200 m-bin means. Note that the x-axis is $\log_{10}$-scale. The much lower H_2SO_4 samples (gray points left side of plot) were measured at night.

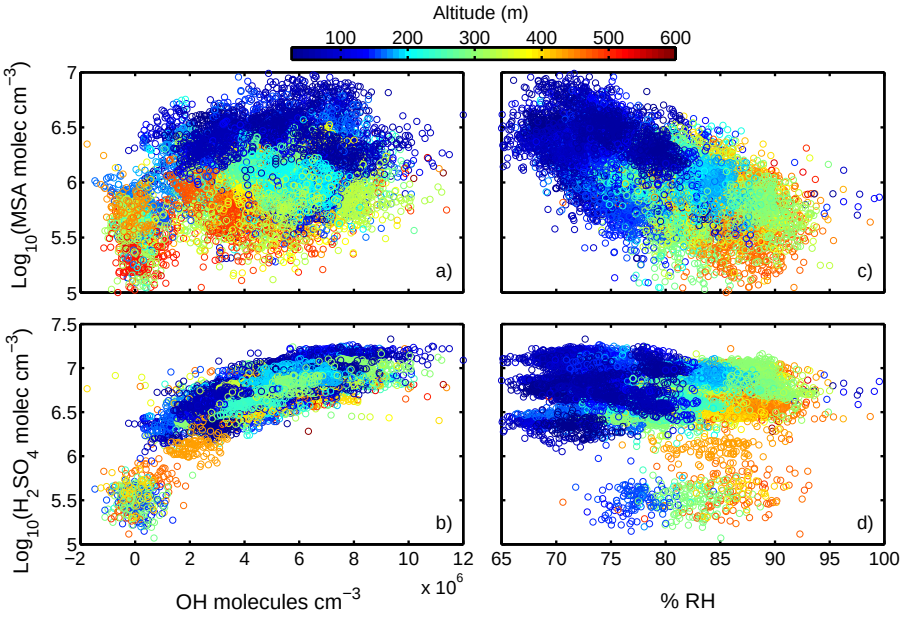

Figure 4.7: $\log_{10}$(MSA) and $\log_{10}(H_2SO_4)$ versus OH molecules/cm^3 (a and b, respectively) and versus %RH (c and d, respectively) in the PASE ML. All samples are color-coded by altitude (m). The LML is represented by dark blue while the TML varies more in color. This illustrates that MSA depends more on RH than the photochemical reactant, while the reverse is true for H_2SO_4.

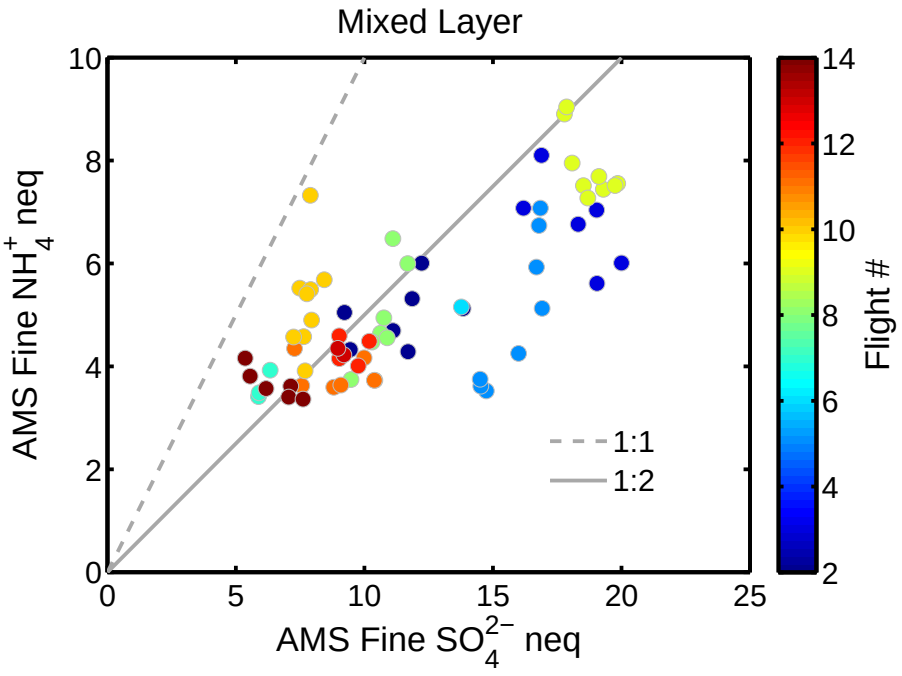

Figure 4.8: AMS submicrometer NH_4^+ neq/m^3 versus SO_4^{2-} neq/m^3 averaged for 30 min level legs in the ML, color-coded by flight number. The least-squares linear regression slope (0.25) indicates that the fine mode NH_4^+ is under-saturated and thus very acidic. Note that RF05, the flight exhibiting the highest MSA vapor in PASE (Fig. 4.5a), contained the most acidic particles farthest below the 1:2 line.

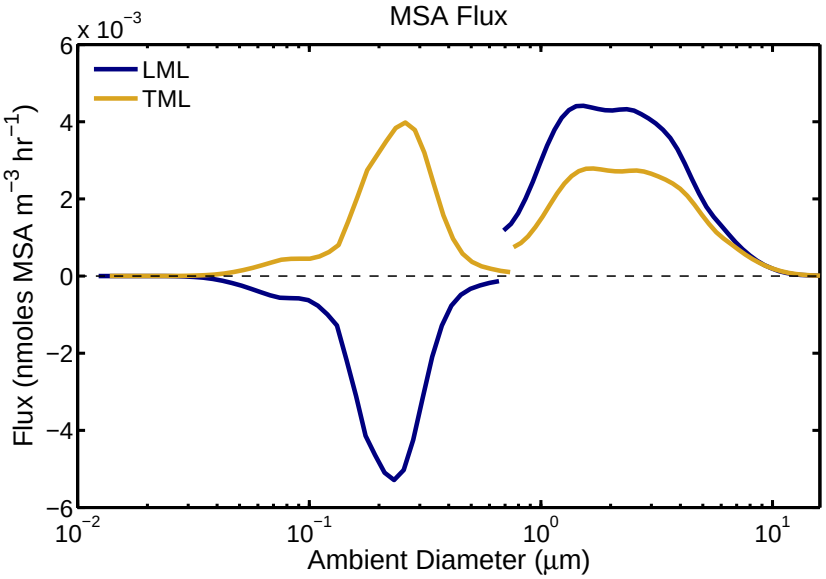

Figure 4.9: Calculated flux of MSA vapor to/from PASE particles in the LML and TML. Submicrometer particle size distributions were measured with a LDMA, and supermicrometer particles were measured with an APS. These fluxes were calculated with $K_H = 3 \times 10^{10}\,\mathrm{M\,atm^{-1}}$.

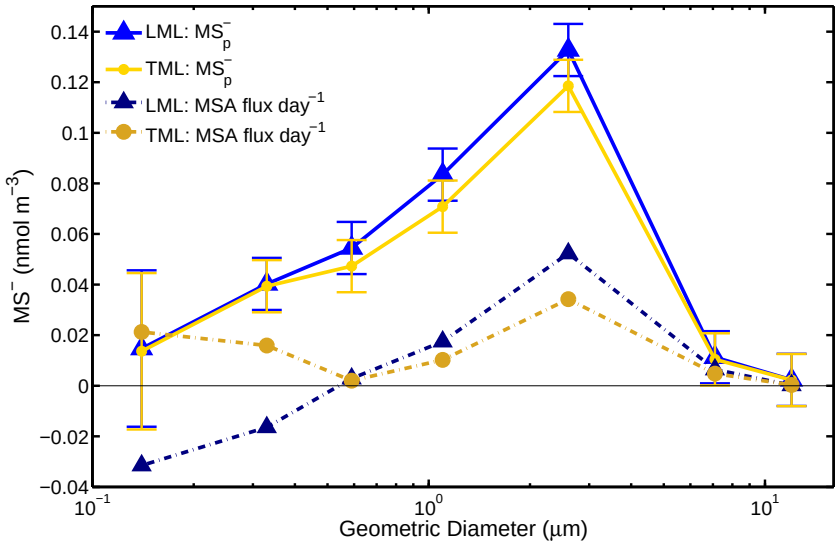

Figure 4.10: Comparison of size-resolved MOI MS^- aerosol molar concentration with calculated total daily fluxes (dotted lines) of MSA vapor to/from each MOI stage. Calculated fluxes are Figure 4.9 fluxes summed for MOI stages.

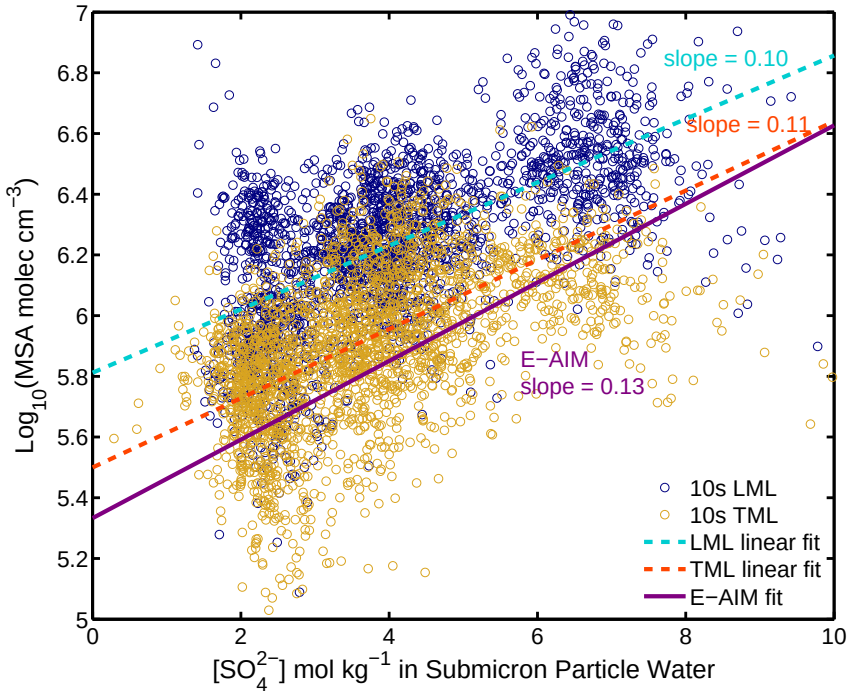

Figure 4.11: $\log_{10}$(MSA) versus submicrometer $[SO_4^{2-}]$ molality ($mol\,kg^{-1}$) in ambient particle volume in the LML and TML. PASE data is compared with the *E-AIM* model output. $[SO_4^{2-}]$ comes from AMS SO_4^{2-} mass divided by the OPC RH-corrected submicrometer aerosol volume.

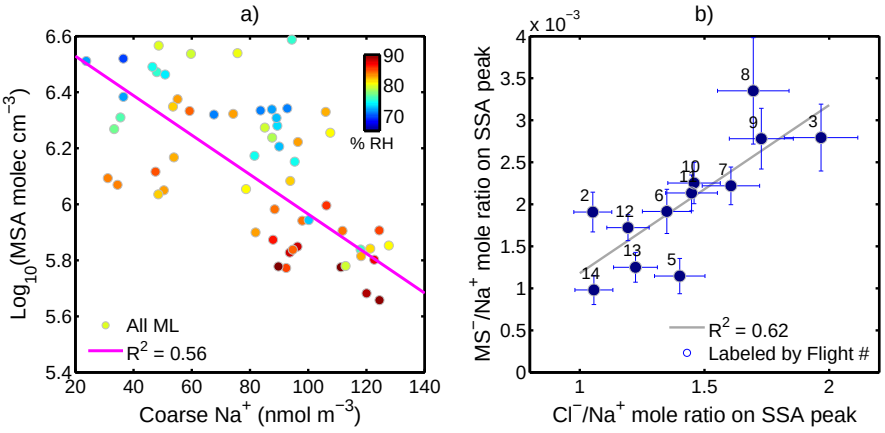

Figure 4.12: a) $\log_{10}$(MSA molecules/cm^3) compared to 30 min MOI coarse-mode Na^+ mass, with data color-coded by %RH. b) Flight-average MS^-/Na^+ molar ratio versus Cl^-/Na^+ ratio on MOI Stage 3, the SSA mass peak.

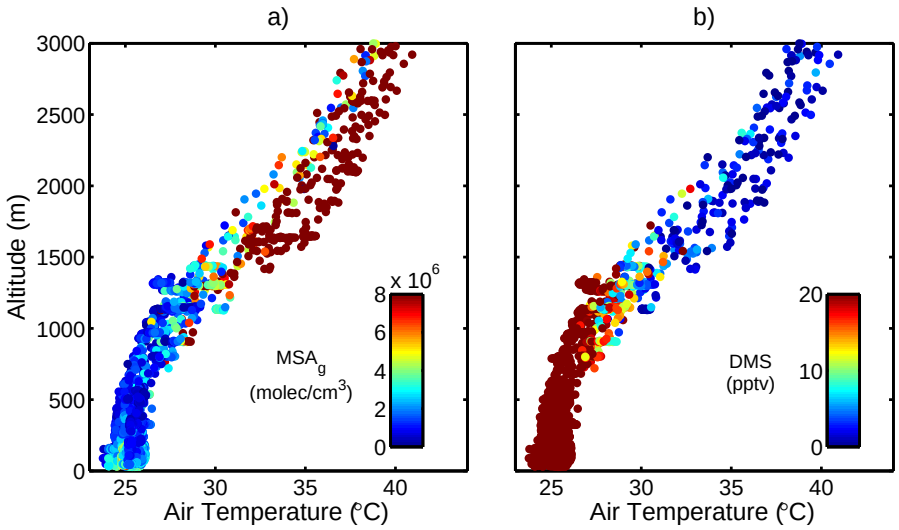

Figure 4.13: Potential temperature (θ) profiles colored by a) MSA molecules/cm^3 and b) DMS pptv.

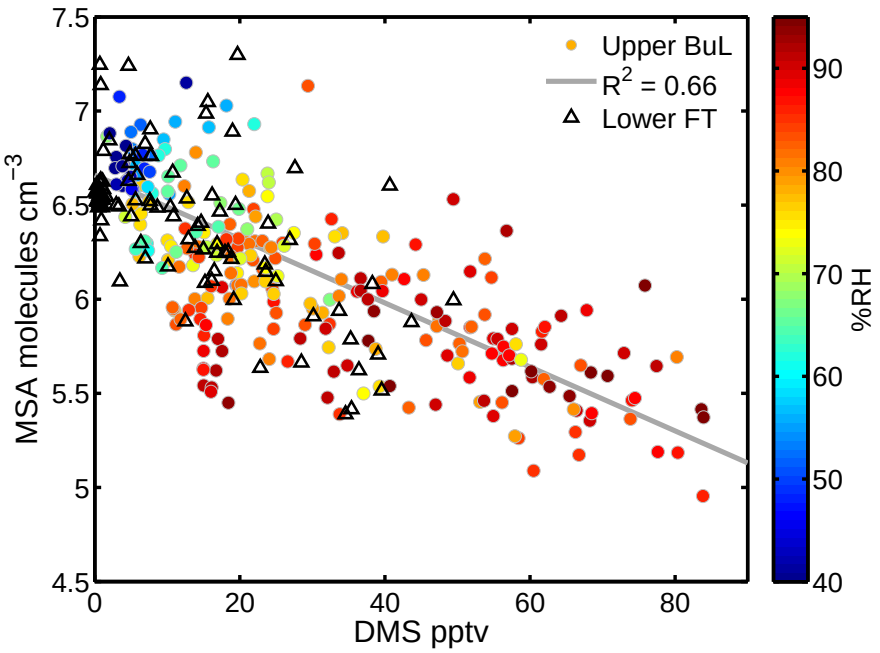

Figure 4.14: $\log_{10}$(MSA molecules/cm^3) versus DMS /pptv in the upper BuL (upper 300 m) colored by %RH, with the lower 200 m of the FT (black triangles) plotted on top. As expected, the boundary between the BuL and FT is variable and not easy to define.

Table 4.1: *E-AIM* Inputs and Outputs.

Inputs: Measurements		**Fine Mode**		**Coarse Mode**	
Layer		LML	TML	LML	TML
%RH		76 %	84 %	76 %	84 %
SO_4^{2-}	neq/m^3	12.2	11.4	0.66	0.52
NO_3^-	neq/m^3	0.27	0.29	2.9	3.1
NH_4^+	neq/m^3	5.3	5.1	0	0
H^+	neq/m^3	7.2	6.6	31.6	22.6
Na^+	neq/m^3	NA	NA	65	65
Cl^-	neq/m^3	NA	NA	93	84
Outputs: Model Calculations					
pH		-0.80	-0.41	-0.80	-0.37
$[MS^-]$	$mol\,kg^{-1}$	0.031	0.028	0.011	0.008
$volume_{(aq)}$	$cm^3\,m^{-3}$	1.09×10^{-6}	1.66×10^{-6}	NA	NA
$\rho_{(aq)}$	$g\,cm^{-3}$	1.31	1.21	NA	NA

Table 4.2: PASE MSA and MS^- concentrations in layers of the central Pacific marine atmosphere.

	MSA	SEM	MS^-_{tot}	MS^- <1 µm[a]	MS^- >1 µm	MSA/MS^-
LML[b]						
$nmol\,m^{-3}$	3.49×10^{-3}		0.32	0.10	0.22	0.01
$molecules/cm^3$	2.10×10^6	4.40×10^4	1.91×10^8			
TML						
$nmol\,m^{-3}$	1.53×10^{-3}		0.30	0.10	0.20	0.005
$molecules/cm^3$	9.23×10^5	1.10×10^4	1.78×10^8			
ML						
$nmol\,m^{-3}$	2.49×10^{-3}		0.31	0.10	0.21	0.008
$molecules/cm^3$	1.50×10^6	2.20×10^4	1.86×10^8			
BuL						
$nmol\,m^{-3}$	2.59×10^{-3}		0.24	0.09	0.15	0.01
$molecules/cm^3$	1.56×10^6	2.30×10^4	1.43×10^8			
FT						
$nmol\,m^{-3}$	1.27×10^{-2}					
$molecules/cm^3$	7.66×10^6	3.30×10^5				

[a] Filter concentrations for MS^- were not measurable due to analytical limitations and thus were inferred using MS^- size distribution data from similar impactors used in the 1994 Christmas Island experiment (*Huebert et al.*, 1996). MOI filter MS^- is likely no greater than 5 % of the total MS^- mass.

[b] LML: lower mixed layer (<200 m); TML: top of the mixed layer (>200 m and below the buffer layer); BuL: buffer layer between the ML and free troposphere, FT (∼1250 m).

Table 4.3: Comparison of total calculated MSA gas-to-particle fluxes assuming different K_H values for MSA.

K_H of MSA M atm^{-1}		Hourly MSA Flux nmol m^{-3} h^{-1}		Daily MSA Flux nmol m^{-3} d^{-1}		MSA Vapor Lifetime h		Adsorb$_{(+)}$/Degas$_{(-)}$ Time h	
		<1 µm	>1 µm	<1 µm	>1 µm	<1 µm	>1 µm	<1 µm	>1 µm
1×10^9									
	LML[a]	-0.9	-0.06	-21	-1.5	0.004	0.13	-0.1	-4
	TML	-0.4	-0.02	-9	-0.4	0.005	0.25	-0.3	-12
3×10^{10}									
	LML	-0.002	0.003	-0.05	0.08	1.9	2.4	-50	70
	TML	-0.002	0.002	0.04	0.05	1.3	1.9	60	100
9×10^{11}									
	LML	0.03	0.005	0.7	0.1	0.14	1.5	3	40
	TML	0.014	0.003	0.3	0.06	0.14	1.4	7	70

[a] LML: lower mixed layer (<200 m); TML: top of the mixed layer (>200 m and below the buffer layer); BuL: buffer layer between the ML and free troposphere, FT (∼1250 m).

References

Albu, M., I. Barnes, K. H. Becker, I. Patroescu-Klotz, R. Mocanu, and T. Benter (2006), Rate coefficients for the gas-phase reaction of OH radicals with dimethyl sulfide: temperature and O_2 partial pressure dependence, *Phys. Chem. Chem. Phys.*, *8*(6), 728–736.

Allen, H. C., E. A. Raymond, and G. L. Richmond (2001), Surface structural studies of methanesulfonic acid at air/aqueous solution interfaces using vibrational sum frequency spectroscopy, *J. Phys. Chem. A*, *105*(9), 1649–1655.

Arsene, C., I. Barnes, K. H. Becker, and R. Mocanu (2001), FT-IR product study on the photo-oxidation of dimethyl sulphide in the presence of NOx – temperature dependence, *Atmos. Environ.*, *35*(22), 3769–3780.

Arsene, C., I. Barnes, K. H. Becker, W. F. Schneider, T. T. Wallington, N. Mihalopoulos, and I. V. Patroescu-Klotz (2002), Formation of methane sulfinic acid in the gas-phase OH-radical initiated oxidation of dimethyl sulfoxide, *Environ. Sci. Technol.*, *36*(23), 5155–5163.

Ayers, G., J. Cainey, H. Granek, and C. Leck (1996), Dimethylsulfide oxidation and the ratio of methanesulfonate to non sea-salt sulfate in the marine aerosol, *J Atmos Chem*, *25*(3), 307–325.

Bandy, A., I. C. Faloona, B. W. Blomquist, B. J. Huebert, A. D. Clarke, S. G.

Howell, R. L. Mauldin, C. A. Cantrell, J. G. Hudson, and B. G. Heikes (2012), Pacific Atmospheric Sulfur Experiment (PASE): dynamics and chemistry of the south Pacific tropical trade wind regime, *J. Atmos. Chem.*, pp. 1–21.

Bandy, A. R., D. C. Thornton, B. W. Blomquist, S. Chen, T. P. Wade, J. C. Ianni, G. M. Mitchell, and W. Nadler (1996), Chemistry of dimethyl sulfide in the equatorial Pacific atmosphere, *J. Geophys. Res.*, *23*, 741–744.

Bandy, A. R., D. C. Thornton, F. H. Tu, B. W. Blomquist, W. Nadler, G. M. Mitchell, and D. H. Lenschow (2002), Determination of the vertical flux of dimethyl sulfide by eddy correlation and atmospheric pressure ionization mass spectrometry (APIMS), *J. Geophys. Res.*, *107*, doi:10.1029/2002JD002472.

Bardouki, H., M. B. Da Rosa, N. Mihalopoulos, W.-U. Palm, and C. Zetzsch (2002), Kinetics and mechanism of the oxidation of dimethylsulfoxide (DMSO) and methanesulfinate (MSI^-) by OH radicals in aqueous medium, *Atmospheric Environment*, *36*(29), 4627–4634.

Bardouki, H., H. Berresheim, M. Vrekoussis, J. Sciare, G. Kouvarakis, K. Oikonomou, J. Schneider, and N. Mihalopoulos (2003), Gaseous (DMS, MSA, SO_2, H_2SO_4 and DMSO) and particulate (sulfate and methanesulfonate) sulfur species over the northeastern coast of Crete, *Atmos Chem Phys*, *3*(4), 3869–3906.

Barnes, I., J. Hjorth, and N. Mihalopoulos (2006), Dimethyl sulfide and dimethyl sulfoxide and their oxidation in the atmosphere, *Chem. Rev.*, *106*(3), 940–975.

Berndt, T., and S. Richters (2012), Products of the reaction of OH radicals with dimethyl sulphide in the absence of NOx: Experiment and simulation, *Atmos. Environ.*, *47*, 316–322.

Campolongo, F., A. Saltelli, N. Jensen, J. Wilson, and J. Hjorth (1999), The role

of multiphase chemistry in the oxidation of dimethylsulphide (DMS). A latitude dependent analysis, *J. Atmos. Chem.*, *32*(3), 327–356.

Capaldo, K. P., and S. N. Pandis (1997), Dimethylsulfide chemistry in the remote marine atmosphere: Evaluation and sensitivity analysis of available mechanisms, *J. Geophys. Res.*, *102*(D19), 23,251–23,267.

Carslaw, K. S., S. L. Clegg, and P. Brimblecombe (1995), A thermodynamic model of the system HCl-HNO_3-H_2SO_4-H_2O, including solubilities of HBr, from < 200 to 328 K, *J. Phys. Chem. A*, *99*(29), 11,557–11,574.

Chen, G., D. Davis, P. Kasibhatla, A. Bandy, D. Thornton, B. Huebert, A. Clarke, and B. Blomquist (2000), A study of DMS oxidation in the tropics: Comparison of Christmas Island field observations of DMS, SO_2, and DMSO with model simulations, *J. Atmos. Chem.*, *37*(2), 137–160, doi:10.1023/A:1006429932403.

Clarke, A., S. Freitag, R. Simpson, J. Hudson, S. Howell, V. Brekhovskikh, T. Campos, V. Kapustin, and J. Zhou (2013), Free troposphere as a major source of CCN for the equatorial Pacific boundary layer: Long-range transport and teleconnections, *Atmos. Chem. Phys.*, *13*(15), 7511–7529.

Clegg, N., and R. Toumi (1998), Non-sea-salt-sulphate formation in sea-salt aerosol, *J. Geophys. Res.*, *103*(D23), 31,095–31, doi:10.1029/98JD02595.

Clegg, S., and P. Brimblecombe (1985), The solubility of methanesulphonic acid and its implications for atmospheric chemistry, *Environ Technol.*, *6*(1-11), 269–278.

Clegg, S. L., and P. Brimblecombe (2005), Comment on the "Thermodynamic dissociation constant of the bisulfate ion from raman and ion interaction modeling studies of aqueous sulfuric acid at low temperatures", *J. Phys. Chem. A*, *109*(11), 2703–2706.

Clegg, S. L., P. Brimblecombe, and A. S. Wexler (1998), Thermodynamic model of the system H^+-NH_4^+-SO_4^{2-}–NO_3–H_2O at tropospheric temperatures, *J. Phys. Chem. A*, *102*(12), 2137–2154.

Conley, S., I. Faloona, D. Lenschow, T. Campos, C. Heizer, A. Weinheimer, C. Cantrell, R. Mauldin, R. Hornbrook, I. Pollack, et al. (2011), A complete dynamical ozone budget measured in the tropical marine boundary layer during PASE, *J. Atmos. Chem.*, *68*(1), 55–70, doi:10.1007/s10874-011-9195-0.

Covington, A. K., and R. Thompson (1974), Ionization of moderately strong acids in aqueous solution. Part III. Methane-, ethane-, and propanesulfonic acids at 25 deg C, *J Solution Chem.*, *3*(8), 603–617.

Dahneke, B. (1983), Simple kinetic theory of Brownian diffusion in vapors and aerosols, *Theory of dispersed multiphase flow*, *2*, 97–133.

Davidovits, P., C. E. Kolb, L. R. Williams, J. T. Jayne, and D. R. Worsnop (2006), Mass accommodation and chemical reactions at gas-liquid interfaces, *Chem. Rev.*, *106*(4), 1323–1354.

Davis, D., G. Chen, P. Kasibhatla, A. Jefferson, D. Tanner, F. Eisele, D. Lenschow, W. Neff, and H. Berresheim (1998), DMS oxidation in the Antarctic marine boundary layer: Comparison of model simulations and field observations of DMS, DMSO, $DMSO_2$, H_2SO_4 (g), MSA (g), and MSA (p), *J. Geophys. Res.*, *103*(D1), 1657–1678.

Davis, D., G. Chen, A. Bandy, D. Thornton, F. Eisele, L. Mauldin, D. Tanner, D. Lenschow, H. Fuelberg, B. Huebert, et al. (1999), Dimethyl sulfide oxidation in the equatorial Pacific: Comparison of model simulations with field observations for DMS, SO_2, H_2SO_4(g), MSA(g), MS and NSS, *J. Geophys. Res.*, *104*(D5), 5765–5784, doi:10.1029/1998JD100002.

De Bruyn, W., J. A. Shorter, P. Davidovits, D. Worsnop, M. Zahniser, and C. Kolb (1994), Uptake of gas phase sulfur species methanesulfonic acid, dimethylsulfoxide, and dimethyl sulfone by aqueous surfaces, *J. Geophys. Res.*, *99*(D8), 16,927–16,932.

DeCarlo, P. F., J. R. Kimmel, A. Trimborn, M. J. Northway, J. T. Jayne, A. C. Aiken, M. Gonin, K. Fuhrer, T. Horvath, K. S. Docherty, et al. (2006), Field-deployable, high-resolution, time-of-flight aerosol mass spectrometer, *Anal. Chem.*, *78*(24), 8281–8289.

Falbe-Hansen, H., S. Sørensen, N. Jensen, T. Pedersen, and J. Hjorth (2000), Atmospheric gas-phase reactions of dimethylsulphoxide and dimethylsulphone with OH and NO_3 radicals, Cl atoms and ozone, *Atmos. Environ.*, *34*(10), 1543–1551.

Freitag, S., A. Clarke, S. Howell, V. Kapustin, T. Campos, V. Brekhovskikh, and J. Zhou (2013), Assimilating airborne gas and aerosol measurements into HYSPLIT: a visualization tool for simultaneous assessment of air mass history and back trajectory reliability, *Atmos. Meas. Tech. Discuss.*, *6*, 5345–5399.

Gerbig, C., S. Schmitgen, D. Kley, A. Volz-Thomas, K. Dewey, and D. Haaks (1999), An improved fast-response vacuum-UV resonance fluorescence CO instrument, *J. Geophys. Res.*, *104*(D1), 1699–1704.

Glasow, R. v., and P. Crutzen (2004), Model study of multiphase DMS oxidation with a focus on halogens, *Atmos. Chem. Phys.*, *4*(3), 589–608.

Gondwe, M., M. Krol, W. Klaassen, W. Gieskes, and H. de Baar (2004), Comparison of modeled versus measured MSA: nss $SO_4^=$ ratios: A global analysis, *Global Biogeochem. Cy.*, *18*(2), GB2006, doi:10.1029/2003GB002144.

González-García, N., À. González-Lafont, and J. M. Lluch (2007), Methanesulfinic acid reaction with OH: Mechanism, rate constants, and atmospheric implications, *J. Phys. Chem. A*, *111*(32), 7825–7832.

Gray, B. A., Y. Wang, D. Gu, A. Bandy, L. Mauldin, A. Clarke, B. Alexander, and D. D. Davis (2011), Sources, transport, and sinks of SO_2 over the equatorial Pacific during the Pacific Atmospheric Sulfur Experiment, *J. Atmos. Chem.*, *68*(1), 27–53.

Hanson, D. (2005), Mass accommodation of H_2SO_4 and CH_3SO_3H on water-sulfuric acid solutions from 6% to 97% RH, *J. Phys. Chem. A*, *109*(31), 6919–6927.

Hatakeyama, S., and H. Akimoto (1983), Reactions of hydroxyl radicals with methanethiol, dimethyl sulfide, and dimethyl disulfide in air, *J Phys Chem*, *87*(13), 2387–2395.

Herrmann, H., B. Ervens, P. Nowacki, R. Wolke, and R. Zellner (1999), A chemical aqueous phase radical mechanism for tropospheric chemistry, *Chemosphere*, *38*(6), 1223–1232.

Huebert, B., D. Wylie, L. Zhuang, and J. Heath (1996), Production and loss of methanesulfonate and non-sea salt sulfate in the equatorial Pacific marine boundary layer, *Geophys. Res. Lett.*, *23*(7), 737–740.

Huebert, B., S. Howell, D. Covert, T. Bertram, A. Clarke, J. Anderson, B. Lafleur, W. Seebaugh, J. Wilson, D. Gesler, et al. (2004), PELTI: Measuring the passing efficiency of an airborne low turbulence aerosol inlet, *Aerosol Sci. Technol.*, *38*(8), 803–826.

Jefferson, A., D. Tanner, F. Eisele, D. Davis, G. Chen, J. Crawford, J. Huey, A. Torres, and H. Berresheim (1998), OH photochemistry and methane sulfonic

acid formation in the coastal Antarctic boundary layer, *J Geophys Res*, *103*(D1), 1647–1656.

Jensen, N., J. Hjorth, C. Lohse, H. Skov, and G. Restelli (1992), Products and mechanisms of the gas phase reactions of NO_3 with CH_3SCH_3, CD_3SCD_3, CH_3SH and CH_3SSCH_3, *J. Atmos. Chem.*, *14*(1-4), 95–108.

Kerminen, V.-M., and C. Leck (2001), Sulfur chemistry over the central Arctic Ocean during the summer: Gas-to-particle transformation, *J. Geophys. Res.*, *106*(D23), 32,087–32,099.

Kolb, C., R. Cox, J. Abbatt, M. Ammann, E. Davis, D. Donaldson, B. C. Garrett, C. George, P. Griffiths, D. Hanson, et al. (2010), An overview of current issues in the uptake of atmospheric trace gases by aerosols and clouds, *Atmos. Chem. Phys.*, *10*(21), 10,561–10,605.

Kukui, A., D. Borissenko, G. Laverdet, and G. Le Bras (2003), Gas-phase reactions of OH radicals with dimethyl sulfoxide and methane sulfinic acid using turbulent flow reactor and chemical ionization mass spectrometry, *J Phys Chem-A*, *107*(30), 5732–5742.

Leck, C., and C. Persson (1996), The central Arctic Ocean as a source of dimethyl sulfide seasonal variability in relation to biological activity, *Tellus B*, *48*(2), 156–177.

Legrand, M., J. Sciare, B. Jourdain, and C. Genthon (2001), Subdaily variations of atmospheric dimethylsulfide, dimethylsulfoxide, methanesulfonate, and non-sea-salt sulfate aerosols in the atmospheric boundary layer at Dumont d'Urville (coastal Antarctica) during summer, *J. Geophys. Res.*, *106*(D13), 14,409–14,422.

Lelieveld, J., and P. Crutzen (1991), The role of clouds in tropospheric photochemistry, *J. Atmos. Chem.*, *12*(3), 229–267.

Lewis, R., and E. Schwartz (2004), *Sea Salt Aerosol Production: Mechanisms, Methods, Measurements and Models – A Critical Review*, vol. 152, American Geophysical Union.

Lucas, D. D., and R. G. Prinn (2005), Sensitivities of gas-phase dimethylsulfide oxidation products to the assumed mechanisms in a chemical transport model, *J Geophys Res*, *110*(D21).

Marandino, C., S. Tegtmeier, K. Krüger, C. Zindler, E. Atlas, F. Moore, and H. W. Bange (2013), Dimethylsulphide (DMS) emissions from the western Pacific Ocean: a potential marine source for stratospheric sulphur?, *Atmos. Chem. Phys.*, *13*(16), 8427–8437.

Massucci, M., S. L. Clegg, and P. Brimblecombe (1999), Equilibrium partial pressures, thermodynamic properties of aqueous and solid phases, and Cl_2 production from aqueous HCl and HNO_3 and their mixtures, *J. Phys. Chem. A*, *103*(21), 4209–4226.

Mauldin, R., D. Tanner, J. Heath, B. Huebert, and F. Eisele (1999), Observations of H_2SO_4 and MSA during PEM-Tropics-A, *Journal of Geophysical Research: Atmospheres (1984–2012)*, *104*(D5), 5801–5816.

Maxwell, J. C. (1888), Diffusion, in *Encyclopædia Britannica*, vol. VII, edited by T. S. Baynes, 9th ed., pp. 214–221, Henry G. Allen and Company, New York.

McNaughton, C. S., A. D. Clarke, S. G. Howell, M. Pinkerton, B. Anderson, L. Thornhill, C. Hudgins, E. Winstead, J. E. Dibb, E. Scheuer, et al. (2007), Results from the DC-8 Inlet Characterization Experiment (DICE): Airborne versus surface sampling of mineral dust and sea salt aerosols, *Aerosol Sci. Technol.*, *41*(2), 136–159.

Mihalopoulos, N., V. Kerminen, M. Kanakidou, H. Berresheim, and J. Sciare (2007), Formation of particulate sulfur species (sulfate and methanesulfonate) during summer over the Eastern Mediterranean: a modelling approach, *Atmos. Environ.*, *41*(32), 6860–6871.

Nowak, J., D. Davis, G. Chen, F. Eisele, R. Mauldin, D. Tanner, C. Cantrell, E. Kosciuch, A. Bandy, D. Thornton, et al. (2001), Airborne observations of DMSO, DMS, and OH at marine tropical latitudes, *Geophy. Res. Lett.*, *28*(11), 2201–2204.

Pfister, G., L. Emmons, D. Edwards, A. Arellano, G. Sachse, and T. Campos (2010), Variability of springtime transpacific pollution transport during 2000–2006: the INTEX-B mission in the context of previous years, *Atmos. Chem. Phys.*, *10*(3), 1345–1359.

Quinn, P., V. Kapustin, T. Bates, and D. Covert (1996), Chemical and optical properties of marine boundary layer aerosol particles of the mid-Pacific in relation to sources and meteorological transport, *J. Geophys. Res.*, *101*(D3), 6931–6951.

Saltzman, E., D. Savoie, J. Prospero, and R. Zika (1986), Methanesulfonic acid and non-sea-salt sulfate in Pacific air: Regional and seasonal variations, *J. Atmos. Chem.*, *4*(2), 227–240.

Savoie, A., and J. Prospero (1989), Comparison of oceanic and continental sources of non-sea-salt sulphate over the Pacific Ocean, *Nature*, *339*, 29.

Scaduto, R. C. (1995), Oxidation of DMSO and methanesulfinic acid by the hydroxyl radical, *Free Radical Bio. Med.*, *18*(2), 271–277.

Sciare, J., M. Kanakidou, and N. Mihalopoulos (2000), Diurnal and seasonal vari-

ation of atmospheric dimethylsulfoxide at Amsterdam Island in the southern Indian Ocean, *J Geophys Res*, *105*(D13), 17,257–17,265.

Shank, L., S. Howell, A. Clarke, S. Freitag, V. Brekhovskikh, V. Kapustin, C. McNaughton, T. Campos, and R. Wood (2012), Organic matter and non-refractory aerosol over the remote southeast Pacific: oceanic and combustion sources, *Atmos. Chem. Phys.*, *12*(1), 557–576.

Simpson, R. (2010), Mechanisms of sulfate formation in the equatorial Pacific marine boundary layer, M.S. thesis, Univ. Hawai'i, Mānoa, Honolulu.

Simpson, R. M., S. G. Howell, B. W. Blomquist, A. D. Clarke, and B. J. Huebert (2014), Dimethyl sulfide: Less important than long-range transport as a source of sulfate to the remote tropical Pacific marine boundary layer, *J. Geophys. Res.*, *119*(14), 9142–9167.

Sørensen, S., H. Falbe-Hansen, M. Mangoni, J. Hjorth, and N. Jensen (1996), Observation of DMSO and $CH_3S(O)OH$ from the gas phase reaction between DMS and OH, *J. Atmos. Chem.*, *24*(3), 299–315.

Tian, Y., Z.-M. Tian, W.-M. Wei, T.-J. He, D.-M. Chen, and F.-C. Liu (2007), Ab initio study of the reaction of oh radical with methyl sulfinic acid (msia), *Chem. Phys.*, *335*(2), 133–140.

Turnipseed, A., and A. Ravishankara (1993), The atmospheric oxidation of dimethyl sulfide: Elementary steps in a complex mechanism, *Dimethylsulfide: Oceans, Atmosphere and Climate*, pp. 185–196.

Turnipseed, A., S. Barone, and A. Ravishankara (1996), Reaction of OH with dimethyl sulfide. 2. Products and mechanisms, *J. Phys. Chem. A*, *100*(35), 14,703–14,713.

Urbanski, S., R. Stickel, and P. Wine (1998), Mechanistic and kinetic study of the gas-phase reaction of hydroxyl radical with dimethyl sulfoxide, *J. Phys. Chem. A*, *102*(51), 10,522–10,529.

Vácha, R., P. Slavícek, M. Mucha, B. J. Finlayson-Pitts, and P. Jungwirth (2004), Adsorption of atmospherically relevant gases at the air/water interface: Free energy profiles of aqueous solvation of N_2, O_2, O_3, OH, H_2O, HO_2, and H_2O_2, *J. Phys. Chem. A*, *108*(52), 11,573–11,579.

Yin, F., D. Grosjean, and J. Seinfeld (1990), Photooxidation of dimethyl sulfide and dimethyl disulfide. I: Mechanism development, *J. Atmos. Chem.*, *11*(4), 309–364.

Zhang, Y., Y. Wang, B. A. Gray, D. Gu, L. Mauldin, C. Cantrell, and A. Bandy (2014), Surface and free tropospheric sources of methanesulfonic acid over the tropical Pacific Ocean, *Geophys. Res. Lett.*, *41*(14), 5239–5245.

Zhou, X., A. J. Davis, D. J. Kieber, W. C. Keene, J. R. Maben, H. Maring, E. E. Dahl, M. A. Izaguirre, R. Sander, and L. Smoydzyn (2008), Photochemical production of hydroxyl radical and hydroperoxides in water extracts of nascent marine aerosols produced by bursting bubbles from Sargasso seawater, *Geophys. Res. Lett.*, *35*(20).

Zhu, L., J. M. Nicovich, and P. H. Wine (2003a), Temperature-dependent kinetics studies of aqueous phase reactions of hydroxyl radicals with dimethylsulfoxide, dimethylsulfone, and methanesulfonate, *Aquatic sciences*, *65*(4), 425–435.

Zhu, L., J. Nicovich, and P. Wine (2003b), Temperature-dependent kinetics studies of aqueous phase reactions of so 4- radicals with dimethylsulfoxide, dimethylsulfone, and methanesulfonate, *Journal of Photochemistry and Photobiology A: Chemistry*, *157*(2), 311–319.

Zhu, L., A. Nenes, P. H. Wine, and J. M. Nicovich (2006), Effects of aqueous organosulfur chemistry on particulate methanesulfonate to non–sea salt sulfate ratios in the marine atmosphere, *J Geophys Res*, *111*(D5).

Appendix. Derivation of divergence losses

Start with the divergence integral.

$$D_{\mathrm{S}} = \int_0^{z_2} div(z)[\mathrm{S}](z)dz \tag{4.17}$$

As mentioned in section 2.2, $div(z)$ is near zero at z_2, increasing more or less linearly through the BuL to the ML, where it is constant. Call D_M the value of $div(z)$ in the ML. Then

$$div(z) = \begin{cases} D_M & \text{if } 0 < z \leq z_1 \\ D_M(z_2 - z)/(z_2 - z_1) & \text{if } z_1 < z < z_2 \end{cases} \tag{4.18}$$

Similarly, the concentration of a substance S is roughly constant in the ML at $\mathrm{S_M}$ and changes linearly through the BuL to the FT value $\mathrm{S_F}$. So

$$[\mathrm{S}](z) = \begin{cases} \mathrm{S_M} & \text{if } 0 < z \leq z_1 \\ \mathrm{S_F} + (\mathrm{S_M} - \mathrm{S_F})(z_2 - z)/(z_2 - z_1) & \text{if } z_1 < z < z_2 \end{cases} \tag{4.19}$$

Split Eq. 4.17 into ML and BuL parts and substitute in Eqns. 4.18 and 4.19 to get

$$D_{\mathrm{S}} = \int_0^{z_1} D_{\mathrm{M}} \mathrm{S}_{\mathrm{M}} dz + \int_{z_1}^{z_2} D_{\mathrm{M}} \frac{z_2 - z}{z_2 - z_1} \left[\mathrm{S}_{\mathrm{F}} + (\mathrm{S}_{\mathrm{M}} - \mathrm{S}_{\mathrm{F}}) \frac{z_2 - z}{z_2 - z_1} \right] dz \tag{4.20}$$

The first term is trivially $D_{\mathrm{M}}\mathrm{S}_{\mathrm{M}} z_1$; the second is aided by substituting

$$Z = z_2 - z \quad \text{and} \quad dZ = -dz \tag{4.21}$$

and simplifying a bit to get

$$D_{\mathrm{S}} = D_{\mathrm{M}}\mathrm{S}_{\mathrm{M}} \int_0^{z_1} dz - \frac{D_{\mathrm{M}}\mathrm{S}_{\mathrm{F}}}{z_2 - z_1} \int_{z_2 - z_1}^{0} Z dZ - \frac{D_{\mathrm{M}}(\mathrm{S}_{\mathrm{M}} - \mathrm{S}_{\mathrm{F}})}{(z_2 - z_1)^2} \int_{z_2 - z_1}^{0} Z^2 dZ \tag{4.22}$$

which can be solved and simplified to

$$D_{\mathrm{S}} = D_{\mathrm{M}}\mathrm{S}_{\mathrm{M}} z_1 + \left[\frac{1}{6} D_{\mathrm{M}}\mathrm{S}_{\mathrm{F}} + \frac{1}{3} D_{\mathrm{M}}\mathrm{S}_{\mathrm{M}} \right] (z_2 - z_1) \tag{4.23}$$

All of the quantities are measured except D_{M}, which can be determined by noting that total divergence must equal entrainment:

$$\omega_e = \int_0^{z_2} div(z) dz = \int_0^{z_1} D_{\mathrm{M}} dz + \int_{z_1}^{z_2} D_M \frac{z_2 - z}{z_2 - z_1} dz \tag{4.24}$$

$$= D_{\mathrm{M}} z_1 + \frac{1}{2} D_{\mathrm{M}} (z_2 - z_1) \tag{4.25}$$

Solving for D_{M} gives

$$D_{\mathrm{M}} = \frac{2\omega_e}{z_1 + z_2} \tag{4.26}$$

Substituting Eq. 4.26 back into Eq. 4.23 and simplifying yields

$$D_{\mathrm{S}} = \omega_e \mathrm{S}_{\mathrm{M}} \left[\frac{2z_1}{z_2 + z_1} + \left(\frac{2}{3} + \frac{1}{3} \frac{\mathrm{S}_{\mathrm{F}}}{\mathrm{S}_{\mathrm{M}}} \right) \frac{z_2 - z_1}{z_2 + z_1} \right] \tag{4.27}$$

Significance

While $\omega_e S_M$ is straightforward, the rest of Eq. 4.27 is rather opaque. It is not immediately obvious whether it makes any particular difference. For comparison with the naïve formula $D_S = \omega_e \bar{S}$, it is useful to derive $\bar{S}$, the mean concentration in the MBL:

$$\bar{S} = \frac{1}{z_2}\left[S_M z_1 + \frac{S_F + S_M}{2}(z_2 - z_1)\right] \tag{4.28}$$

If column concentration is fairly constant with height, then $S_M = S_F = \bar{S}$, and Eq 4.27 reduces to $D_S = \omega_e S_M = \omega_e \bar{S}$, as one would expect. Similarly, if a strong inversion and weak convection lead to a very thin BuL, as is often the case in stratocumulus-topped boundary layers, then $z_1 \approx z_2$ and $D_S \approx \omega_e \bar{S}$

The largest effect is when $S_F = 0$, as is the case with DMS. In that case, with $z_1 = 550$ and $z_2 = 1250$, we get

$$D_S = 0.87\,\omega_e\,S_M \text{ and} \tag{4.29}$$

$$\bar{S} = 0.72\,S_M, \text{ so} \tag{4.30}$$

$$D_S = 1.2\,\omega_e\,\bar{S} \tag{4.31}$$

The net effect is a 20% increase in divergence flux over the simple formula. Essentially, because divergence is maximal where the concentration is highest, the divergence flux is amplified. The effect is small for SO_2, where FT concentrations are close to the MBL, 10% for NSS under low CO conditions and 4% at high CO.